Optimization studies on the calorimetric second level tau trigger of the ATLAS experiment at the Large Hadron Collider

by

Estel Pérez i Codina

Treball de Recerca de tercer cicle de Física

Facultat de Ciències
de la Universitat Autònoma de Barcelona

April 2008

Directora: Martine Bosman

Tutor: José Maria Crespo Vicente

“I love deadlines.
I like the whooshing sound
they make as they fly past”

D. Adams

Contents

List of Figures

List of Tables

1 Introduction

The Standard Model of particle physics (SM) is the theory that currently describes the strong and electroweak interaction between fermions. In this model, fermions (spin 1/2 particles) interact among them through gauge bosons (spin 1 particles).

Despite its large phenomenological success, there is still a missing building block of the SM: the Higgs boson. Such scalar boson, which has not been observed yet, plays a fundamental role: it gives mass to every elementary particle via the electroweak symmetry breaking mechanism.

Furthermore, there are strong reasons to believe that the SM is only a low energy effective theory of a more fundamental theory. The Supersymmetric theory (SUSY) is a good candidate to be the extension of the SM. The minimal version of SUSY model (MSSM) doubles the number of elementary particles, introducing for each known SM particle a supersymmetric partner. Each known fermion has a supersymmetric boson associated, and vice versa, and their couplings are related. In this scheme, the masses of the supersymmetric particles are of the order of 100 GeV to 1 TeV.

The Large Hadron Collider (LHC) is a proton-proton collider at CERN in Geneva, that will produce soon the first interactions. The LHC will extend the frontiers of particle physics with its unprecedented high energy and luminosity. Inside the LHC, bunches of up to 10^{11} protons will collide 40 million times per second to provide 14 TeV proton-proton collisions at a design luminosity of $10^{34}\,\mathrm{cm}^{-2}\mathrm{s}^{-1}$. It will provide a rich physics potential, ranging from more precise measurements of Standard Model parameters to the search for new physics phenomena.

One of the main goals of the LHC is to search for supersymmetric particles. At the energies reachable by the LHC the cross section for the production of supersymmetric particles is dominated by strongly interacting gluinos and squarks. The decay chains of supersymmetric particles contain jets and leptons. Additionally, this events are characterized by the lack of visible energy. This "*missing energy*" is due to light supersymmetric particles produced in the decay chains, which only undergo weak interaction and therefore escape detection. Observation of an excess of this kind of events with respect to those predicted by the SM can be the key for the discovery of "*new physics*".

Regarding the Higgs boson, results from other collider experiments lead to an experimental lower bound for the SM Higgs mass of 114.4 GeV at 95% confidence level. From the theoretical point of view the highest possible mass scale allowed for the Higgs is around 1 TeV. As the search for the Higgs boson is one of the main motivations for the LHC, the LHC's energy range was designed to perfectly suit the possible Higgs masses, allowing also the discovery of possible new physics which is expected at the TeV scale.

The ATLAS experiment is one of the two main general-purpose detectors designed to explore this new energy frontier. Installation of the ATLAS detector down in the ATLAS cavern is now nearing completion. The primary physics goals of ATLAS are to understand the mechanism for electroweak symmetry breaking and to search for new physics at the TeV energy scale.

At LHC's design luminosity, the interaction rate inside the detector will be of 10^9 proton-proton interactions per second. Due to limitation of the number of events which can be stored, the output rate is limited to $\sim$200 Hz. ATLAS is therefore equipped with an on-line multi-stage selection system (Trigger) which must achieve the required rejection maintaining a high efficiency for the interesting events.

The tau (τ) particle is a lepton, equivalent to electron and muon, the only differential property being its mass. However, due to its much higher mass (m_τ=1777 MeV, m_e=0.5 MeV), it is the only lepton able to decay into hadrons.

The tau trigger aims at selecting hadronic tau decays, while leptonic tau decays are triggered by the electron or muon trigger. Hadronic taus are detected as narrow jets with low track multiplicity. These characteristics will help to distinguish them from QCD jets, the dominant background.

The outline of this document is as follows. Chapter 2 describes the ATLAS experiment, its physics goals, the detector layout and specially the trigger system. Chapter 3 is dedicated to the ATLAS tau trigger and addresses the following subjects. First of all the physics channels reachable with such triggers, as well as the characteristics used for tau identification, are described. Tau offline reconstruction algorithms are presented. A description of the three trigger levels and their performance is then given. Tau trigger menus as well as the selection strategy for different luminosities are presented. The menu for early running is discussed comparing tau with electron and muon slices. Chapter 4 presents the optimization studies for the calorimetric part of the first and second level of the tau trigger. Finally, conclusions and outlook can be found in chapter 5.

2 The ATLAS experiment

2.1 Introduction to LHC

The Large Hadron Collider (LHC) will provide proton-proton collisions at a center of mass energy of 14 TeV, the highest energy ever reached in collider experiments. The start-up is programmed for the second half of this year 2008.

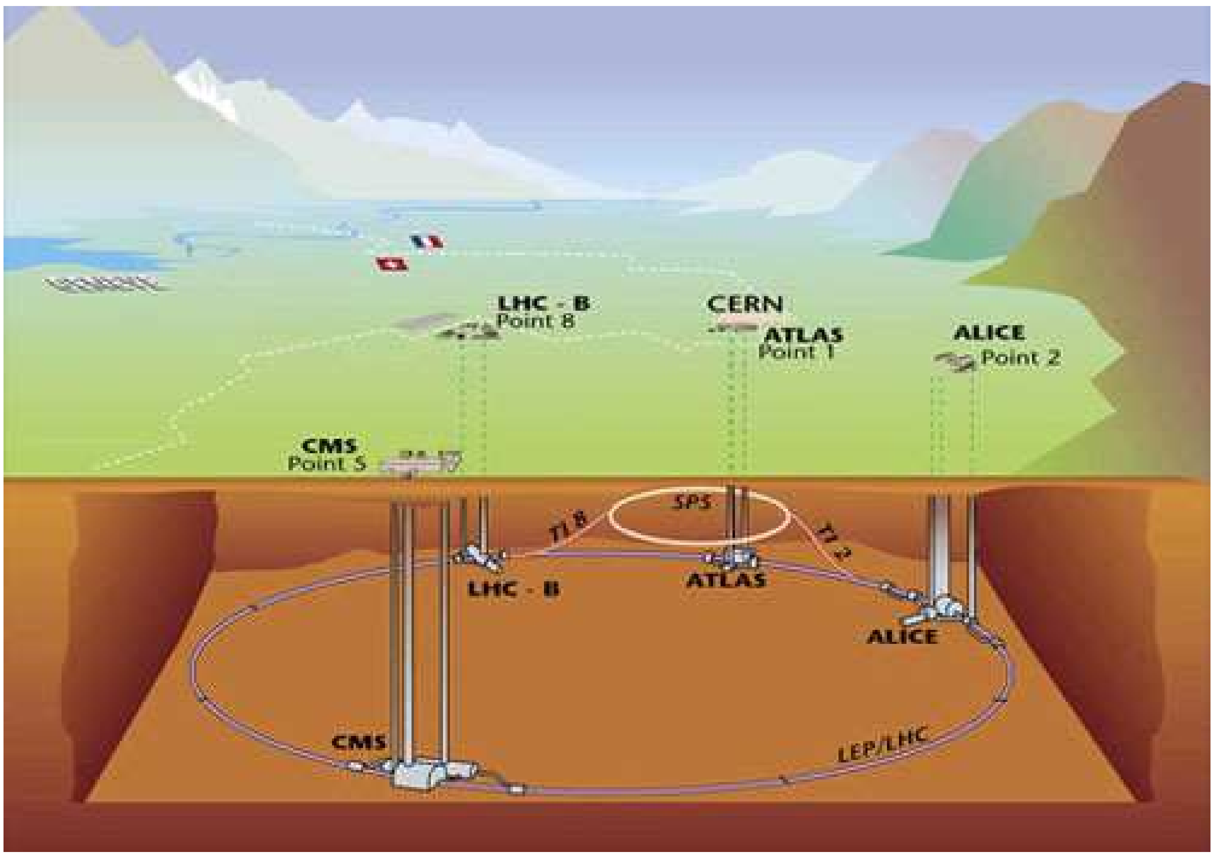

Figure 2.1: Overall View of the CERN LHC Experiments

The accelerator has been built in the 27 Km perimeter tunnel which used to host the LEP machine. Superconducting magnets will provide magnetic fields of about 10 Tesla which will hold the protons on their orbit and will allow the desired 7 TeV energy per beam.

Each beam is nominally constituted by ∼2800 bunches containing approximately 10^{11} protons per bunch. A bunch crossing will occur at each interaction point every 25 ns. These conditions lead to very high interaction rates of almost 10^9 interactions per second.

Initial luminosity foreseen for start-up and commissioning in 2008 is $\sim 10^{31} cm^{-2} s^{-1}$. The following year this luminosity will increase to reach the "low luminosity" scenario with peak luminosity of about $10^{33} cm^{-2} s^{-1}$. Finally the LHC's design luminosity of $\sim 10^{34} cm^{-2} s^{-1}$ is expected to be reached 3 years after start-up. [1]

The high value of the design luminosity, combined with the unprecedented center-of-mass energy implies that heavy particles can produced with high statistics up to the TeV scale. High precision tests of QCD, as well as electroweak interactions and flavor physics will be enabled. The top quark will be produced at the LHC at a rate of a few tens of Hz, providing the opportunity to test its couplings and spin.

The LHC has four *interaction points* where the two beams collide and therefore particle detectors are placed. Accordingly, there will be four experiments taking measurements at LHC. Consequently ATLAS (A Toroidal LHC ApparatuS) and CMS (Compact Muon Solenoid) are general-purpose detectors designed to exploit the full discovery potential of physics at the LHC. The other two experiments in the LHC are: ALICE (A Large Ion Collider experiment), dedicated to the study of heavy ions, and LHCb, devoted to CP-violation and B-physics studies.

2.2 The ATLAS detector

ATLAS (A Toroidal LHC ApparatuS) [2] is a general purpose $p-p$ spectrometer designed to exploit the full discovery potential of the LHC.

The primary goal of the experiment is to operate at high luminosity ($10^{34} cm^{-2} s^{-1}$) with a detector that provides as many signatures as possible. The variety of signatures is considered to be important in the harsh environment of the LHC in order to achieve robust and redundant physics measurements with the ability of internal cross-check.

In this section, the physics processes that are expected to be observed and measured with the ATLAS experiment are described. Besides, the requirements that the harsh environment and the needed precision and robustness of the measurements impose to the detector are explained. Next, an overview of the detector layout is given, together with a more detailed description of the calorimeters.

2.2.1 Physics goals

The main physics goals of ATLAS will be the search for the Standard Model Higgs boson over an energy range of $115 < m_H < 1000\,\text{GeV}$ and the search for physics beyond the SM (such as Supersymmetry and Extra-dimensions) up to the TeV-range, as well as precise measurements of SM parameters: W mass; top mass, couplings and decay properties; Higgs mass, spin and couplings (if Higgs found); and many others.

The search for the Standard Model Higgs boson has been used as a benchmark to establish the performance of important sub-systems of ATLAS. It is a particularly important process since there is a range of production and decay mechanisms, depending on the mass of the Higgs boson (m_H). At low masses ($m_H < 2m_Z$), the predominant decay mode into hadrons would be difficult to detect due to QCD backgrounds, and the two-photon decay channel would be an important one. For masses above 130 GeV, Higgs-boson decays, H $\rightarrow$ ZZ, where each Z decays into a pair of oppositely charged leptons, would provide the experimentally cleanest channel to study the properties of the Higgs boson. For masses above $\sim$ 600 GeV, WW and ZZ decays into jets or involving neutrinos would be needed to extract a signal.

Searches for the Higgs boson beyond the Standard Model, for such particles as the neutral (A) and heavy ($H^{\pm}$) Higgs of the MSSM, require sensitivity to processes involving τ-leptons and good b-tagging performance. Should the Higgs boson be discovered, it would need to be studied in several modes, regardless of its mass, in order to fully disentangle its properties and establish its credentials as belonging to the Standard Model or an extension thereof.

The decays of supersymmetric particles, such as squarks and gluinos, would involve cascades which, if R-parity is conserved[1], always contain a lightest stable supersymmetric particle (LSP). As the LSP would interact very weakly with the detector, the experiment would measure a significant missing transverse energy ($\not{E}_T$), in the final state. The rest of the cascade would result in a number of leptons and jets. In schemes where the LSP decays into a photon and a gravitino, an increased number of hard isolated photons is expected.

Several new models propose the existence of extra dimensions leading to a characteristic energy scale of quantum gravity in the TeV region. In terms of experimental signatures, this could lead to the emission of gravitons which escape into extra dimensions and therefore generate $\not{E}_T$.

Other experimental signatures could be anomalous high-mass di-jet production, and miniature black-hole production with spectacular decays involving democratic production of fundamental final states such as jets, leptons, photons, neutrinos, Ws, and Zs.

2.2.1.1 Early discoveries and measurements

Already half a year after the start-up, the amount of data collected (expected to be a few tens of pb^{-1}) could be enough to observe the first top quarks in Europe. New physics such as Supersymetry, could be seen after the first year of data taking, with first few $100\,pb^{-1}$. Possible observation of the Higgs particle (in case it exists with low mass) will need at least $1\,fb^{-1}$ of data, but we will probably have to wait at least a couple of years for the awaited Higgs discovery.

In figure 2.2 a general view of the possible LHC discoveries and the expected amount of data and time needed is presented.

2.2.2 Detector description

2.2.2.1 Coordinate System

The coordinate system used for describing the ATLAS detector and the particles emerging from the $p-p$ collisions are briefly summarized here as they are used repeatedly throughout this document.

- The beam direction defines the z-axis and the x-y plane is transverse to the beam direction.
- The azimuthal angle ϕ is measured around the beam axis, and the polar angle θ is the angle from the beam axis.
- The pseudorapidity [2] [3] is defined as $\eta = -ln\,tan\,\frac{\theta}{2}$.
- The transverse momentum p_T , the transverse energy E_T , and the missing transverse energy $\not{E}_T$ are defined in the x-y plane, i.e. $E_T = E/cosh(\eta)$.
- The distance ΔR in the pseudorapidity-azimuthal angle space is defined as $\Delta R \equiv \sqrt{(\Delta\eta)^2 + (\Delta\phi)^2}$.

[1] In the MSSM, baryon and lepton number are no longer conserved by all of the renormalizable couplings in the theory. Since these number's conservation has been tested very precisely, these couplings need to be very small in order not to be in conflict with experimental data. R-parity is a symmetry acting on the MSSM fields that forbids such couplings. All Standard Model particles have R-parity of 1 while supersymmetric particles have R-parity -1. If R-parity is preserved, the lightest supersymmetric particle (LSP) can not decay.

[2] In hadron collider physics, the rapidity is preferred over the polar angle θ because, particle production probability is constant as a function of rapidity. Also the difference in the rapidity of two particles is independent of Lorentz boosts along the beam axis.

[3] The rapidity (y) is defined as: $y = \frac{1}{2}\ln\left(\frac{E+p_L}{E-p_L}\right)$ where p_L is the component of the momentum along the beam direction. In the relativistic limit, pseudorapidity (η) is numerically close to rapidity.

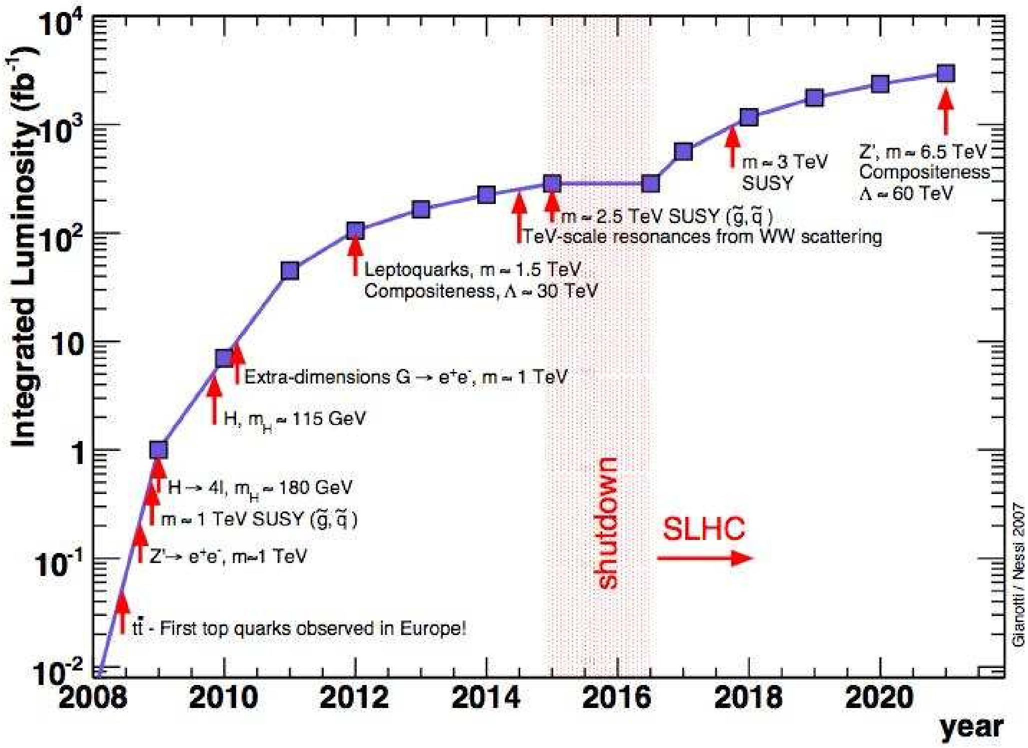

Figure 2.2: Overall View of timescale for LHC discoveries

2.2.2.2 Detector Requirements

The LHC experimental environment poses severe requirements on detectors in terms of speed (to avoid integrating over too many bunch crossings), granularity (to avoid that the same detector element is traversed by particles from different interactions) and radiation hardness (the high flux of particles induces radiation damage).

At the same time, given the large statistics available, the precision measurements will be dominated by systematic effects, thus calling for a very good control of the detector performance.

Therefore the main design criteria of the detector include the following:

- Very good electromagnetic calorimetry for electron and photon identification and measurements is needed, in addition to full-coverage hadronic calorimetry for accurate jet and missing transverse energy measurements.
- Good charged-particle momentum resolution and reconstruction efficiency in the inner tracker are essential. Furthermore, for offline tagging of τ-leptons and b-jets, vertex detectors close to the interaction region are required to observe secondary vertices.
- High-precision muon momentum measurements over a wide range of momenta are desired, together with the capability to guarantee accurate measurements at the highest luminosity using the external muon spectrometer alone.
- Large acceptance in pseudorapidity (η) with full azimuthal angle (ϕ) coverage is required for good measurement of $\not{E}_T$.

- Triggering and measurements of particles at low-p_T thresholds, is essential for providing high efficiencies and sufficient background rejection for most physics processes of interest.

2.2.2.3 Detector Layout

ATLAS follows the typical layout of a collider physics spectrometer.

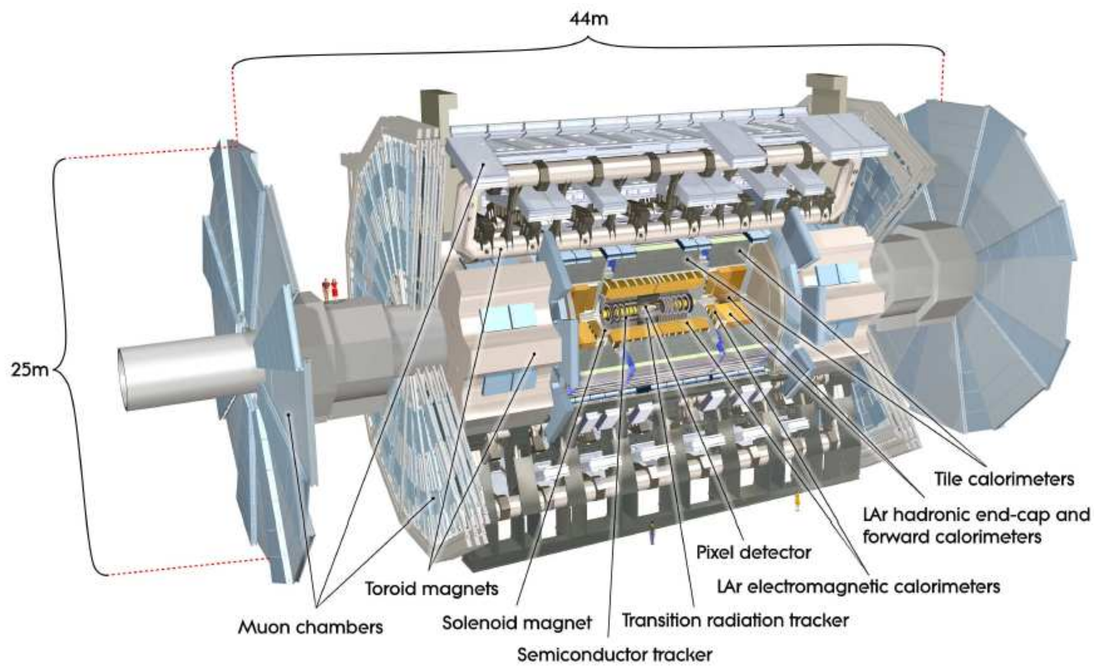

Figure 2.3: Cut-away view of the ATLAS detector.

The magnet configuration is based on an inner thin superconducting solenoid surrounding the inner detector cavity, and large superconducting air-core toroids consisting of independent coils arranged with an eight-fold azimuthal symmetry outside the calorimeters.

Proceeding outwards from the beam, the following subdetectors are found:

- The Inner Detector (ID) is contained in a 2 T solenoidal magnetic field and covers up to $|\eta| < 2.5$. Pattern recognition, momentum and vertex measurements, and electron identification are achieved with a combination of discrete high-resolution semiconductor pixel and strip detectors in the inner part of the tracking volume, and continuous straw-tube tracking detectors with the capability to generate and detect transition radiation in its outer part.

- Highly granular liquid-argon (LAr) electromagnetic (EM) sampling calorimeters, with excellent performance in terms of energy and position resolution, cover the pseudorapidity range $|\eta| < 3.2$. In the end-caps, the LAr technology is also used for the hadronic calorimeters (HAD), which share the cryostats with the EM end-caps. The same cryostats also house the special LAr forward calorimeters which extend the pseudorapidity coverage up to $|\eta| = 4.9$. The bulk of the hadronic calorimetry is provided by scintillator-tile calorimeter (tile), which is separated into a large barrel and two smaller extended barrel cylinders, one on each side of the barrel. The overall calorimeter system provides a very good jet and $\not\!\!E_T$ performance of the detector.

- The calorimeter is surrounded by the muon spectrometer. The air-core toroid system, with a long barrel and two inserted end-cap magnets, generates a large magnetic field volume with strong bending power within a light and open structure. Multiple-scattering effects are thereby minimized, and excellent muon momentum resolution is achieved with three layers of high-precision tracking chambers. The muon instrumentation also includes, as a key component, trigger chambers with a very fast time response.

The ATLAS detector (figure 2.3) is 44 m long and the overall weight is about 7000 Tons. It is the largest volume particle detector ever constructed.

2.2.2.4 Calorimeter Description

As in later sections discussion will be centered on the calorimetric part of the Trigger, it is worth briefly describing its structure here in some more detail. A more extensive description can be found in [3].

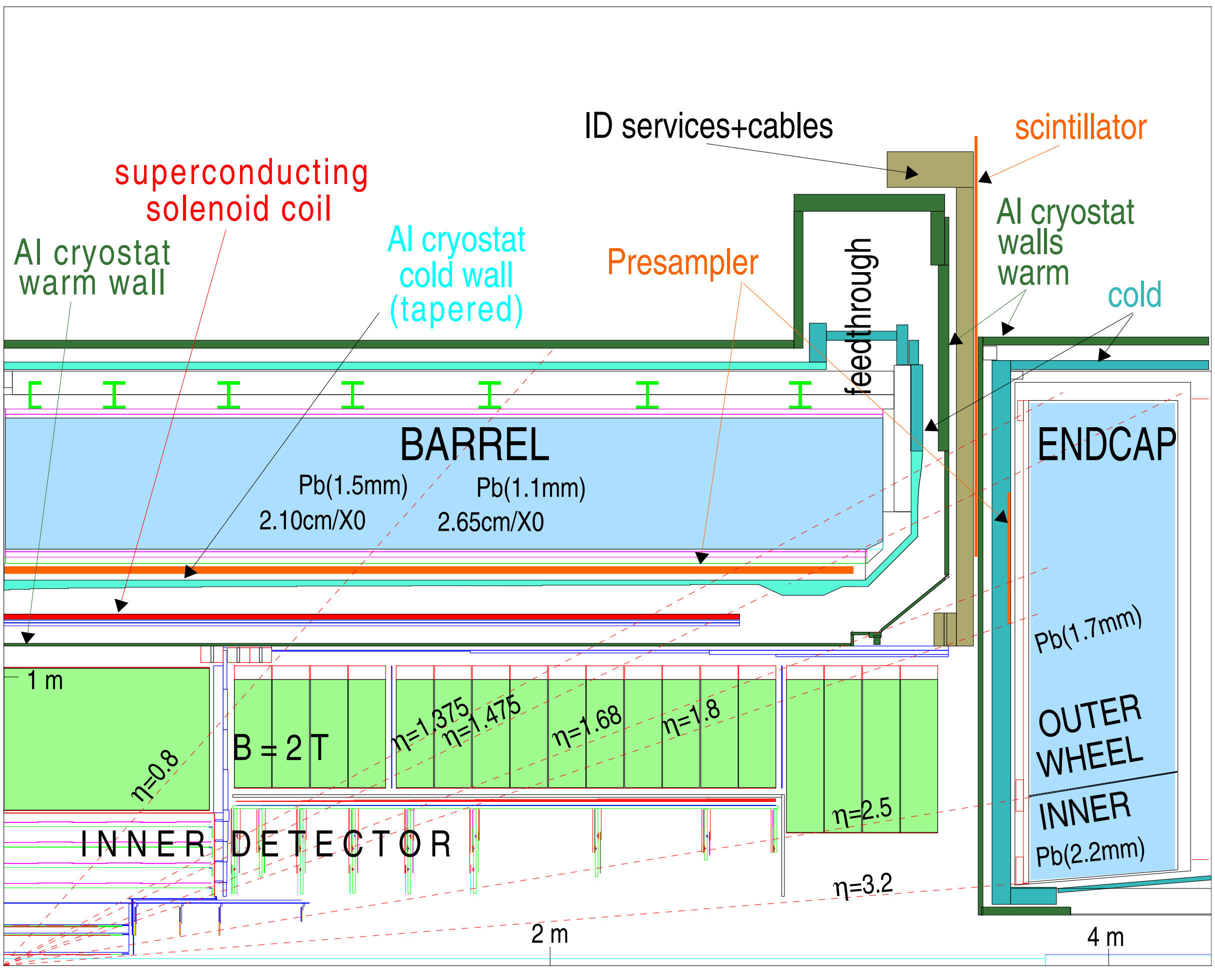

Figure 2.4: Longitudinal view of a quadrant of the ATLAS EM Calorimeter.

Over the region matched to the inner detector $|\eta| < 2.5$, the fine granularity of the EM calorimeter is ideally suited for precision measurements of electrons and photons. The coarser granularity of the rest of the calorimeter is sufficient to satisfy the physics requirements for jet reconstruction and $\not\!\!E_T$ measurements.

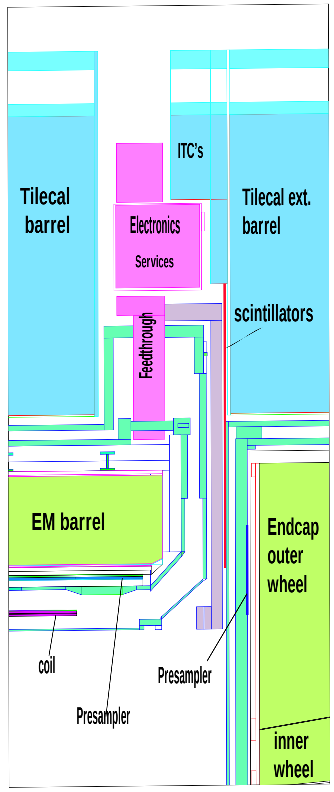

Figure 2.5: Longitudinal view of a quadrant of the vertical gap between the barrel and the extended barrel Hadronic Tile Calorimeters.

Calorimeters must provide good containment for electromagnetic and hadronic showers, consequently the thickness of the EM calorimeter is already ~ 24 radiation lengths (X_0).

The electromagnetic calorimeter in its most central ($\eta = 0$) region is divided into 4 samplings:

- Pre-sampler (sampling 0): is located just after the coil and it is used to correct for the energy lost by electrons and photons upstream of the calorimeter.
- Strips (First sampling): very high granularity in the η direction ($\Delta\eta \times \Delta\phi = 0.003 \times 0.1$) and constant thickness as a function of η (radiation length $\sim 6X_0$) allows this section to act as a "preshower" detector, enhancing particle identification (γ/π^0, $e^{\pm}/\pi^{\pm}$ separation, etc.) and providing a precise position measurement in η.
- Middle (Second sampling): segmented into square $\Delta\eta \times \Delta\phi = 0.025 \times 0.025$ towers, the middle layer accounts for the bulk thickness of the EM calorimeter (total thickness up to the end of this layer is $\sim 24X_0$).
- Third sampling: the back layer is designed to have coarser η granularity ($\Delta\eta \times \Delta\phi = 0.05 \times 0.025$) and has a non uniform thickness (from 2 to $12X_0$).

Instead the hadronic calorimeter in the central region (tile calorimeter) consists only of 3 samplings: the first two with a granularity of $\Delta\eta \times \Delta\phi = 0.1 \times 0.1$ and the last one of $\Delta\eta \times \Delta\phi =$

0.2×0.1.

Due to technical reasons there are regions in η with large amount of dead material. This is the case for the transition region between the barrel and the end-caps in the EM calorimeter, located at $1.37 < \eta < 1.52$. It is also the case for the 68 cm vertical gap between the barrel ($\eta < 1.0$) and the extended barrel ($0.8 < \eta < 1.7$) in the tile calorimeter. This gap provides space for cables from the ID, feedthrough and service pipes, as well as front-end electronics for the EM calorimeter. Another discontinuity in the EM calorimeter is the change of the lead thickness in the absorber plates at $\eta = 0.8$. Furthermore, the EM calorimeter barrel is divided into two identical half-barrels leaving a small vertical gap of 6 mm at $z = 0$. These are some of the main discontinuities in the calorimeter and in the material in front of it, which cause non-constant η response of the detector. They need to be kept in mind when analyzing η distributions in the following chapters.

A longitudinal view of the EM calorimeter is shown in figure 2.4, and a similar view of the vertical gap between the barrel and the extended barrel in the HAD calorimeter is presented in figure 2.5.

2.3 ATLAS Trigger

2.3.1 Physics Challenge

The formidable LHC luminosity and resulting interaction rate are needed because of the small cross-sections expected for many of the interesting physics processes detailed in previous section 2.2.1. However, the LHC's total inelastic cross-section of 80 mb implies that every hard scattering (candidate event for interesting physics) will on average be accompanied by 23 softer inelastic events.

Cross sections for the most frequent processes at $p-p$ (or $p-\bar{p}$) colliders are plotted as a function of the center of mass energy in figure 2.6.

Production of jets coming from QCD interactions [4] dominate over the rare processes mentioned above. Interesting events such as production of top quark are a factor of 10^3 less frequent than QCD jet production. This factor is even smaller (about $5 \cdot 10^4$) for light SM Higgs production.

2.3.2 Trigger description

The proton-proton interaction rate at the design luminosity is approximately 1 GHz, while the event data recording, based on technology and resource limitations, is limited to about 200 Hz (assuming an event size of ≈ 1.5 MB).

Hence the trigger and data acquisition (T/DAQ) system must work in this challenging environment trying to identify and accept interesting physics events while reducing by a factor of $5 \cdot 10^6$ the overall data rate.

To achieve this, ATLAS has designed a three-level trigger system.

In the following sections the ATLAS Trigger is described. Both the division into the 3 levels and into vertical "*slices*" are explained.

2.3.2.1 Level description

The entire ATLAS trigger system is organized in three levels.

[4] Quarks and gluons inside the protons can undergo hard interactions. As the partons separate from the interaction point fragmentation occur and a jet of collimated particles reaches the detector.

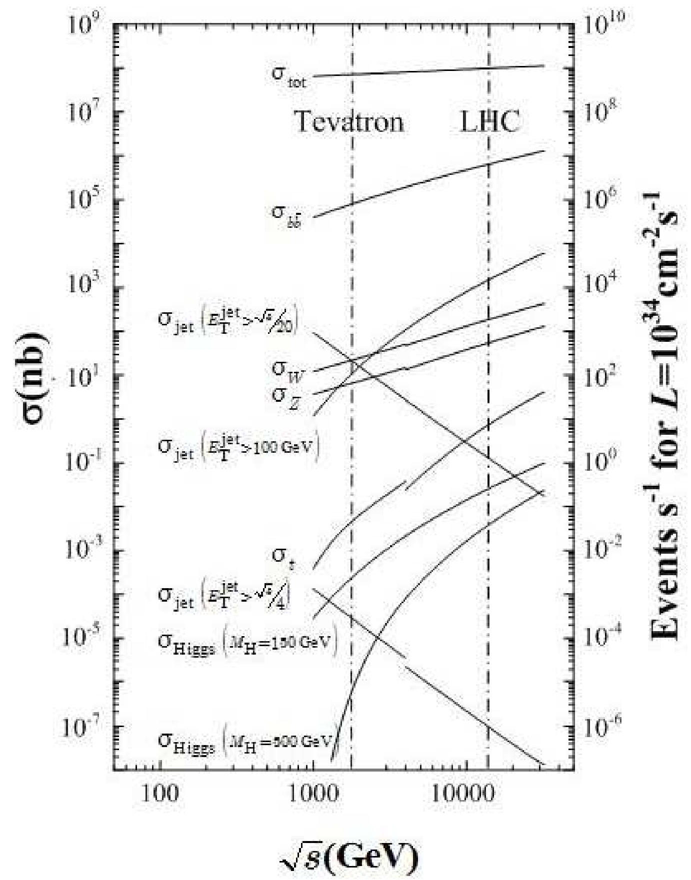

Figure 2.6: Production cross-section as a function of the center of mass energy for the most frequent physics processes at $p{-}p$ ($p{-}\bar{p}$) colliders.

The first level (L1) is designed to reduce the collision rate from 40 MHz to 75 kHz with a maximum processing time per event of 2.5 μs. It is a hardware system based on muon trigger detectors and calorimeter information with reduced granularity of roughly $\Delta\eta \times \Delta\phi = 0.1 \times 0.1$. The L1 calorimeter aims to identify high transverse energy objects (electron/photon (EM), jet/hadronic tau (HA)) as well as events with large missing E_T (XE) and total E_T (TE). Isolation for trigger objects can also be required. For each cluster of energy deposition in the calorimeter, L1 defines a “Region of Interest” (RoI) around it, which is passed to the next trigger level.

The second (L2) and third (Event Filter, EF) trigger levels constitute the so called High Level Trigger (HLT), they are software based and therefore are fully flexible and configurable, even after data taking has started. Their goal is to reduce the event rate to 3.5 kHz and 200 Hz respectively. These triggers have roughly 40 ms (L2) and 4 s (EF) per event to take a decision. L2 analyzes calorimeter and tracking data only within the RoI provided by L1 in order to speed up the execution. EF can restrict event processing to the RoIs passed by L2 as well as refine the calculation of overall event variables like missing transverse energy. Fast reconstruction algorithms are used at L2, while the actual offline reconstruction algorithms can be used at EF as the available time is larger. EF also benefits from more detailed calibration and alignment than L2. The HLT triggers are able to perform a more refined event reconstruction and even add topological requirements such as mass cuts and b-tagging.

More details on differences between trigger levels specific to tau Trigger are given in section 3.2.

2.3.2.2 Menus, chains and signatures

The trigger [4] is divided into vertically integrated "chains" (*Slices*) of inclusive, high E_T objects. Each slice has the goal of identifying a different particle or signature.

The full trigger menu contains electron (e), photon (g), muon (mu), tau (tau), jet (j), b-jet (b), missing energy (xe), total energy (te), jet energy (je) and B-physics triggers, in single, multiple and combined triggers with various thresholds each. The b-jet, missing energy and total energy triggers will require a good understanding of the detector, and hence will not be reliable for the first data taking.

The trigger software supports prescale[5] (PS) and pass-through[6] (PT) triggers. Prescales will be used to control the rates of triggers which will vary with the luminosity[7] and beam conditions. Both prescale and pass-through are also used to record lower thresholds and rejected events [8] at each level of the trigger. This is essential for commissioning, debugging and efficiency calculations.

Each trigger has associated a generic name, with a corresponding LVL1 item, LVL2 chain and EF chain.

The L1 selection strategy is depicted in figure 2.7. Trigger objects are built, and multiplicities are checked. A satisfied requirement that also survives the prescaling results in a L1 accept.

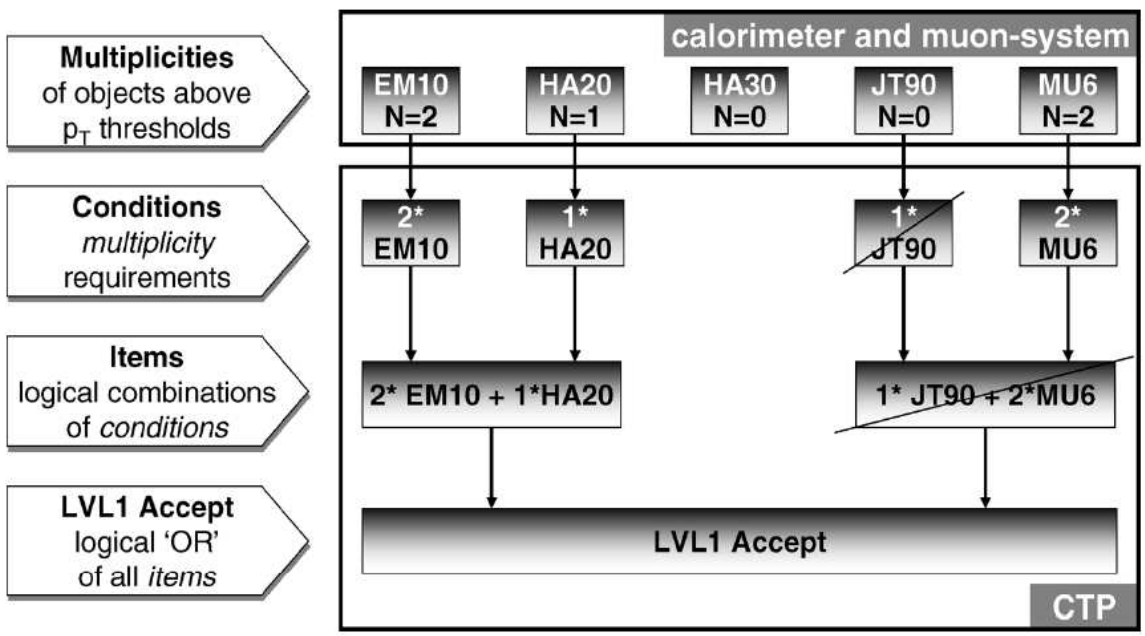

Figure 2.7: Level 1 trigger selection strategy. Trigger objects are built by the muon-system and calorimeter trigger hardware. Their numbers are counted and the multiplicities are checked against the requirements of the trigger item. A satisfied requirement that also survives the prescaling issues a LVL1 accept. The complete collection of trigger items form the LVL1 part of the trigger menu.

A HLT chain [5] is an ordered list of trigger *signatures* that are evaluated sequentially. Each step (trigger signature) represents one or more *algorithms*, and is specified in terms of *Trigger*

[5]When only a fraction of the accepted events are recorded.

[6]When the event is recorded independently of the HLT decision.

[7]L1 prescales can be changed during a run at a luminosity block boundary, while L2 and EF prescales must be configured before the run begins.

[8]By using prescale and pass-through, debug information is available for rejected events too.

Elements (TEs). TEs are abstract objects which represent the state of the reconstruction. *Sequences* define how a given TE is transformed to one or more output TEs via one or more algorithms. These concepts are illustrated in figure 2.8.

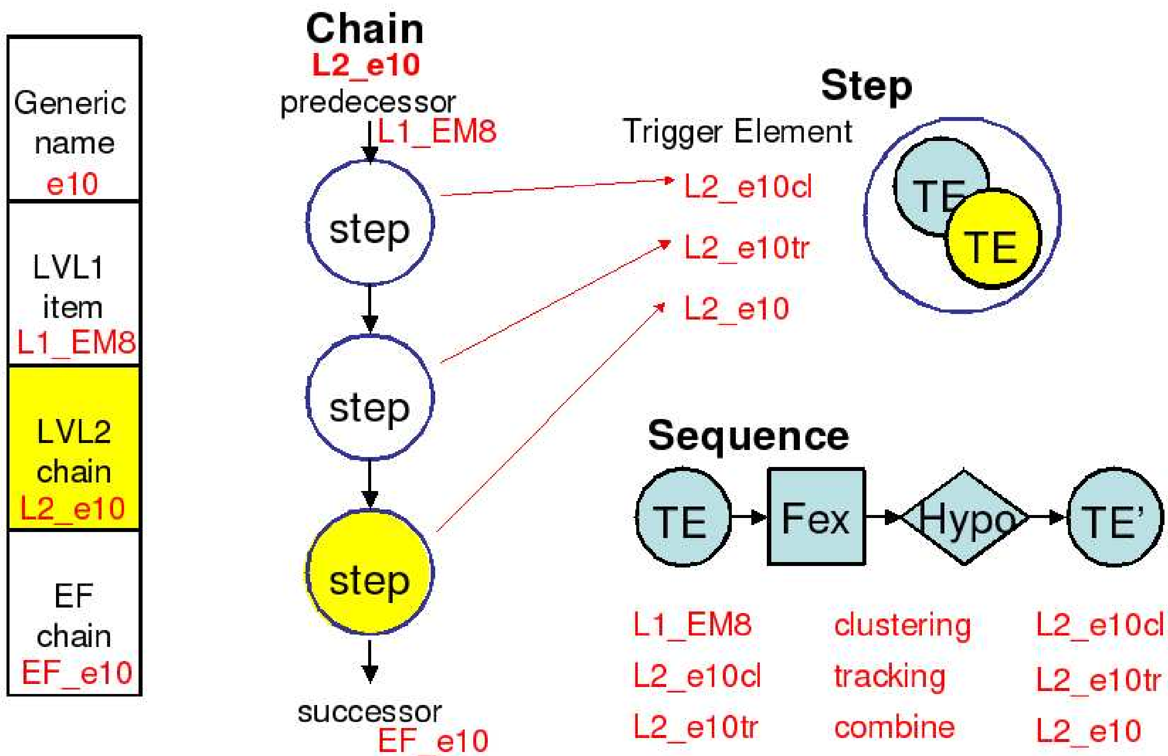

Figure 2.8: Illustration of the main configuration concepts of the HLT Steering. The labels included in this diagram are merely an example.

The chain shown is the L2 e10 chain from this trigger. The preceding chain to this is L1 EM8, and the successor is EF e10. The three steps of the L2 e10 chain are defined by the TEs. They require: L2 e10cl, L2 e10tr and L2 e10. Sequences are shown which create these TEs from the previous ones. For example, a calorimeter-clustering algorithm is configured to transform a LVL1 EM cluster (L1 EM8) to a LVL2 EM cluster (L2 e10cl).

Following the early reject trigger principle, chain execution proceeds up to the step where a signature is not satisfied, at that point the chain is deactivated for the current event. An event is registered if it is selected by at least one of these chains.

A typical sequence consists of a single input TE, a *features extraction algorithm* (FEX) that create trigger objects such as tracks or clusters , an *hypothesis algorithm* (Hypo), that validate the trigger elements based on properties of the trigger objects, and a single output TE. Other types of algorithm and more complex logic (multiple inputs and outputs) are also possible.

A caching mechanism is included to avoid unnecessary execution of sequences and algorithms. In the frequent case where the same sequence is used in more than one chain, the sequence is run on each RoI only the first time it is needed, and the results taken from the cache after that. It is also common that several sequences will be defined with the same FEX algorithm but different hypothesis algorithms (e.g. in order to apply different thresholds to the same calorimeter cluster). In this case, the FEX algorithm will only be run once for a given RoI, after which the cached results will be used.

3 Tau Trigger

3.1 Introduction

3.1.1 Tau Physics

Tau leptons [6] (and particularly their hadronic decays) will play an important role at LHC in the measurements of the electroweak bosons properties and in studies of the top quark properties. However they will play the most remarkable role by providing an excellent probe in searches for new phenomena: the SM Higgs boson at low masses, the MSSM Higgs and Supersymmetry.

Tau leptons are massive particles[1] with a measurable life-time undergoing only electroweak interactions. They couple to SUSY particles via Yukawa coupling free from QCD effects.

Due to its relatively large lifetime, the production and decay vertices of τ leptons in typical LHC collisions are well separated in space, therefore providing some potential for measurements of the polarization, spin correlations and parity of the resonances decaying to τ leptons. The excellent knowledge about their decay modes from low energy experiments make them indeed an ideal signature for the observations of New Physics.[2]

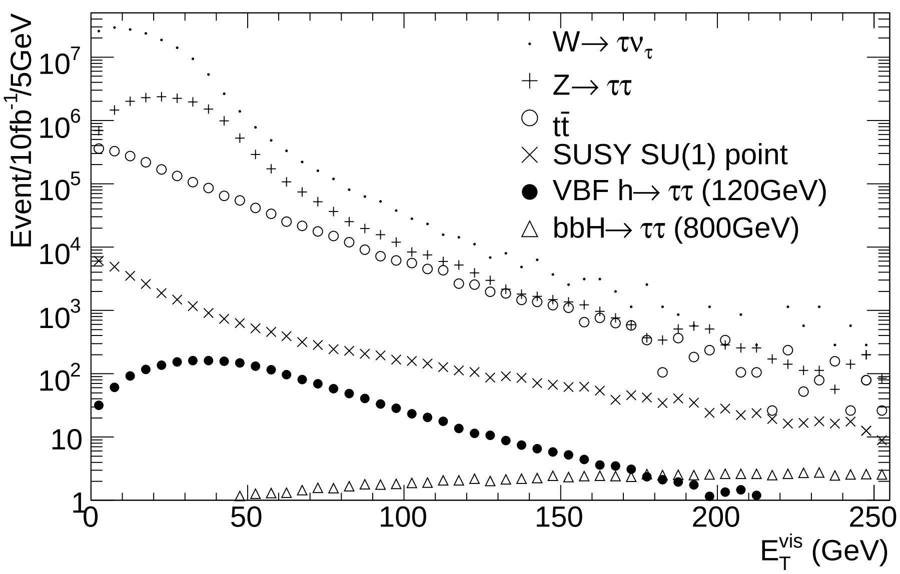

Figure 3.1: The transverse visible energy of τ leptons for different physics processes: top quark decay, W, Z, Standard Model VBF Higgs production of 120 GeV mass with $H \to \tau\tau$, also for τ leptons from low energy Supersymmetry with a light stau (SU1 sample), and heavy Higgs bosons in MSSM scenario from bbH production, with $\tan\beta = 45$ for mass 800 GeV.

The interesting transverse momentum range of τ leptons spans from below 10 GeV up to 500 GeV. Experiments at the LHC will thus have to identify τ leptons in this momentum range. The low energy range should be optimized for analysis related to W and Z boson observability

[1] Their mass is about 3500 times the electron's mass.

[2] $H \to \tau\tau$ is indeed the channel where the Higgs has long been searched for at the Fermilab experiments

in decays to τ leptons, Higgs boson searches and SUSY cascade decays. The higher energy range is mostly of interest for the heavy Higgs boson search in the MSSM models and for extra heavy W and Z gauge bosons. For illustration, figure 3.1 shows the transverse momentum spectrum of the visible decay products of the τ lepton from different processes of interest, normalized to the cross-section with which they will be produced at the LHC. The number of events corresponds to an integrated luminosity of 10 fb^{-1}.

3.1.2 Relevance of the Tau trigger for Tau physics

At the lowest luminosity the focus of the tau trigger will be to collect samples enriched in Standard Model physics useful for understanding the detector and the tau reconstruction software. Tau signatures in combination with missing transverse energy will be essential to collect data samples enriched in W$\rightarrow \tau\nu$ events, for understanding of tau identification. Additionally, single tau signatures of various p_T thresholds heavily prescaled will be used to collect samples for tau fake rates studies. Moving towards higher luminosities, the tau trigger will cope with the rate increase by either using higher p_T thresholds or tighter identification, or using more complex menus combining several signatures together.

At high luminosity, the tau trigger will be essential for collecting data samples for searches based on single tau final states, like MSSM $H^{\pm} \rightarrow \tau\nu$ [7], and to this purpose single high p_T tau signatures or moderate p_T tau signatures in combination with missing transverse energy or jet trigger signatures will be used.

The tau trigger will also be very important in collecting data samples for searches based on more than one tau lepton in the final state, like SM Higgs [8], MSSM Higgs [9], Z' [10] decaying into two taus, or SUSY decay chains containing tau leptons. To this purpose single tau signatures with moderate p_T thresholds in combination with other leptonic or tau or missing transverse energy signatures will be used, to increase the significance in various searches for New Physics.

3.1.3 Tau Identification

Tau Decay Topology

Tau leptons [11] decay leptonically (in electron or muon and two neutrinos) in 35% of cases. In the remaining 65% of cases they decay hadronically, mainly in one or three charged pions plus neutrals and one neutrino.

Reconstruction of τ leptons is usually understood as the reconstruction of the hadronic tau decay modes. It would be hard to distinguish leptonic modes from primary electrons and muons, and such cases are considered as a subject of isolated lepton reconstruction.

From the detection point of view hadronic modes are divided (counting number of charged pions among decay products) into single-prong (one charged π) and three-prong decays (three charged π).

Single prong taus contribute ~76% to the hadronic decays, while 3 prong taus represent only ~22.5% of them. Other hadronic decay modes of the τ are less frequent and more difficult to trigger on. Such decays include: 5 prong decays (which are hard to detect in the jet environment) and decays into K-mesons ($K^{\pm}$ decays which look like $\pi^{\pm}$ and decays into K^0_S for which the number of prongs depend on decay mode and decay point within the detector).

Thus, the τ reconstruction in ATLAS has to focus on one prong and three prong (or multi-prong) decays.

Due to the relatively low mass ($m_\tau \approx 1777$ MeV) of tau leptons, already for an energy of a few GeV the τ decay products are well collimated. Besides, tau decay vertex is separated from the interaction point since τ lifetime is relatively large ($c_\tau = 87$ μm). Therefore, other characteristics of τ hadronic decays are well collimated high momentum tracks and non-zero impact parameter.

Tau identification in the detector

Hadronic τ decays can be efficiently reconstructed and identified using information from the Calorimeter and Inner Detector. Reconstruction is done only for the visible part of the decay products, however for specific analysis like $H \to \tau\tau$ decays, usually assumption like the collinear approximation is being made (neutrino momenta parallel to the visible products momenta) and the complete invariant mass of the $\tau\tau$ system is reconstructed as well.

The reconstruction of tracks from charged π arising in τ decays is an important ingredient of the τ reconstruction algorithms. The charge of the τ candidate is determined by summing up the charge of the track system. The tracking information is further used in τ identification by considering quantities such as track multiplicity, impact parameter and quality of the fit to the secondary vertex (for multi-track candidates).

Calorimeter τ-jets are collimated low multiplicity jets with hadronic and electromagnetic energy deposits. These narrow showers have a significant pure electromagnetic component since in the case of the single-prong decays about 55% of the energy is carried by π^0s. The high calorimeter granularity allows a detailed description of the energy deposition from the shower of τ visible decay products. The radius of the EM shower together with the number of hits and the transverse energy width in the η strip layer are some of the quantities used to characterize showers from τ-jets. The granularity of the ATLAS EM calorimetry will also permit the identification of isolated subclusters from π^0 in the reconstructed hadronic τ decays [6].

Tau-jet QCD-jet Separation

Despite a strong physics motivation for exploring data with τs in the final state, τ reconstruction at hadron colliders remains a very difficult task in terms of distinguishing interesting events from backgrounds dominated by multi-jet production.

Hadronically decaying τ leptons are distinguished from QCD jets on the basis of the low track multiplicity, characteristics of the track system and shapes of the calorimetric showers. Isolation from the rest of the event is required both in the Inner Detector and the Calorimeter. From this information, a set of identification variables is built, to which either a traditional selection with cuts or multi-variate discrimination techniques are applied.

Tau Reconstruction strategies

Tau leptons are typically reconstructed by matching calorimetric clusters with tracks. The hadronic tau reconstruction efficiency is dominated by the efficiency for track reconstruction from charged $\pi^{\pm}$. An efficient and precise reconstruction of calorimetric clusters allows a confirmation of the (η, ϕ) direction obtained from the Inner Detector and a measurement of the visible energy of the τ lepton.

However, an alternative approach has been explored in order to improve identification in the low τ energy range. The idea is to measure the direction from the Inner Detector information only and to use the EM part of the calorimeter to determine the τ energy, applying an energy-flow scheme (a combination of the energy of reconstructed tracks for $\pi^{\pm}$ and energy deposition in EM presampler+strips+middle layers for π^0). The E-flow algorithm [12] takes advantage of the two main features specific to showers from the hadronic τ decays: the significantly higher energies of the reconstructed track(s) and the absence of neutral hadronic energy. Roughly speaking, the E-flow algorithm estimates the τ energy by measuring the neutral component with the EM calorimeter and uses the precisely measured track momentum instead of the HAD calorimeter to estimate the charged component of the energy.

3.1.4 Tau Offline reconstruction

Presently, in ATLAS tau offline reconstruction software, two complementary algorithms are implemented [6]: the first one relies on calorimeter-based (calo-based) seeds for reconstructing hadronic τ decays, whereas the second algorithm relies on track-based seeds and an energy-flow approach.

3.1.4.1 Calo-based algorithm

The calo-based algorithm (*tauRec*) starts from the reconstructed cluster in the hadronic and electromagnetic calorimeter and then builds identification variables based on information from the tracker and calorimeter.

These clusters are provided by a sliding window cluster algorithm, which runs on *CaloTowers*. CaloTowers are the sum of all calorimeter layers on a grid of $\Delta\eta \times \Delta\phi = 0.1 \times 2\pi/64$. The algorithm returns a cluster which corresponds to $\Delta\eta \times \Delta\phi \sim 1.0 \times 1.0$. On that basis, energy and position are calculated. Only clusters with $E_T > 15\ GeV$ are considered.

In the near future, τ-jet reconstruction from topological clustering [13] (*Topoclusters*), instead of sliding-window clustering *Caloclusters* will be possible. Topoclusters, based on topological association of cells, discriminate better between true low energy deposits and electronic noise. They have better energy resolution and therefore the background discrimination improves. Figure 3.2 shows these improvements for the reconstruction efficiency as a function of the true visible p_T of the τ lepton. In particular, the improvement at low p_T is clearly visible.

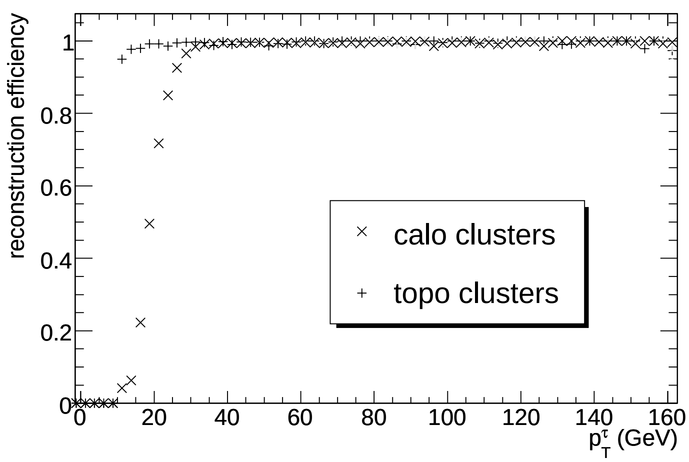

Figure 3.2: Reconstruction efficiency as a function of the τ visible p_T for sliding-window (calo-clusters) and topological (topo-clusters) algorithms.

To calculate the quantities involved in τ identification the full granularity of the calorimeters is used. All cells within $\Delta R < 0.4$ around the barycenter of the cluster are calibrated with an H1-style calibration [14], with a fudge factor applied to correct the overall τ-scale with respect to the jet scale.

The calibration aims to correct various effects which degrade the measurement of the jet energy in the calorimeter, namely: detector driven effects (noise, non-compensation, cracks, dead-material, magnetic field effects, pile-up) and physics driven effects (underlying event, showering effects, clustering). Cell-weights are functions of the cell-energy density, η, and the calorimeter region and they are obtained by optimizing the jet resolution in QCD jet samples. For τ leptons the same H1-style cell weights are used as for jets, while the fudge factor, function of E_T , η and the number of tracks, is obtained by comparing the reconstructed E_T after applying the H1 weights and the E_T of the true hadronic τ.

The addition of electronic noise in the calorimeter cells causes a change for calorimeter variables which is generally small, except for the R_{em} for τ-jets at low E_T . Only cells with energy $> 2\sigma(noise)$ are used to build the τ-Id quantities in this case.

The rejection power with respect to QCD jets comes almost entirely from the identification procedure. The calo-based algorithm currently uses a multi-variate method for τ identification. A likelihood function is built as a one dimensional likelihood ratio based on 8 variables:

- three discrete variables: Number of tracks in the cluster core ($\Delta R < 0.3$), number of hits in the η strip layer, and total charge of the associated tracks.
- and five continuous variables: EM radius, isolation in the calorimeter, transverse energy width in the η strip layer, lifetime signed pseudo impact parameter significance, and E_T over p_T of the leading track

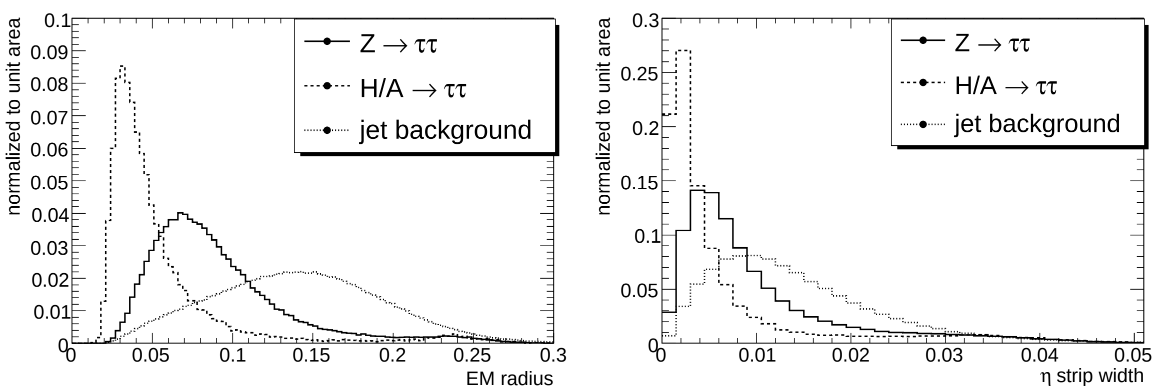

Figure 3.3: Electromagnetic radius (left) and shower width in the η strip layer (right) for τ and non τ showers.

Although it is well known that there are important correlations between the different variables, these are neglected by this approach, since the available statistics was not sufficient to make use of two dimensional PDFs. The distributions of the likelihood value for τ-jets and QCD-jets is given in figure 3.4 (left).

Despite the use of E_T bins the LLH shows a residual E_T dependence. Therefore a fixed cut on the LLH value neither will result in a generally flat efficiency, nor will it be optimal. [15] The fixed cut on the LLH value will also introduce a strong bias towards suppressing three-prong with respect to single-prong taus (see figure 3.4-right).

A rejection of 100-10000 depending on the energy range and required efficiency is obtained with this method.

3.1.4.2 Track-based algorithm

The track-based algorithm (*tau1p3p*), is optimized for low p_T taus with transverse momenta of 10-50 GeV and it is seeded by good quality tracks (one of them with transverse momentum above 9 GeV).

This algorithm clearly separates *reconstruction* and *identification* steps:

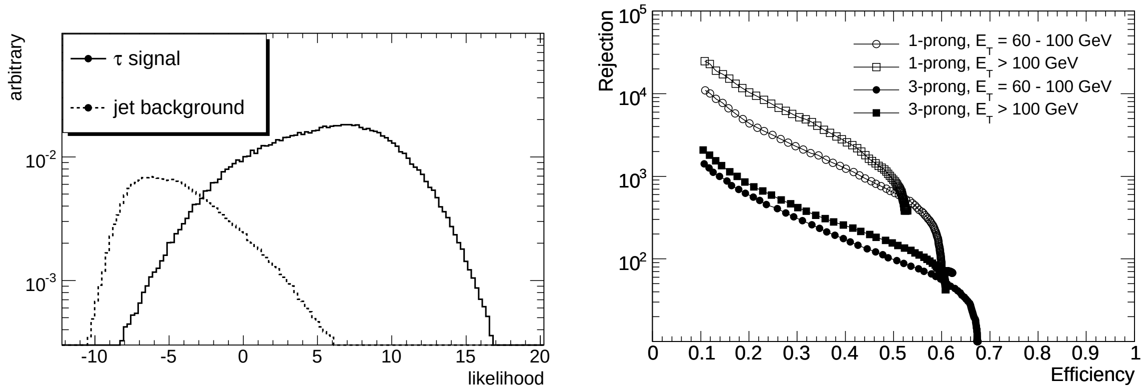

Figure 3.4: Left: The Likelihood (LLH) distribution for τ-jets (solid) and QCD-jets (dashed). Candidates with a LLH < -10 had variables outside the boundaries of histograms used when obtaining the PDFs. The LLH is applied after a preselection of $1 \leq N_{Tr} \leq 3$. Right: Expected performance for calo-based algorithm with likelihood selection. The rejection against Monte-Calo truth jets as a function of efficiency for hadronic τ-decays for various ranges of the visible transverse energy is shown. Used CSC production with 12.0.6 processing. For signal events $Z \to \tau\tau$ and $bbH, H \to \tau\tau$ with mH=800 GeV were used, for QCD background the dijet-samples.

- Reconstruction
  - Identify and qualify a leading hadronic track which becomes a seed for building the candidate;
  - Create candidates with up to 3 tracks in a core region (at most 3 good quality tracks); define (η, ϕ) position and the energy of the candidate; check charge consistency for three-prong candidates;
- Identification
  - Calculate calorimetric and tracking quantities;
  - Calculate *cut based*, *NN based* and *PDRS based* discriminants.

Requiring that the leading track has $p_T^{\pi\pm} > 9$ GeV reduces the physics efficiency for observing hadronic τ in low p_T range, the advantage being the strong rejection power against QCD background already at the reconstruction step. Lowering the base-line threshold to 6 GeV would increase the fraction of τs passing the threshold from 63% to 81% for $W \to \tau\nu$ and from 70% to 82% for $Z \to \tau\tau$ events, but it might require much more stringent selection to reject background candidates at the identification step.

For a single-prong mode, exactly one qualified track with no nearby tracks in the core ($\Delta R =$ 0.2) region is required. For multi-prong modes, exactly two or three nearby tracks are required; figure 3.5 shows the efficiency for reconstructing `tau1p3p` candidates as a function of the visible τ energy. For the single-prong mode, the reconstruction efficiency is of order of 80%, following the efficiency for the track reconstruction. Including two-track candidates allows to recover the reconstruction efficiency for three-prong decays from 50% to 80% for $E_T^{visible} = 20$ GeV (similar as for the single-prong ones) but introduces about 10 times more background.

The energy scale of the τ candidate is defined using an *energy flow* algorithm, as described in section 3.1.3. The advantage from using the above approach comes from the fact that it significantly underestimates the nominal energy of the fake candidates from jets, since a cone of $\Delta R = 0.2$ is too narrow to collect efficiently the energy of a QCD jet and since the neutral

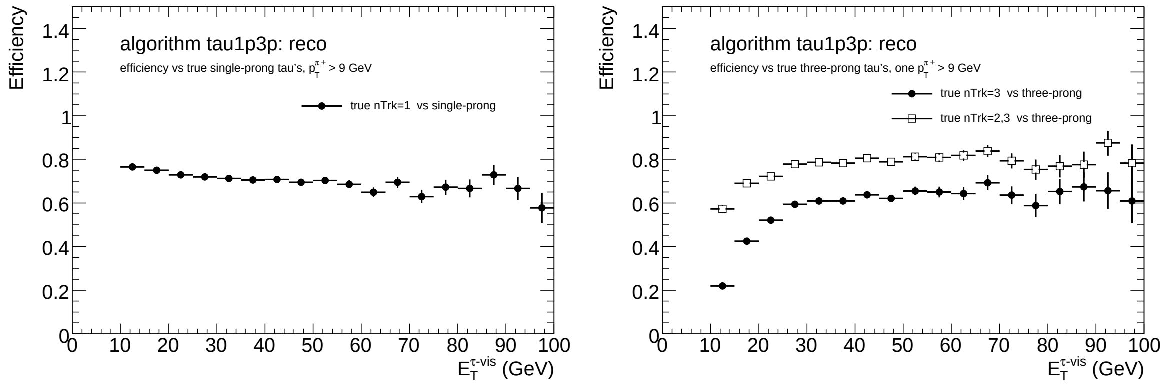

Figure 3.5: Efficiency for reconstructing the tau1p3p candidates as a function of the visible τ transverse energy for single prong candidates (left) and three prong candidates (right). The efficiency is normalized to τ s with the leading charged $\pi^{\pm}$ $p_T > 9$ GeV. Signal events from $W \to \tau\nu$ sample are used.

hadronic component is largely omitted in the energy definition itself. This energy estimate leads to lower background compared to the calibrated calorimetric clusters used by the calo-based algorithm (section 3.1.4.1).

For three-prong τ decays reconstructed as the two track candidates the energy reconstruction does not work well. The momentum carried by the lost track is missing from the energy balance, as in most cases no energy is deposited in the EM calorimetry and/or is taken only at the EM scale.

In the track-based algorithm, calorimetric and tracking identification quantities are calculated from cells/tracks in a distance from a seed of $\Delta R = 0.2$. The isolation criteria are checked in the isolation cone $\Delta R = 0.2 - 0.4$. Some of the variables used are specific of multi-prong decays.

- Tracking quantities: Number of tracks in the isolation cone, width of tracks weighted with their transverse momenta (only for two and three-track candidates), and invariant mass of the tracks system (only for two and three-track candidates).

- Calorimetric quantities: EM radius, number of strips with energy deposition, width of the energy deposition in strips, fraction of the transverse energy deposited in the $0.1 < \Delta R < 0.2$ radius with respect to the total energy, and energy (at the EM scale) deposited in the *isolation* region in the electromagnetic and hadronic calorimeter.

- Tracking+calorimetric quantities: Invariant visible mass of the candidate, energy in the EM calorimeter (at the EM scale) deposited in the *isolation* region with respect to that in the *core* region, energy in the HAD calorimeter (at the EM scale) deposited in the *core* region with respect to the sum of the tracks transverse momenta.

Figure 3.6 shows some of these variables distributions for taus and fake-taus.

A rejection factor of 10-100 is achieved against QCD jets at the reconstruction stage. A further identification procedure explores tracking and calorimetric quantities on which basic *cut* methods and multi-variate analysis [6] (sliding-cuts, artificial neural network (NN) and range-search probability density (PDRS)) are applied, bringing an additional rejection of 5-100.

One of the criteria for the optimization was to arrive at a well balanced efficiency/rejection performance between the single-prong and the three-prong decays, not to bias the characteristic

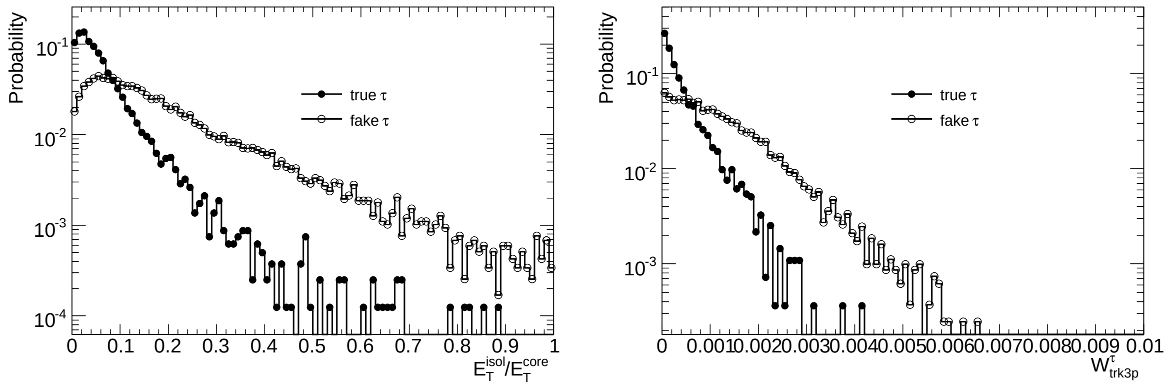

Figure 3.6: Distribution of some of the quantities used for identification selection for τ decays: E_T^{isol}/E_T^{core} for single prong decays (left) and width of tracks for three-prong decays (right). True τ signal candidates from $W \to \tau\nu$ sample with charged $\pi^{\pm} > 9$ GeV are shown. For background events used candidates reconstructed from QCD dijet process with $p_T^{hard} = 17 - 35$ GeV.

spectrum on N_{trk} for signal events. The rejection of this algorithm is illustrated in figure 3.7 as a function of the energy.

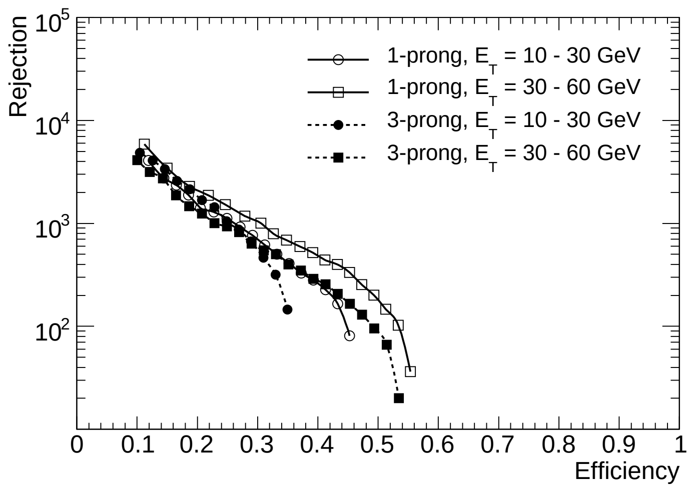

Figure 3.7: Expected performance for track-based algorithm with NN selection likelihood selection. The rejection against Monte-Calo truth jets as a function of efficiency for hadronic τ-decays for various ranges of the visible transverse energy is shown. Used CSC production with 13.0.30 processing. For signal events $Z \to \tau\tau$ and $bbH, H \to \tau\tau$ with mH=800 GeV were used, for QCD background the dijet samples.

3.1.4.3 Offline algorithms overlap

It is clear that both algorithms are optimized very differently, the calo-based one favors single-prong candidates but leads to much better signal-to-background ratio . The track-based one is optimized to be equally efficient for single and three-prong candidates, and to bias as little as possible the track multiplicity spectrum for fake candidates from QCD dijet.

The track-based algorithm provides, already at the reconstruction step, considerable rejection against QCD jets with high track multiplicities. For a similar rejection against QCD events of ~ 1600, the efficiency of the calo-based algorithm is $\sim 10\%$ higher than that of the track based algorithm [6]. However, this slightly higher efficiency is obtained at the expense of a strong distortion of the multiplicity spectrum for the identified τs. In addition, the track-based algorithm permits a control of the fake τ by using track multiplicity spectrum, for track multiplicity larger than 3. Figure 3.8 shows the normalized track-multiplicity spectra for hadronic τ-candidates, with visible transverse energy above 20 GeV, from $Z \rightarrow \tau\tau$ decays and from QCD jets, respectively. The distributions are shown for both reconstruction algorithms after the reconstruction step, and after identification.

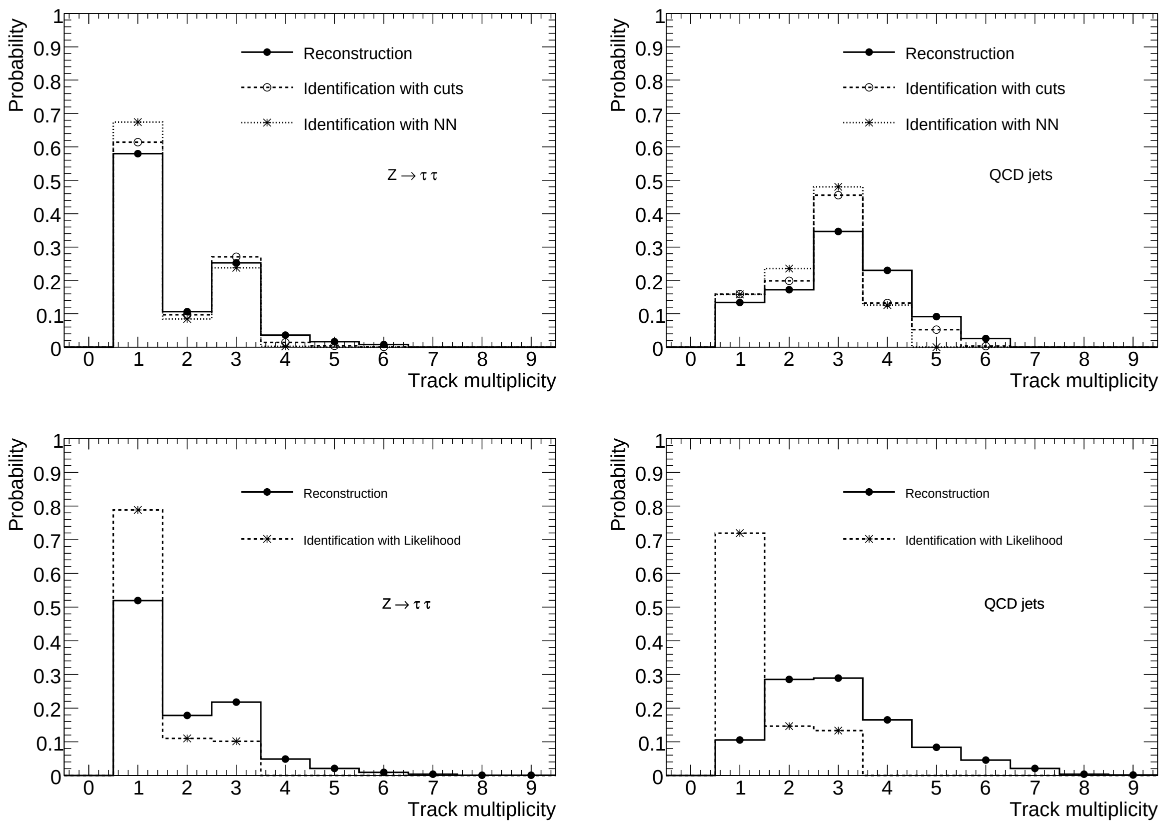

Figure 3.8: Top (Bottom): Track multiplicity distributions obtained for hadronic τ-decays with visible transverse energy above 20 GeV and below 60 GeV using the track-based (calo-based) τ-identification algorithm. The distributions are shown after reconstruction, after cut-based identification and finally after applying the neural network discrimination technique (after applying the likelihood discrimination technique) for an efficiency of 30% for the signal (left) and background (right).

Following the two offline algorithms different criteria, it is not surprising that they select somewhat different tau candidates.

This difference is quantified in table 3.1 which shows the identification efficiency of both reconstruction algorithms. Efficiency is detailed for single-prong and three-prong tau decays, as well as globally for all hadronic decays. Even if the global identification efficiency is similar for both algorithms, it has to be noticed that the fraction of overlap events (those identified by both algorithms) is quite small (about a 50%). This poses delicate questions to trigger developers, as the trigger selection has to be optimized to give the highest efficiency possible for the offline identified hadronic taus. Offline reference for trigger optimization is discussed more in depth in

Offline Identification package	all taus	1-prong	3-prong
Calo-based	31	40	10
Track-based	39	35	48
Calo- OR Track-based	53	54	51
Calo- AND Track-based	17	21	7.7

Table 3.1: Identification efficiencies in percentage for different offline references calculated on $W \to \tau\nu$ sample. Identification cuts used are likelihood>4 for tauRec and NN discriminant==1 for tau1p3p.

section 4.1.2

In figure 3.9 the E_T spectrum of taus identified by the two offline algorithms can be compared. TauRec maintains a quite flat efficiency plateau in the plotted energy range, while for tau1p3p the efficiency for high-p_T taus clearly decreases. However, for taus with p_T <20 GeV tauRec efficiency is very poor and only tau1p3p is able to reconstruct a reasonable fraction. It is important to highlight that different subsample of τs are selected by each algorithm in the reconstruction and identification steps. In addition to different optimization criteria, the most important reason for this being the different pre-selection cuts applied to τ jets: the cut on minimum leading track p_T of 9 GeV for tau1p3p at the level of reconstruction, and the low reconstruction efficiency of tauRec for p_T <20 GeV taus.

For this reason, the merging of both algorithms is under consideration. A first step towards unification will be loosening of the leading track p_T threshold to 6 GeV in tau1p3p, and the use of TopoClusters in tauRec, which perform better at low p_T .

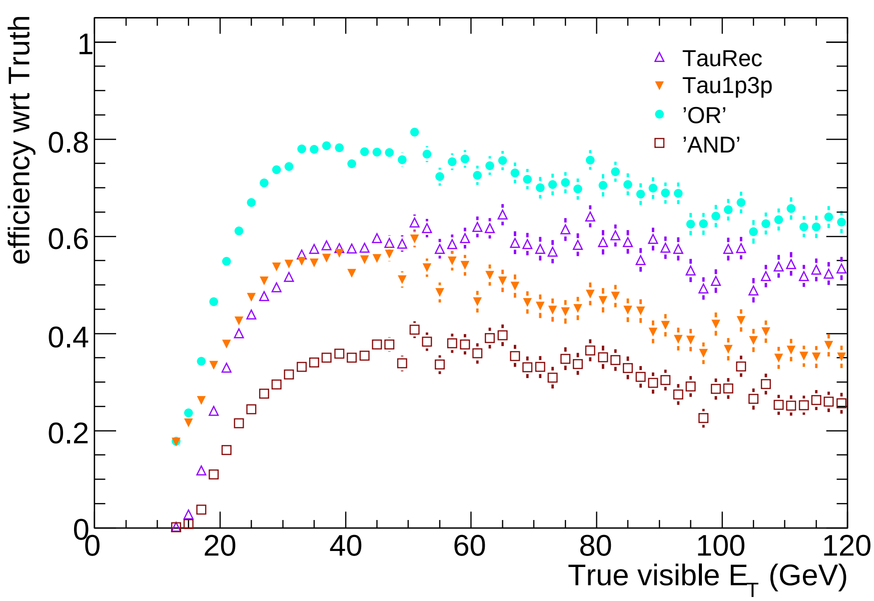

Figure 3.9: Identification efficiency for Tau Offline reconstruction algorithms. Efficiency is calculated with respect to the true taus. Likelihood>4 for tauRec and discriminant==1 for tau1p3p were used as identification cuts.

3.2 Tau Trigger Description

This section briefly presents the three tau trigger levels. A more complete description can be found in reference [16]. Selection variables are defined, and selection strategy at each level is shortly discussed.

3.2.1 Level 1

The L1 tau trigger, is a hardware trigger based on electromagnetic and hadronic calorimeter information, which uses trigger towers of about $\Delta\eta \times \Delta\phi = 0.1 \times 0.1$, with a coverage up to $|\eta| < 2.5$ (limit of inner-detector coverage and of high-granularity electromagnetic calorimetry used in further steps).

The trigger towers are formed by analogue summation of calorimeter cells, and the tower size was determined to reach a compromise between rejection of jet background and cost and complexity of the trigger processor. Note that jet triggers use $\Delta\eta \times \Delta\phi = 0.2 \times 0.2$ towers instead, as jets produce wider showers in the calorimeters. Trigger tower words are 8 bits with, nominally, 1 GeV of transverse energy (E_T) per count, which means that the towers saturate above 255 GeV. There are separate sets of trigger towers from the electromagnetic and hadronic calorimeters, among other reasons because the calorimeter response to electromagnetic and hadronic showers is not equal.

A 2×2 tower electromagnetic (EM) cluster and a 2×2 hadronic (HAD) cluster are used to identify a Region of Interest (RoI). The RoI cluster must be a local E_T maximum compared to its neighbors. Its center is defined as the center of this 2×2 tower.

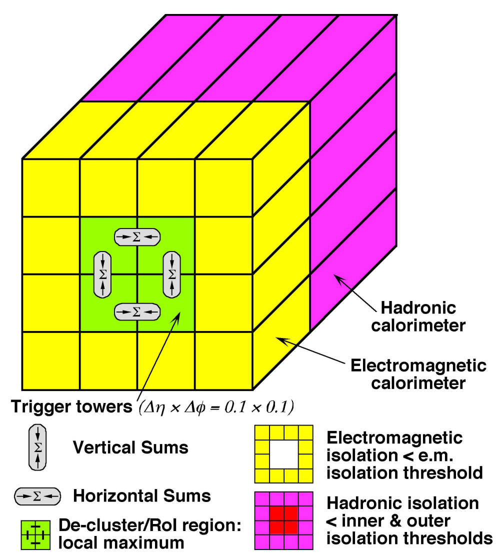

Figure 3.10: Trigger towers used in the electron/photon and tau/hadron L1 triggers.

The algorithm considers a rectangular window of 4×4 towers (0.4×0.4 in $\Delta\eta \times \Delta\phi$) in both the EM and hadronic calorimeters, and makes use of different elements, each formed by summing E_T over a group of towers (figure 3.10). The algorithm uses the following selection quantities:

- **TauCluster** is the energy contained in the two most energetic neighboring central towers in the EM calorimeter plus the central 2×2 towers of the hadronic calorimeter.

- **EmIsol** is the energy in the EM isolation ring (region between 2×2 and 4×4 towers in the EM calorimeter).
- **HadIsol** is the energy in the hadronic isolation ring (region between 2×2 and 4×4 towers in the hadronic calorimeter).

Conditions on this variables are to be satisfied for the L1 cluster to be accepted as a L1 tau trigger candidate. Particularly TauCluster must be greater than a given threshold, while energy in the isolation ring (EmIsol, HadIsol) must not exceed a given energy threshold.

Energy calibration procedure is the same as for jet calibration: adjusting the overall gains of the towers to provide a uniform jet response in η.

For the electron/photon and tau/hadron cluster triggers there are a total of sixteen trigger E_T thresholds available. Eight of the thresholds are dedicated to the EM cluster trigger, and the other eight thresholds are individually programmable to be either an EM cluster trigger or hadronic cluster trigger. Therefore, a maximum of eight trigger thresholds are available at L1 for taus. Each threshold being a combination of E_T thresholds for TauCluster, EmIsol and HadIsol[3].

3.2.2 Level 2

At the second level trigger, tracking and calorimeter information are available with full granularity and the allowed average time per event is about 40 ms.

This allows L2 to improve the energy resolution and to define a refined tau candidate exploiting more of the characteristics of a hadronic tau decay, (such as collimation and low track multiplicity) to further reject the QCD jet backgrounds by an additional factor of 5-10.

Tau trigger consists of 3 sequences: calorimeter-based selection (*L2Calo*), tracking-based selection (*L2ID*), and the final matching of the two, which only requires a calorimeter and tracking object to match within a certain ΔR. L2Calo is seeded by a region of interest (RoI) determined by the L1 signature. Seed position is refined an passed to the L2ID. The final seed position given to the EF is a combination of both Calo and tracking directions.

3.2.2.1 Level 2 Calorimeter

This stage of the tau trigger makes use of calorimeter shape variables and the cluster energy to enrich the sample of tau candidates. Shape variables are calculated using only the second electromagnetic sampling layer while the cluster energy is calculated with all available EM and hadronic layers. Three different rectangular window sizes are defined, centered on a *seed* cluster, with areas of $\Delta\eta \times \Delta\phi = 0.1 \times 0.1$ (narrow, *Nar*), 0.2×0.2 (wide, *Wid*), and 0.3×0.3 (normal, *Nor*).[4]

The algorithm consists of several steps: First of all, the *seed* of the cluster is found by refining the L1 RoI position using the second EM sampling. The algorithm unpacks cells in the *Nor* region around the L1 RoI position, and finds the cell with the highest energy deposition. In a *Wid* region around the most energetic cell, the cluster position (*seed*) is defined as the energy weighted mean position of the cells in this window. Then, shape variables are reconstructed, using different window sizes around the seed. At the same time, the total energy in all calorimeter samplings is computed. Finally, the total energy is corrected with a simple sampling calibration.[5]

[3] In the present menus the hadronic isolation variable is not used for selection (see section 4.2).

[4] The RoI window size is currently subject of optimization studies which are detailed in section 4.4

[5] More details on calibration are given in section 3.2.2.2 and 4.5.1

At L2 shape variables are calculated in the second sampling of the EM calorimeter contrarily to EF and offline, where all EM samplings are used. Historically, time consumption of the algorithm was dominated by the data unpacking time (data access and preparation), and this was done as a provision for possible speed-up of the algorithm. Now the unpacking strategy has improved [17], but the same approach is kept for simplicity, since it has been checked that using all EM samplings does not improve the rejection of the shape variables at L2.

In the trigger algorithm, no noise suppression is applied when selecting cells[6], contrarily to the offline.

The rejection variables used by the L2 Calorimeter are the following:

- **EMRadius** is the energy weighted squared radius of the cluster, calculated in a *Nor* region around the *seed*, in the second sampling of the EM calorimeter[7] .

$$EMRadius = \frac{\sum\limits_{Nor} E_{cell} \cdot R^2_{cell}}{\sum\limits_{Nor} E_{cell}} \tag{3.1}$$

- **IsoFrac**[8] is the difference in energy between the *Nar* and *Wid* region, normalized to the *Wid* region. It is calculated in the second sampling of the EM calorimeter.

$$isoFrac = \frac{\sum\limits_{Wid} E_{cell} - \sum\limits_{Nar} E_{cell}}{\sum\limits_{Wid} E_{cell}} \tag{3.2}$$

- **stripWidth**[9] is the width of the energy deposition, defined as the energy weighted standard deviation in η. It is calculated in a *Nor* region around the seed, in the second sampling of the EM calorimeter.

$$stripWidth = \sqrt{\frac{\sum\limits_{Nor} \eta^2_{cell} \cdot E_{cell}}{\sum\limits_{Nor} E_{cell}} - \left[\frac{\sum\limits_{Nor} \eta_{cell} \cdot E_{cell}}{\sum\limits_{Nor} E_{cell}}\right]^2} \tag{3.3}$$

- **EtCalib** is the calibrated total transverse energy, calculated in the EM and hadronic calorimeters, in a *Nor* region around the seed.

The distributions of EMRadius, IsoFrac and stripWidth are shown in figure 3.11 using $W \rightarrow \tau\nu$ as signal and low p_T QCD dijets as background, both required to be accepted by L1 tau selection and identified by either one of the two tau offline algorithms.

[6]To suppress the electronic noise in the calorimeter cells, only cells with an energy deposition greater than two times the deviation value of the noise in that cell are considered.

[7]This variable is also used by EF and offline reconstruction algorithms, defined as the energy weighted radius calculated in all the EM samplings of the calorimeter. At L2 the squared radius is used instead, since it was proven to give slightly better rejection.

[8]This variable is used as well by EF and offline algorithms, calculated in all EM samplings.

[9]This variable is calculated by the offline algorithms using the first sampling (Strip) instead of the middle one. At the second level trigger the name of this variable is maintained for analogy.

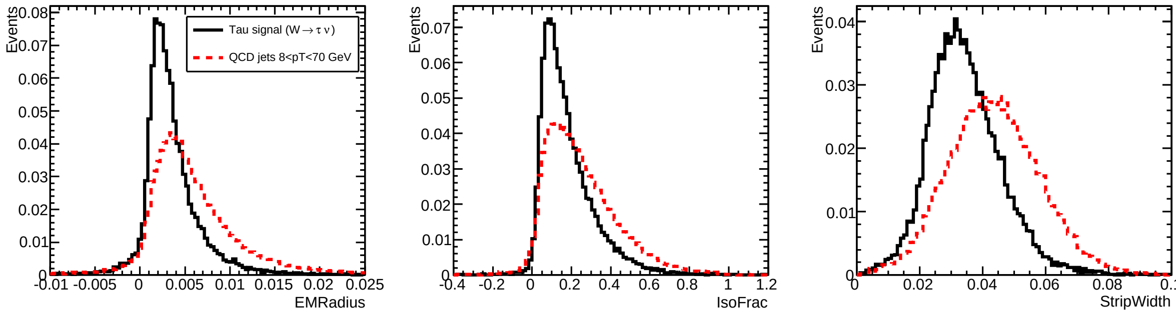

Figure 3.11: Calorimeter L2 variables to distinguish QCD background from tau leptons

3.2.2.2 L2 Calibration

A simple *Sampling* calibration is used in the L2 calorimeter algorithm for reconstruction of the tau energy. This method is fast ($\approx 7\mu s$) compared to the one used by the offline calibration [14] in which a cell by cell correction is performed. Although this calibration could apply a weight per calorimeter sampling, in the current implementation only 2 layers are considered (EM and hadronic compartments) and the weights are energy and η dependent.

More information on calibration and calibration performance can be found in section 4.5.

The performance of a new energy-flow type variable to estimate τ's E_T at L2 is under investigation. This method makes use not only of the calorimeter but also of the tracking information. As a first attempt this variable has been constructed taking the sum of the most energetic tracks plus the raw (non-calibrated) energy in the first 3 samplings of the EM calorimeter. One of the main advantages of this approach would be the ability to handle differently single prong and multi prong decays. This simple approach showed worse signal/background separation than calorimetric energy alone.

3.2.2.3 Level 2 Tracking

The standard L2 tracking reconstruction [18] is used at L2 in the tau slice, except that no extrapolation in the Transition Radiation Tracker is used within the L2 tau trigger. Tracks with $p_T > 1.5$ GeV are reconstructed and a rectangular region $\Delta\eta \times \Delta\phi = 0.6 \times 0.6$ centered on the L2 Calorimeter seed is used.

The output of the L2 Tracking algorithm is a list of tracks found in the RoI. Two window sizes are defined, corresponding to a distance $\Delta R = 0.15$ (*Core*) and $\Delta R = 0.3$ (*Nor*) with respect to the highest p_T track. An isolation ring (*Iso*) with ΔR between 0.15 and 0.3 is also defined.

The following selection criteria are then calculated from the track list:

- **Pt leading** is the p_T of the highest p_T track found. By requiring a minimum Pt, this criterion also effectively requires that at least one track is found in the RoI.

- **Pt Iso/Core** is the ratio of the scalar sum of track p_T in the *Core* and *Iso* region $\sum p_T^{\rm iso} / \sum p_T^{\rm core}$.

- **N Slow tracks** is the number of slow tracks found in the *Core* region. A slow track is defined as a track with p_T below some threshold, typically 7.5 GeV/c.

- **Charge** is defined as the absolute value of the sum of charges of all tracks found in the *Nor* region.

- **N Tracks** is the total number of tracks found in the *Nor* region.

The L2 track cuts further enrich the tau sample requiring at least one track to be found with a minimum Pt leading, a maximum fraction of energy deposited in the *Iso* region and a maximum number of slow tracks. The requirements on charge and total number of tracks are set very loose. The distributions of Pt Iso/Core and N Slow tracks are presented in Fig. 3.12.

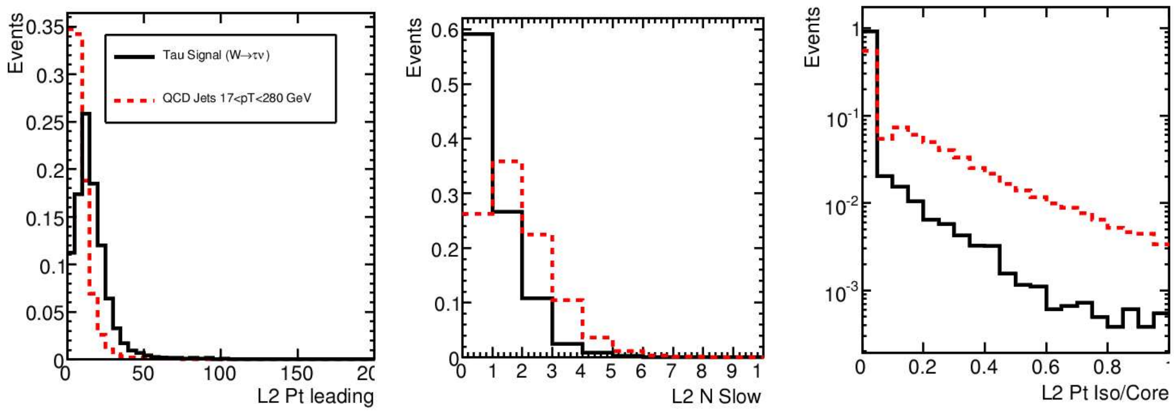

Figure 3.12: Tracking L2 variables to distinguish QCD background from tau leptons.

The requirement on the maximum number of tracks will be loosen at both L2 and EF, following the requirement of the Tau Offline Group, given that the high multiplicity part of the spectra is used in the offline reconstruction to extrapolate the background distribution.

3.2.3 Event Filter

At the Event Filter level, a mean processing time per event of about 4 seconds is possible, allowing a much more refined algorithm to be implemented.

As in L2, at EF level the selection is performed with a calorimeter algorithm first, and with a tracking algorithm afterwards.

The EF calorimeter algorithm collects cells in a rectangular region of $\Delta\eta \times \Delta\phi = 0.6 \times 0.6$ centered around the L2 seed. Then it recalculates the seed direction, and cells in a cone around that seed are used to reconstruct energy and calorimeter identification variables.

The tracking reconstruction at the EF is described in [18]. Tracking is performed in a rectangular region $\Delta\eta \times \Delta\phi = 0.4 \times 0.4$ centered around the L2 seed.

The final step of the EF tau trigger runs the offline calorimeter based identification algorithm [6]. The energy and the variables used for identification are calculated as follows. The L2 seed is refined, some very loose criteria are applied to tracks and if more than one track is found a common vertex is reconstructed. Then, the EM energy and the calorimeter shape variables are obtained using as center the new direction. Finally, an overall calibration [14] is applied to all cells, and after that a tau specific jet calibration is applied to the tau object. This final calibration is derived from simulated samples of high and low pt tau lepton sources, like Z and Higgs bosons.

The following variables are currently used for tau identification at EF:

- **EMRadius** is an energy weighted radius, which exploits the small transverse shower profile of τ leptons. The differences with L2 variable are that the radius is used instead of the square, and that all EM samplings are used. In addition, transverse energy of the cell rather than energy is used for the weighting.

- **IsoFrac** is the energy deposited in an annular region between $0.1 < \Delta R < 0.2$ divided by the energy deposited in $\Delta R < 0.3$. Here the difference with the L2 definition is that all EM samplings are used and that the square regions should be replaced by the annuli in this case.
- **N Tracks** is the number of associated tracks with $p_T > 2$ GeV found in a $\Delta R < 0.2$ region around the seed.
- **$\mathbf{p_T}$ leading track** is the highest p_T track among the tracks found in a $\Delta R < 0.2$ region around the seed.
- **EtCalib** is the energy calculated in all EM and hadronic cells found in the $\Delta R < 0.3$ region around the seed, and calibrated with the standard jet calibration (using an H1-style procedure described in [14]) and an additional tau specific calibration.

No noise suppression is applied when selecting cells used by EF.

A simple cut based selection is applied on the variables above described. Typically a further background rejection factor of 2 is achieved with the current implementation, for a signal efficiency above 90%.

3.3 Tau Trigger Performance

This section summarizes the performance of the tau Trigger, presenting the efficiency and resolution obtained at the different levels [16], as well as the efficiency for the different single tau signatures.

3.3.1 Trigger signatures

In the ATLAS trigger, there are different tau trigger signatures implemented, corresponding to different E_T thresholds[10]: `tau10i`, `tau15i`, `tau20i`, `tau25i`, `tau35i`, `tau45i`, `tau60`, `tau100`. For some E_T thresholds, additional signatures are defined which do not make use of isolation criteria at L1 (e.g. `tau10`).

L1 items are named with the actual E_T threshold applied. On the other hand, for HLT chains the selection criteria are adjusted to give high efficiency for true taus with visible E_T above the nominal energy as specified in the signature name[11], while reducing the backgrounds as much as possible. Due to the E_T resolution at the two HLT levels, the actual cut applied on E_T at each stage is significantly less than the nominal E_T.

3.3.2 Efficiency definition

The tau trigger was optimized to select with high efficiency events where a tau lepton is likely to be reconstructed and identified by the offline reconstruction. Efficiencies are quoted with respect to hadronically-decaying tau leptons where the visible tau momentum ($p^{\alpha}_{\text{vis}} = p^{\alpha}_{\tau} - p^{\alpha}_{\nu}$) is

[10] The first symbol of the signature represents the particle type, the following number is the E_T threshold and the "i" indicates that an isolation requirement is made in addition.

[11] Optimization criteria is described in section 4.1. This is the convention for the Tau slice only. Other slices use different naming conventions. For instance, electron and photon signatures are named according to the actual E_T threshold applied at EF. [19]

in the sensitive region of the detector ($|\eta| \leq 2.5$). Additionally, for any given signature, the true visible E_T for signal taus must be greater than the nominal E_T threshold for that signature.

Tau decays were only considered for calculating signal efficiencies in case they were also selected by one of the two offline tau reconstruction algorithms[12] [6]. In particular, offline tau candidates found by the calorimeter based algorithm with a Likelihood probability > 4 or by the track based algorithm using the cut selection (discriminant cut = 1) are used as a reference. Unless otherwise specified, all efficiencies quoted assume a matching to a selected offline tau candidate.

3.3.3 Energy and Angular Resolution

The resolution on E_T and direction (η,ϕ) at different levels of the tau trigger are shown in figure 3.13 for `tau20i` signature. It is calculated using $W \rightarrow \tau\nu$, $H/A \rightarrow \tau\tau$ and $Z \rightarrow \tau\tau$ samples.

The behavior is rather flat as a function of the true visible E_T and of the true visible η. The angular resolution improves between L1 and L2. At EF the direction is set according to the offline calorimeter based tau reconstruction, hence the resolution is slightly worse than at L2 where tracking information is also used to determine the cluster direction.

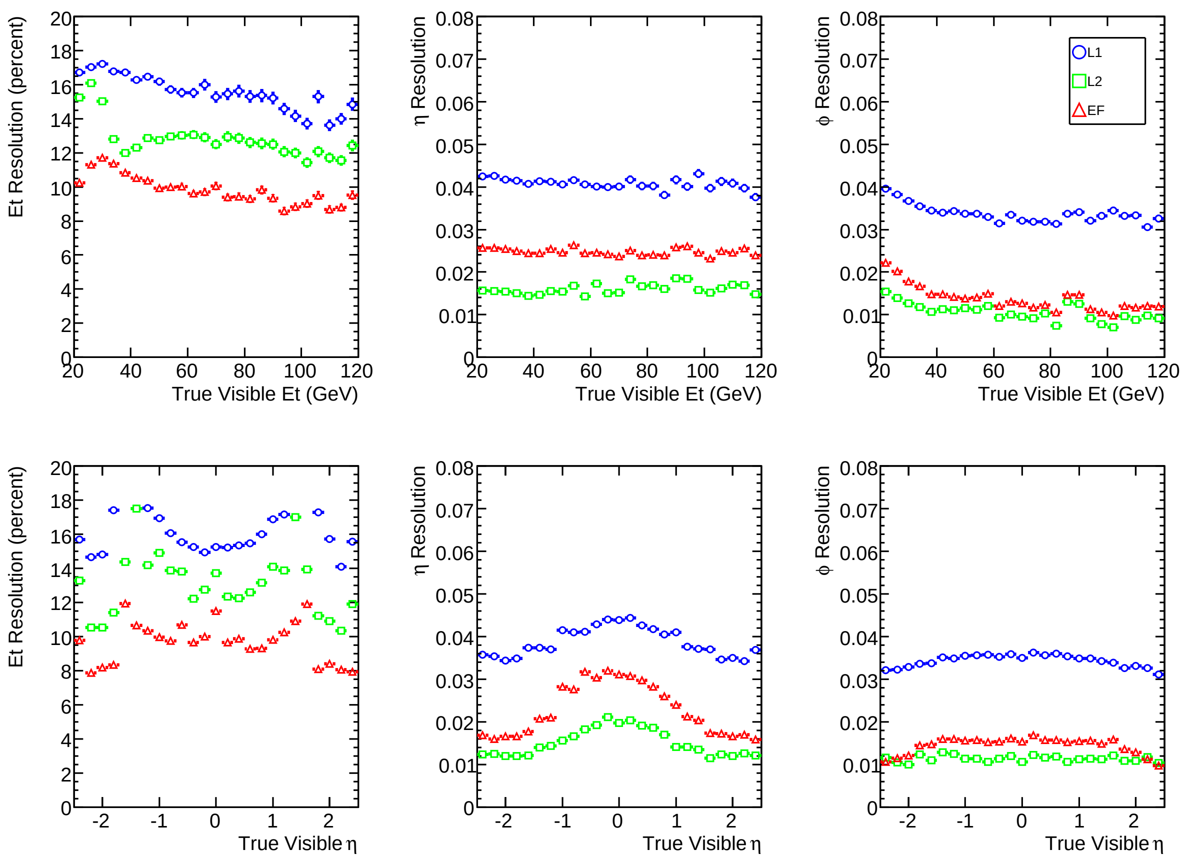

Figure 3.13: E_T , η and ϕ resolution as a function of true visible E_T (top row) and η (bottom row). It is calculated with a variety of signal samples passing the `tau20i` signature.

[12]Offline reference for optimization is introduced in 3.1.4.3 and discussed in section 4.1.

3.3.4 Efficiency for different levels

Using the efficiency definition detailed in section 3.3.2, the efficiency for the three trigger levels is plotted as a function of the τ's visible p_T in figure 3.14. It is calculated for the `tau35i` signature using a variety of signal samples.

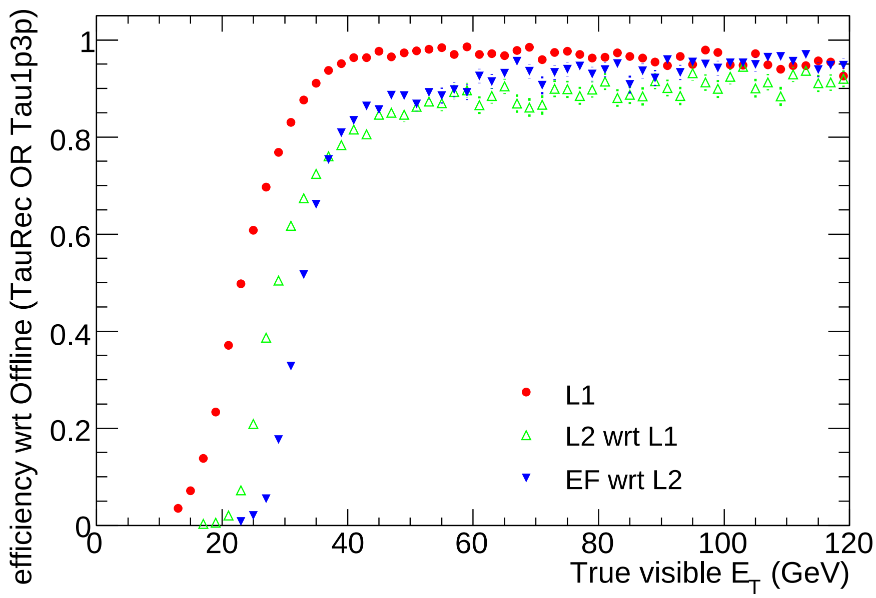

Figure 3.14: Efficiency for `tau35i` as a function of the tau visible E_T for the three trigger levels.

The efficiency of the each level is not a step function due not only to the resolution of the E_T estimation but also to the shape variables selection, which are correlated with E_T . In particular, the cut on p_T of the leading track at L2 and EF is causing the fact that the efficiency does not reach a plateau until about 60 GeV, since it is a cut on the absolute p_T value and it is highly correlated with the cluster's E_T .

The L1 turn-on curve has the less steep slope. To ensure the start of the plateau at the threshold, the cut on E_T at L1 (16 GeV) is set significantly lower than at L2 (26.5 GeV) and at EF (31 GeV).

The main factors causing different resolution and efficiency turn-on shape are described below:

- The hardware scheme [20] for collecting and setting the scale of the τ jet energy at L1 causes inevitably a biasing and smearing of the reconstructed τ transverse energy with respect to the true τ visible transverse energy: L1 energy digitization is typically 1 GeV per count and position is found using towers of low ($\Delta\eta \times \Delta\phi = 0.1 \times 0.1$) granularity.

  L1 energy resolution (the rather slow turn-on of efficiency curve) limits the rejection power at L1, since the background distribution is steep and concentrated at low p_T . The L1 efficiency plateau is not flat due to the isolation selection criteria, which is a cut on the absolute value of the energy in the isolation region and therefore is less efficient at higher energies.

- At L2 the calibration is applied per sampling (only two samplings -EM and hadronic- are considered) instead of the cell by cell basis calibration used in the offline reconstruction and at EF. Cell-based calibration allows better energy resolution but the procedure is too slow to be used at L2.

The noise suppression algorithm used offline is not applied at L2, hence the noise contribution deteriorates the performance of the calorimeter variables.

The addition of tracking information at L2 allows better discrimination between true hadronic tau decays and jet backgrounds. However the L2 tracking algorithm is about 95% efficient for tracks with p_T above 5 GeV, and only 90% of taus (from $W \rightarrow \tau\nu$ sample) passing the L2 calorimeter selection are found to have at least one track with $p_T > 5$ GeV. Thus, the L2 plateau reaches a maximum efficiency of about 90% due to the tracking reconstruction efficiency.

Besides, the two L2 sequences (L2Calo and L2ID) were optimized separately (see section 4.1.1) to give > 90% efficiency each, therefore the allowed efficiency loss was overall larger than at L1.

- At EF, a cell-based calibration is applied, but noise suppression algorithm is not used. Due to a better energy resolution, EF has fastest turn-on in the efficiency curve. The efficiency plateau is higher than at L2 since events with a good quality reconstructed track are already selected.

  As described in section 3.2.3, currently at EF the tau trigger makes use directly of the offline calorimeter based algorithm for tau identification. It is also foreseen to implement an alternative, "particle-flow" type algorithm at EF, in analogy with the offline (tau1p3p), in order to better trigger on low E_T tau leptons. It is important for optimization to have this second approach at EF, given that the efficiency tries to be maximized with respect to both offline algorithms (see section 4.1).

3.3.5 Efficiencies and rates for single tau signatures

As in the following chapter 4 optimization of single tau items will be discussed, it is worth including here a short summary with the resulting efficiencies and rates for single tau items.

Rates shown in table 3.2 are those foreseen for the initial low luminosity of $10^{31}\,\text{cm}^{-2}\text{s}^{-1}$ if prescale factors would not be applied.

3.4 Tau Trigger Menus

The different types of tau trigger signatures currently implemented in the trigger software and the physics goals they address are described in this section[16]. Given the large abundance of fake τ candidates at low energies from QCD backgrounds, the soft p_T tau trigger items will be used in combination with other trigger signatures, while high p_T items might be used *standalone.*

Menu items and thresholds in this section refer to those planned for the low (start-up) luminosity of $10^{31}\,\text{cm}^{-2}\text{s}^{-1}$.

3.4.1 Tau Trigger items

- **Single tau** triggers.

  The single tau signatures, except very high p_T ones such as `tau60` and `tau100`, will be used in combination with other triggers. Some signatures will be run standalone with prescale factors during commissioning period. The single tau item with the lowest threshold that will be available without prescale is `tau60`.

Signature	L1 item	L1 Rate (Hz)	EF eff.	EF Rate (Hz)
tau10	TAU6	14290	82.6±0.3	2266±26
tau10i	TAU6	14290	78.7±0.4	1583±21
tau15	TAU6	14290	78.2±0.4	1186±19
tau15i	TAU6	14290	74.1±0.4	864±16
tau20i	TAU9I	4767	68.5±0.5	359±10
tau25i	TAU11I	2751	66.5±0.6	185±7
tau35i	TAU16I	921	65.8±0.9	63±4
tau45	TAU25	311	82.7±1.3	75±5
tau45i	TAU25I	219	72.1±1.5	23±5
tau60	TAU40	77	77.5±2.6	7.3±1.5
tau100	TAU40	77	83.9±6.6	1.2±0.6

Table 3.2: Efficiencies and rates for 10^{31} cm^{-2}s^{-1} luminosity. Rates are shown for single tau signatures without prescales. Most of this items will be prescaled in the start up menu (see section 3.4). Efficiencies are calculated on $W \rightarrow \tau\nu$ sample, and rates are extracted using minimum bias events ($\sigma = 70mb$).

- **Single track** triggers.

  In addition to single *tau* items there will be a single *track* trigger, highly optimized to select RoIs with one track only. The majority of such candidates should be charged pions with significant contribution from ρ and K mesons. The main purpose of such trigger is alignment of the tracker. However, a variation of this trigger with well defined L1 trigger could be used to select a sample with higher purity of single prong tau decays.

Combination of tau triggers with other signatures include:

- **tau+missing** E_T **(**$\not{E}_T$ **)** triggers.

  This group of triggers covers a wide spectrum of physics channels. At low luminosity, when the trigger rejection can be relaxed, the selection of events with $W \rightarrow \tau\nu$ is the priority. $t\bar{t}$ events with a tau lepton in the final state are also selected by this trigger. Such events are characterized by relatively soft p_T taus as well as low $\not{E}_T$. The tau+$\not{E}_T$ signatures at design luminosity are oriented for Higgs (neutral or charged) searches as well as for searches of new exotic particles or processes. In combination with missing E_T , the lowest threshold unprescaled signature is `tau20i_xe30`.

- **tau+**ℓ**(+jets)** triggers where $\ell = e, \mu$ aim at selecting events with 2 relatively soft taus in the final state. Two taus are found in events with Z boson, neutral Higgs or SUSY. The tau+ℓ combination selects also events with multiple leptons like $t\bar{t}$ or lepton flavor violating processes. The combination of two signatures allows to use softer thresholds than the one in single signatures, the lowest threshold unprescaled signatures being `tau20i_e10` and `tau20i_mu6`.

- **tau+tau(+jets)** trigger is an extension of tau+ℓ signature and records events where both taus decay hadronically. While the rejection rate is less favorable than in tau+ℓ case, the sample collected is complementary to the former, so it increases statistics and allows to reduce systematic uncertainties due to lepton identification. It is a trigger menu highly relevant for Higgs discovery and for searches of exotics. SUSY double tau end point analysis will also benefit from above signature or from double taus combined with extra jets. The lowest accessible unprescaled di-τ signature will be `2tau25i`.

- **tau+jets, tau+bjets** combinations are an interesting option for $t\bar{t}$ studies. At low luminosity, they will allow to study events with low jet thresholds, while at high luminosities the mixed triggers will be necessary to reduce QCD and multiple interaction events. In combination with jets, the lowest threshold unprescaled item is `tau20i_j70`, while if we require the jet to be b-tagged, efficiency decreases but jet threshold can be further lowered: `tau25i_b35`.

- **Commissioning** items, such as `tau15i_PT` and `2tau25i_PT`. These items, have HLT signatures run, however, the HLT decision is neglected, and all events are written out to tape together with HLT decision. This allows full debugging of HLT chain and HLT decision, as well as understanding run-to-run variations of the rate and variables used for identification. As the output rate of pass_through item is equal to L1 rate, only a small fraction can be recorded, typically $\sim$ 0.1 Hz after prescale.

The optimization of the rate allowed for the signature of given type is based on number of interesting physics events it selects and extra rate it gives on top all other triggers. The number of interesting events which are not triggered otherwise are also taken into consideration. The prescales and rates allocated in the trigger menus currently implemented are not optimized and will be tuned further before the start-up as well as during the commissioning period with data.

3.4.2 Tau Trigger menus for various luminosity periods

ATLAS will collect data at different luminosities, starting from low $10^{31}\,\mathrm{cm^{-2}s^{-1}}$ and increasing to high $2 \cdot 10^{33}\,\mathrm{cm^{-2}s^{-1}}$ within several months. While the input rate will highly increase, the maximal output rate of the complete trigger will remain at 200 Hz, subject to storage capacities and recording speed.

The low luminosity run will mostly coincide with commissioning of detector and trigger itself. During this period, the focus is on Standard Model physics and events necessary for calibration and efficiency studies.

The transition to higher luminosity will be done smoothly. The change of trigger menu will happen in several steps, dropping items used for commissioning and the ones with unacceptably large rate, and leaving *unprescalable* items which focus on discovery physics. In some cases, the thresholds and cuts will be tightened (e.g. using *tight* instead of *loose* single high p_T tau item or *e25i* instead of *e15i* in tau+e combination), while in other cases the extra signatures will be added (e.g. tau+ℓ+(jets) trigger).

Several interesting samples like Higgs, SUSY or $t\bar{t}$ will be triggered by different tau trigger items. This is very useful feature because:

- it allows to increase statistics

- it is a robust approach against failure or inefficiency of particular trigger line (e.g. due to detector problems)

- it allows to reduce systematic uncertainty by comparing results of the same analysis repeated on samples selected with different trigger items.

3.4.3 Trigger menu for early running

A summary with the most relevant trigger signatures for the start-up period with low luminosity of $10^{31}\,\mathrm{cm^{-2}s^{-1}}$ is presented in table 3.3. [21]

The goal of this section is to compare the tau Trigger with the other lepton triggers. The physics motivation, topology of the decay, identification strategy and rejection power of trigger selection are very different among the lepton triggers, and so it is their trigger menu for first data taking.

3.4.3.1 Electron Trigger

Electrons will be very important for many physics analysis as they are relatively easy to identify and trigger on. In the early days processes such as $Z \to ee$, $J/\psi \to ee$ and $W \to e\nu$ will be crucial for the commissioning and understanding of the detector.

Electrons leave a much cleaner signature in the detector than tau leptons. They are reconstructed as single tracks matched to a shower fully contained in the EM calorimeter. Therefore electrons are more efficiently separated from QCD jets, as jets are multi-track objects with an important fraction of their energy deposited in the HAD calorimeter. The high granularity of the strip EM sampling allows distinction of electrons from π^0 decaying into two photons, as the two peaks from photon showers can be separated in η direction. Only at HLT the rejection factor is of the order of 100, while for taus is one order of magnitude smaller.

The approach that will follow the electron slice [19] at the beginning of data taking will be to use only prescaled triggers with pass-through the first days in order to understand the rates. After that they will move to the optimized menus in table 3.3, where the lowest p_T unprescaled item is `e10`.

From figure 3.15 the better energy resolution of electron trigger can be appreciated. The efficiency changes from 0 to its maximum within 5 GeV, while for taus it does within roughly 20 GeV.

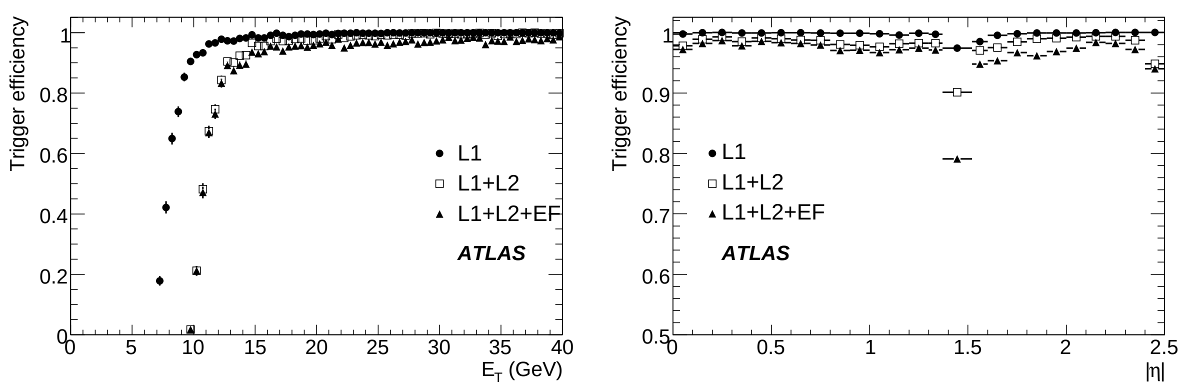

Figure 3.15: Trigger efficiencies at L1, L2 and EF as a function of true electron E_T (left) and $|\eta|$ (right) for the `e10` menu item. The efficiencies are obtained for single electrons using ideal detector geometry electron scan sample and are normalized with respect to medium set of offline electron cuts. Note that $|\eta|$ plot has an additional cut of $E_T > 15$ GeV.

3.4.3.2 Muon Trigger

Muons offer a clean channel in the harsh environment of the LHC. High-p_T muons are important for many known processes, that can be used for monitoring and calibration ($Z \to \mu\mu$), as well as for searches for new phenomena (Higgs, SUSY).

Due to their higher mass ($\sim$ 210 times the electron's) and long lifetime, muons are not stopped in the detector. They leave a track in the inner detector but they generally go through the calorimeter without producing a shower. Therefore their momentum is measured in the muon spectrometer (MS), which was designed for this scope, with help from the ID.

In-flight decays of pions and kaons are the main source of L1 trigger rate at low p_T. For a track from such decays the χ^2 of the fit is worse than for prompt muon tracks. Also the ratio of the p_T values measured in the ID and MS is closer to one for prompt muons.

The muon trigger [22] has already a good rejection at L1. In the menu for early running, the HLT is used only in low p_T items and it has a quite low rejection factor of the order of 5-15. For items with p_T higher than 20 GeV the L1 rate is low enough and triggers are left with HLT pass-through.

Figure 3.16 shows efficiency curves at EF level for muon triggers. As an important difference with respect to other lepton triggers, it has to be noticed the sharp turn-on of the efficiency curve, which goes form 0 to the efficiency plateau within 2 GeV (for low p_T triggers).

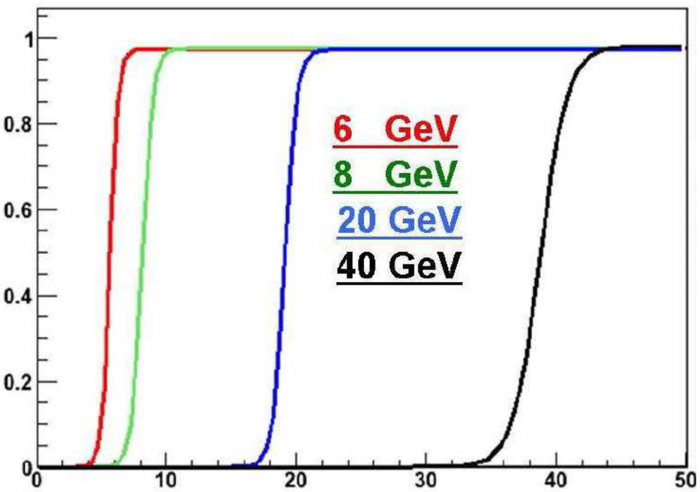

Figure 3.16: Muon Trigger EF efficiency curves for different p_T thresholds.

3.5 Tau Commissioning

In this section preliminary strategies for systematics and calibration of τ objects with first experimental data are summarized. Also an overview on SM signal observability is presented. Finally, a short summary of the results achieved at the Tevatron Collider regarding tau leptons is included.

Two stages can be discussed in the commissioning context, the first one after collecting 1 - 10 pb^{-1} and the second one with 100 pb^{-1} collected. [23]

In the first stage, assuming collected 1 - 10 pb^{-1}, the available sample will be almost *signal free*, just dominated by fake-τ candidates from QCD jets. This amount of data should nevertheless allow to understand performance of tracking and cluster reconstruction, track and cluster matching, and vetoing fake candidates from electron and muon tracks. It will also allow to monitor the fake-τ energy scale versus the energy scale from a reference jet algorithm, to prepare training for background with multi-variate identification schemes and also to prepare parametrization for fake rates, still using Monte Carlo modeling for signal candidates.

In the second stage, assuming 100 pb^{-1} collected, the Standard Model processes of W, Z and $t\bar{t}$ pair production will provide enough signal events for the first observability and interesting

Signature	L1 item	L1 Rate	Prescale	EF rate
2e5	2EM3	6.5 KHz	1	6 Hz
2g10	2EM7	0.5 KHz	1	<0.1 Hz
e10	EM7	5.0 KHz	1	21 Hz
2e10	2EM7	0.5 KHz	1	0.4±0.2 Hz
g20	EM18	0.3 KHz	1	5.4±0.2 Hz
e20	EM18	0.3 KHz	1	4.3±0.2 Hz
em105_PT	EM100	1 Hz	1	1.0±0.1 Hz
mu4_PT	MU4	1 KHz	1000	1 Hz
mu6	MU6	224 Hz	1	48 Hz
mu6_PT	MU6	224 Hz	200	1 Hz
mu10	MU10	112 Hz	1	7 Hz
mu10_PT	MU10	112 Hz	100	1 Hz
mu15	MU15	19 Hz	1	2 Hz
mu15_PT	MU15	19 Hz	20	1 Hz
mu20i_PT	MU20	14 Hz	1	14 Hz
mu40_PT	MU40	8 Hz	1	8 Hz
2mu6_PT	2MU6	4 Hz	1	4 Hz
2mu20_PT	2MU20	<1 Hz	1	1 Hz
tau45	TAU25	311 Hz	20	4.1 Hz
tau45i	TAU25I	219 Hz	10	2.5 Hz
tau60	TAU40	77 Hz	1	10.7 Hz
tau100	TAU40	77 Hz	1	2.4 Hz
tau20i_MET30	TAU9I_XE30	154 Hz	1	4.9 Hz
tau20i_e10	2TAU6_TAU9I_EM7	1 KHz	1	1.2 Hz
tau20i_mu6	TAU9I_MU6	47 Hz	1	2.8 Hz
2tau25i	2TAU9I	407 Hz	1	2.6 Hz
tau20i_3j23	TAU9I_3J5_2J23	314 Hz	1	0.9 Hz
tau20i_j70	TAU9I_2J5_J35	423 Hz	1	7.1 Hz

Table 3.3: Example of lepton trigger menu for start-up luminosity of 10^{31} cm^{-2}s^{-1}.

physics measurements. The analysis which can be envisaged, are discussed in [23]. Here only strategy for efficiency measurements and in-situ calibration are briefly mentioned.

Overall τ identification efficiency

A measurement of the overall τ identification efficiency using SM signal samples will only be only possible with 100 - 300 pb^{-1}. [6] Several methods can be foreseen, with statistics of about a few thousand to a few hundreds of signal events and a signal-to-background ratio between 1:1 and 1:5. Possible strategies for efficiency measurements are the following:

- Measure the $W \to \tau\nu$ and $Z \to \tau\tau$ cross-section and measure the efficiency with respect to $W \to e\nu$ ($W \to \mu\nu$) and $Z \to ee$ ($Z \to \mu\mu$). Like this the relative $\tau/e(\mu)$ efficiency can be obtained.
- Use a Monte Carlo + data approach: for the data with $Z \to \mu\mu$ events, subtract the information on the muon and replace it by the full detector simulation of τ decays. Subtract background using the same-sign events, and then compare with the pure Monte Carlo events and with the pure data events. This way, the MC description is reduced to the tau decays, all the rest of the event comes from real data. This strategy is useful to reduce supplementary bias from MC.
- Use $t\bar{t}$ production to measure the efficiency in higher transverse energy region.

The $W \to \tau\nu$ and $Z \to \tau\tau$ samples will allow also to study trigger efficiencies, e.g. using unbiased $Z \to \tau\tau$ events triggered with the electron or muon stream and monitoring response of the tau trigger. The tau stream with $W \to \tau\nu$ will also provide a cross-check for an unbiased measurement of the electron trigger efficiency.

Calibration with $Z \to \tau\tau$ events

With integrated luminosity of 100 pb^{-1}, the observed $Z \to \tau\tau$ events can be used for in-situ calibration of the reconstructed objects from hadronically decaying τ. After events selection and subtraction of the same-sign background from the opposite-sign events, the invariant mass of the lepton-τ system will allow to in-situ calibrate τ energy scale. The sensitivity of the measured visible Z mass, as obtained from reconstructed $\tau\tau$ pairs, to the absolute τ energy scale, will allow to confirm this scale with $\pm 7\%$ error with 100 pb^{-1} integrated luminosity.

3.5.1 Tau leptons in SM processes

The goals for early τ physics at ATLAS [23] include acquiring a sample of τ leptons from the data with as high purity as possible so the τ identification efficiency can be measured and the simulation can be tuned.

Collecting data with the integrated luminosity of 100 pb^{-1} and with the instantaneous luminosity of 10^{31} $\mathrm{cm}^{-2}\mathrm{s}^{-1}$ will lead to samples of a few thousands to a few hundred identified hadronic τ decays from SM processes. It will provide unique opportunity to access and understand statistically significant τ samples from SM processes at relatively low transverse momenta.

The inclusive $W \to \tau\nu$ process with hadronic τ decays will lead to a few thousands of identified τ for 100 pb^{-1}. Observability in this channel would require already well developed and excellent rejection capability with respect to fake candidates from overwhelming QCD jets background. Identified τ leptons will have to be first triggered with the tau trigger, requiring then well tuned procedure to correct for the inevitable bias introduced into τ identification. The expected signal to background ratio will be of the order of one and the observability will be proven by looking at the track multiplicity spectra of the identified candidates.

The inclusive $Z \to \tau\tau$ process will provide signature at 10 times lower rates, but with more robust prospects for analysis. It will be possible to cross-check channels with electron-τ_{had} and muon-τ_{had}, to control background comparing observed number of events in the same-sign and opposite-sign samples. Moreover, events will be primarily triggered with lepton trigger, just providing unbiased sample of the hadronic τ leptons which could also serve for understanding efficiencies of the hadronic tau trigger. Measurement of the visible mass of the lepton-τ_{had} system, for analysis with low background level will give sensitivity to the energy scale of the reconstructed τ jets.

The $t\bar{t}$ production with one $W \to \tau\nu$ and second one decaying hadronically or leptonically will provide physics signature involving missing energy, several jets and leptons including especially τ leptons.

3.5.1.1 Tau lepton measurements at the Tevatron Collider

It is interesting to recall measurements which have been published by the CDF and DO collaborations with a comparable amount of the data.

- The preliminary measurement by the CDF Collaboration [24] with $W \to \tau\nu$ channel, was reported with the integrated luminosity of 72 pb^{-1} and 2345 event observed. The cross-section measurement of $\sigma(p\bar{p} \to W)BR(W \to \tau\nu) = 2.62 \pm 0.07(stat) \pm 0.21(sys) \pm 0.16(lum)$ nb was possible. Comparison of the $W \to \tau\nu$ yields to those in $W \to e\nu$ channel allowed for measurement of the ratio $BR(W \to \tau\nu)/BR(W \to e\nu) = 0.99 \pm 0.04(stat) \pm 0.07(syst)$. One should note partial cancellation of the systematic error here. These results were then used to constrain the ratio of the couplings $g_e/g_\tau = 0.99 \pm 0.02(stat) \pm 0.4(syst)$.
- Also by the CDF Collaboration was published measurement [25] on the cross-section for the inclusive $Z \to \tau\tau$ production in electron-hadron channel. This measurement was based on 350 pb^{-1} of CDF Run II data. Using a sample of 504 opposite sign e-τ events with a total expected background of 190 events, was obtained cross-section $\sigma(p\bar{p} \to Z)BR(Z \to \tau\tau) = 264 \pm 23(stat) \pm 14(syst) \pm 15(lumi)$ pb, in agreement with the (next-to)-next-to-leading order QCD prediction. This was the first CDF published cross-section measurement using hadronically-decaying τ leptons in Run II.
- For the top-pair production with dilepton signature including τ lepton, the evidence for such observation was reported by the CDF Collaboration [26] with the integrated luminosity of 350 pb^{-1}. The 5 events were observed with expected background of 2.7 ± 0.4. The expected total number from SM process for signal+background was $5.0. \pm 0.5$.

The measurements by the CDF Collaboration discussed above should be kept in mind when discussing prospects for ATLAS experiment in the same channels and comparable integrated luminosity.

Because of low statistics at the Tevatron Collider, tau lepton can not provide competitive precision measurements of SM quantities. At ATLAS, SM measures from tau lepton will neither aim to precision measurements but will be used for commissioning analysis. On the other hand, tau lepton will be very useful for New Physics searches, as being the heaviest lepton it has stronger couplings to new particles.

4 Tau Trigger Optimization Studies

Tau Trigger optimization is ongoing and will be revised when the first data taking will start.

In this section, the tau trigger optimization strategy is described, together with the discussion about which offline reference has to be used for optimization. Next, optimization studies specific from the calorimetric part of the second level trigger (L2Calo) are described in detail. These studies include a discussion on energy estimation and calibration, a comparison of performance considering different window sizes to calculate L2Calo variables, as well as the description of a systematic procedure to optimize simultaneously the L2Calo selection variables.

4.1 Optimization Reference

Tau trigger standalone signatures are optimized taking as a reference the tau objects that can be reconstructed and identified offline. Identification cuts used are the default selection proposed by the two packages. The aim is to keep the trigger as efficient and unbiased as possible with respect to offline reconstructed and identified taus.

4.1.1 Optimization Criteria Overview

The aim of the optimization is to keep a high efficiency for tau objects while reducing the rates to an acceptable level, considering that tau signatures will appear in the menu mainly in combination with other objects and it is the rate of combined triggers that is relevant.

The total allowed rate at each trigger level is to be shared among the different slices (electron, muon, tau, jet,...), the final distribution of rate limitations for each slice will depend on the physics priorities of the Collaboration. The tau trigger could take about 20% of the EF bandwidth which means roughly 40 Hz. However, optimization of the bandwidth allowance is a complicated subject, as the overlap of the different triggers (events selected by more than one slice) as well as the limitations at each level, have to be taken into account. Since the Tau HLT rejection is relatively low, tau trigger rate is limited by the EF bandwidth (see table 3.3). In contrast, the electron trigger is limited by the L1 acceptance rate and, being the HLT rejection larger, the EF output rate fits well in the allowed bandwidth.

Unless otherwise stated, the efficiency definition explained in section 3.3.2 will be used in this section, i.e. tau objects reconstructed offline and with a true visible p_T greater than the nominal E_T threshold of the signature considered are taken as a reference.

The optimization strategy followed is to optimize the variables thresholds (cuts) of each level taking as a reference the objects accepted by the previous trigger level. The optimization goal is to reach an efficiency as close as possible to 90% for each of the three trigger levels.

For instance, L1 E_T threshold was set to reach 90% efficiency at the nominal E_T threshold of the signature, while the EM isolation threshold[1] was set to be the same for all isolated items. Having the same isolation threshold ensures that the sample selected by a high p_T signature is a subsample from a lower p_T one. This will be useful for understanding trigger efficiencies on

[1] At L1 only two variables are used (Energy and EM Isolation), they are described in section 3.2.1.

real data, as low p_T triggers can then be used to study the efficiency of higher p_T signatures. L1 optimization is discussed in more detail in section 4.2.

L2 was optimized in two steps, first the calorimeter part (L2Calo) and the tracking part afterwards (L2ID). For L2Calo, 95% efficiency was required for shower shape variables, and the E_T threshold was set such to give also $\sim$ 95% efficiency at the signature's nominal threshold level.[2] L2ID was not yet systematically optimized, the only signature dependant cut being on the p_T of the leading track.[3] The efficiency reached is about 75-85%, depending on the signature [27]. However it is important to notice that this is due in part to the track reconstruction efficiency (without any L2ID cuts applied) that is already $\sim$ 90%.

The four continuous EF variables[4] were optimized in pairs, i.e. the shower shape variables on one side and the E_T variables on the other, requiring >90% efficiency for each pair. However, EF optimization studies are ongoing as it is following up the newest improvements from offline algorithms.

The results of this optimization can be checked in figure 3.14, where an example using `tau35i` is presented. The plot shows efficiency curves for each trigger level with respect to the previous level, taking the offline as a reference.

4.1.2 Difficulties associated to differences between offline algorithms

There has been a long discussion about which offline reference should be considered for the optimization. Ideally, high efficiency should be reached with respect to both offline reconstruction algorithms, so that the end user is able to choose which algorithm to use. However, the differences outlined below make this difficult:

- Tau1p3p is optimized for low p_T taus, and it maintains equal efficiency for one prong and three prong taus. As the algorithm is seeded by a relatively high p_T track, it discriminates QCD jets already at the level of reconstruction.

- TauRec aims to reach a constant efficiency for taus in a large range of p_T . Reconstruction algorithm starts from a calorimeter cluster, and therefore it has a high efficiency for both taus and QCD jets. All the rejection power comes from the identification step, based mainly on the shape of the calorimeter cluster. The global rejection achieved is higher than in the case of tau1p3p.

The cut on the minimum p_T of the seed track for tau1p3p is the main responsible for the small overlap that the two algorithms show.[5]

The following facts should be taken into account:

- L1, EF and L2Calo algorithms are similar to tauRec algorithm in the sense that they start the reconstruction from a calorimeter cluster. On the other hand, L2ID is more along the line of the tau1p3p selection because it requires a reconstructed track.

- The relative number of one prong and three prong taus is crucial for the offline $W \rightarrow \tau\nu$ analysis. Therefore the trigger should not introduce a significant bias between one and multi-prong taus.

[2] L2Calo optimization is described in detail in section 4.3
[3] L2ID selection variables are described in section 3.2.2.3.
[4] Described in section 3.2.3.
[5] The fraction of taus reconstructed by both packages is about 50%. See section 3.1.4.3.

- Offline algorithms are still under active development: The use of *Topocluster* is being implemented in the tauRec algorithm, and also the possibility to merge both offline algorithms (or at least make more similar the pre-selection criteria) is under investigation.

The decision taken was to use as a reference taus reconstructed and identified by at least one of the reconstruction algorithms, keeping in mind that the trigger will need to follow up offline developments.

In figure 4.1 the efficiency for each trigger level is plotted versus the tau true visible E_T . Efficiency is shown taking as reference different samples: all true taus, true taus identified by either tauRec or tau1p3p, true taus identified by tauRec and true taus identified by tau1p3p. These can be compared to the offline efficiency for different algorithms plotted in figure 3.9.

In the top-left plot it can be noticed that the trigger efficiency is dominated by the L1 selection. It can be appreciated how the L1 efficiency decreases with the tau E_T due to the isolation criteria.

The top-right plot shows the efficiency curves with respect to the reference used for optimization. The E_T dependence of L1 efficiency in the plateau is clearly reduced, since the offline reference has a similar E_T dependence (see figure 3.9). Efficiency at the threshold level is 90% for L1 but it is lower for L2 and EF, as the effect of the three turn-on curves adds up.

In the middle-left plot the high efficiency of L1 when taking as a reference tauRec is expected, as they use a similar clustering algorithm (sliding-window), and because tauRec selects low p_T taus also favored by the L1 selection criteria. In contrast, low efficiency of L2 with respect to tauRec is mainly due to the tracking efficiency and to the cut on the p_T of the leading track.

On the other hand, the middle-right plot shows that the efficiency loss with respect to tau1p3p is more distributed among the different levels, as all levels have a calorimetric part. It can be observed that the L1 efficiency is lower at low p_T , while in the L2 is higher with respect to the previous case.

The bottom row plots in figure 4.1 show the efficiency for true taus selected by the trigger (EF) and identified by each offline algorithm. Single prong and three prong candidates have been separated. These are the efficiency curves that the end user will have to deal with when doing an analysis with taus selected by tau trigger.

Users should be aware of the bias that using the tau trigger can introduce to their samples: it will not be equivalent to run the tau reconstruction algorithms on a sample selected by using the tau trigger or on a sample of events triggered by a different signature.

Complementary to these figures, table 4.1 presents trigger efficiency detailed for one prong and three prong taus taking as a reference the different offline algorithms.

	`tau20i`			`tau60`		
Offline package	all taus	1-prong	3-prong	all taus	1-prong	3-prong
tauRec	76	75	83	94	94	86
tau1p3p	69	77	57	88	90	78
tauRec OR tau1p3p	67	71	58	91	93	80
tauRec AND tau1p3p	87	86	88	93	93	86

Table 4.1: Efficiencies in percent for different offline references as calculated with the $W \rightarrow \tau\nu$ sample (`tau20i`) and the $A \rightarrow \tau\tau$ sample (`tau60`) respectively.

The interesting features of this table are, in first place, that an equal efficiency for one prong and three prong candidates is not achieved at the trigger. Only 57% of three prong taus reconstructed by tau1p3p are indeed accepted by the trigger, while the fraction is 77% for single prong taus. The corresponding efficiency for tauRec is higher because tauRec is able to identify very few three prong taus, and most of them are accepted by the trigger as they are already "good-quality" taus. These efficiency differences decrease for taus with higher p_T .

Secondly, one can see that efficiency at low p_T is somewhat lower, in particular for 3-prong decays, while at high p_T it is about 90% with respect to both reconstruction packages. This reflects the need to revise the selection approach at tau trigger for low p_T taus. Recent developments go in the direction of having *tau1p3p*-type selection at trigger level, to improve the low-p_T tau efficiency.

Finally, an important conclusion is that is is very difficult to optimize for both offline packages at the same time since they have so different approaches. The effect that the differences between the algorithms have on the trigger optimization is not easily measurable. A unique merged offline package with loose selection would be very useful as reference for trigger optimization. Moreover, a merged offline algorithm could take advantage of the strong variables in each algorithm. It could be able to relax pre-selection criteria (e.g. minimum p_T of the leading track), compensating the loss of rejection with best performing variables from the other algorithm. This possibility is under consideration in the Tau Working Group.

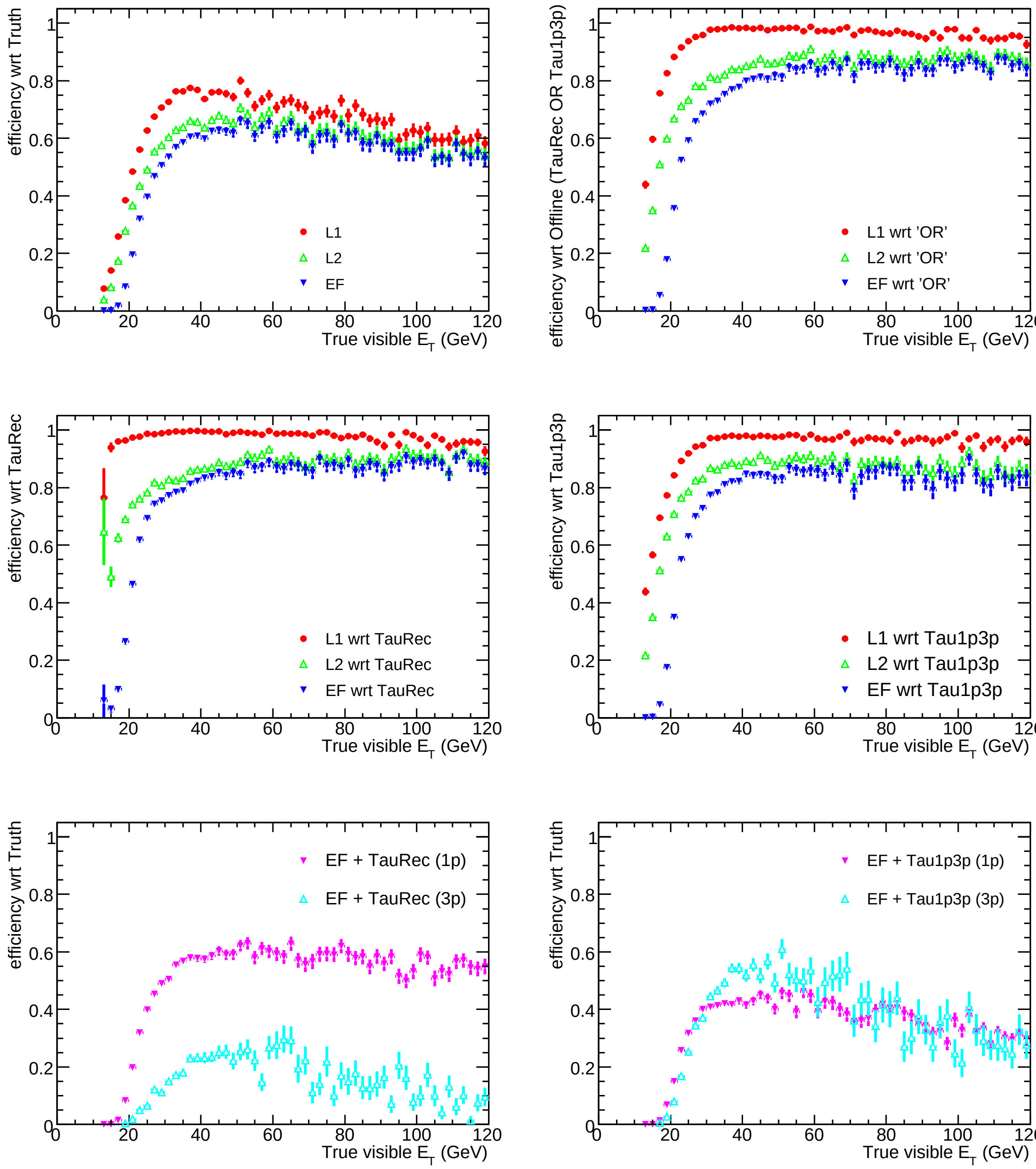

Figure 4.1: Efficiency for the 3 trigger levels with respect to different references: true taus (top-left plot); true taus matched to an offline reconstructed object - by any tau algorithm - (top-right plot); true taus matched to an offline object reconstructed by tauRec (middle-left) and by tau1p3p (middle-right). Plots in the bottom line are for taus reconstructed by tauRec (left) and tau1p3p (right) with respect to true taus. The end-user doing analysis will have to deal with these latest efficiency curves. Selection corresponds to `tau20i` signature. $W \rightarrow \tau\nu$, $H/A \rightarrow \tau\tau$ and $Z \rightarrow \tau\tau$ samples have been used.

4.2 Level 1 Optimization

There are three selection variables at L1: TauCluster (E_T), EmIsol and HadIsol, which are described in section 3.2.1. However HadIsol has been proven [28] to give less background rejection than EmIsol, and therefore the former is not used for selection.

EmIsol has low rejection power for low p_T taus (< 15 GeV) thus it is not used for `tau10i` and `tau15i` signatures. As illustrated in figure 4.2, the rejection due to isolation criteria increases with the tau energy. Yet, isolation cut reduces the efficiency of high energy taus and introduces a p_T dependence in the efficiency curve. This is because, even if high energy τ-jets are more collimated, the energy released in the isolation area is larger. This effect is compensated by introducing in the menu non isolated high p_T signatures which can recover the lost events. The same isolation threshold has been set for all isolated items. As already discussed in section 4.1.1, this will be useful specially at the beginning to understand trigger efficiencies from data. The EmIsol threshold has been set to 6 GeV, this cut is considered to be loose enough to ensure that the L1 acceptance is not sensitive to some increase of the electronic noise level of the calorimeter.

On the other hand, the E_T threshold is optimized to reach 90% efficiency at the nominal E_T threshold of the considered signature. In table 3.2 the L1 E_T thresholds can be found for each signature. Efficiency curves for such signatures are plotted in figure 4.3.

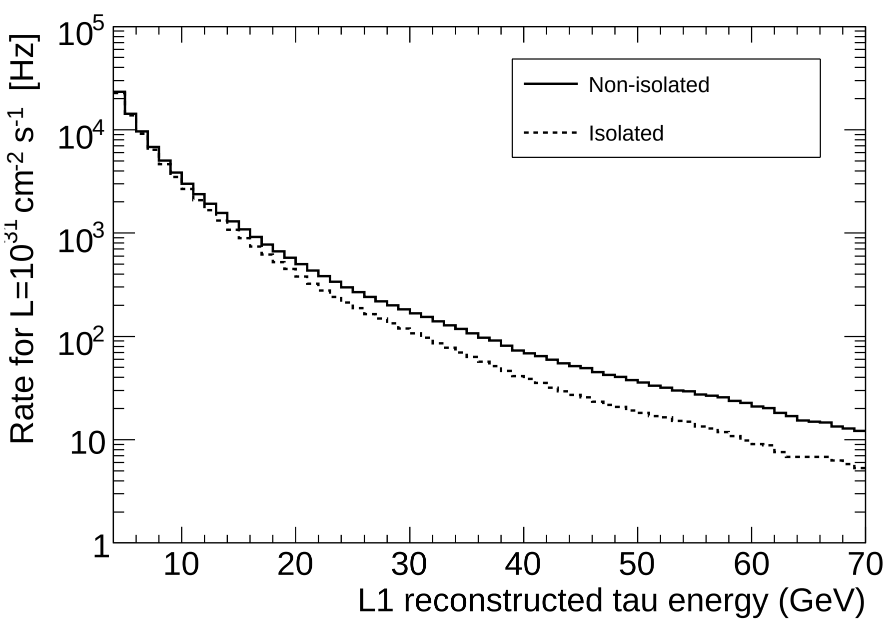

Figure 4.2: Minimum bias L1 rate for $\sigma = 70\,\text{mb}$ and $\mathcal{L} = 10^{31}\,\text{cm}^{-2}\text{s}^{-1}$ as a function of the cut on tau cluster E_T , with and without isolation cut of 6 GeV.

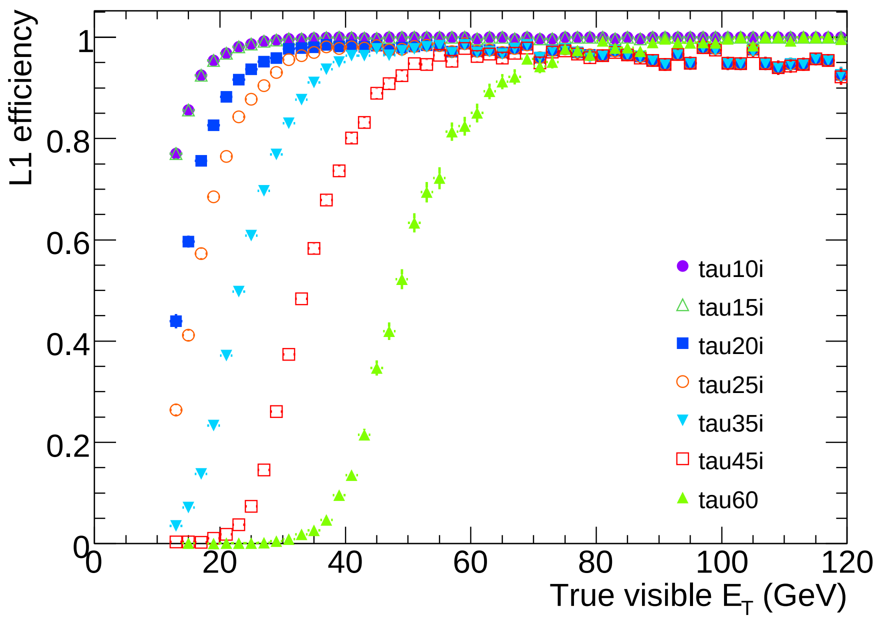

Figure 4.3: L1 efficiency versus true visible E_T for standalone tau signatures. Efficiency is calculated using the standard offline reference.

4.3 Systematic optimization for Calorimetric Level 2

In this section the optimization criteria and procedure used at L2Calo to systematically optimize all tau standalone signatures is described.

A systematic optimization procedure is needed in order to take advantage of the full rejection power of the variables, which might change with the energy of the tau candidate.

4.3.1 Optimization criteria

Two kinds of variables are used at L2 Calo[6], the so-called "shower shape" variables (EMRadius, isoFrac and stripWidth) and the "Et" variables (EtCalib, RawEt). The former use tau characteristic topology (mainly narrowness of the tau shower in the calorimeter) to discriminate against QCD dijets, while the latest kind takes into account only the total energy of the considered object. The main goal of the "Et" variables is not only to reduce the rate but also to select a sample of taus with a given p_T . Shower shape variables are calculated from ratios of energies, thus they are dimensionless, while "Et" variables have, obviously, energy dimensions.

Consequently two different optimization criteria have been used for the "shape" and "Et" variables.

- For "shower shape" variables:
  - The combination of three cut values giving the lowest QCD rate (for a fixed minimum efficiency) is chosen.
  - The combination of cuts is required to fulfill some continuity criteria of the cut value versus efficiency[7], which aims for stability of the selection.
- For "Et" variables:
  - The efficiency for taus in a 5 GeV interval above the E_T threshold must be above a minimum (e.g. 90%[8]), regardless of the rate.
- In general one would aim for "inclusive menus" (i.e. events selected by `tau25i` should be a subsample of those accepted by `tau20i`) having tighter cuts for higher p_T menus. This would make understanding of trigger efficiencies easier.

It is interesting to have an automatic optimization so that optimal set of cuts can be quickly obtained for different menus and for different efficiencies. We expect the optimization to be repeated every time conditions change, i.e. when noise or pile up will be added to the MC simulation, as well as during the commissioning of the trigger with the first data.

4.3.2 Shower Shape Variables Optimization

A systematic optimization has been developed for the three "shower shape" variables together. As the variables are correlated (see figure 4.7), cut values can not be set independently.

Its goal is, given a minimum efficiency for taus, to select a set of stable cuts which minimizes QCD rate.

It consists of the following steps:

[6] Their definition can be found on section 3.2.2.1

[7] Explained in section 4.3.2

[8] This efficiency should actually be considered with respect to the efficiency plateau, as there are unavoidable inefficiencies from reconstruction.

- First of all, a scan in the cut value is performed and efficiency is calculated for each variable independently. A range of the cut value is selected for each variable as a function of the desired efficiency, i.e. if we aim to have a global 95% efficiency, only cut values leading to an efficiency greater than 95% are considered.

- A number (N) of possible cut values is defined inside the selected range.

- Next, efficiency and resulting QCD rate are calculated for all possible combinations of cut values (see figure 4.4). The combination minimizing the rate given a minimum efficiency is chosen as the "best" combination. The number of possible combinations depends on the number of variables to the *Nth* power. Therefore, a compromise has to be reached between precision and speed when setting N.

- Then the procedure is repeated for different values of efficiency. A constrain on continuity of the cut value versus efficiency is applied.[9]Rate is allowed to increase by a certain percentage as we aim for monotonically increasing cut values as a function of efficiency.

- Finally resulting cut values are plotted as a function of the menu's threshold (in figure 4.5) and menu's inclusiveness and cuts consistency are checked. By fitting the cuts obtained as a function of the menu's threshold, extrapolation of the cut value for higher p_T thresholds becomes possible.

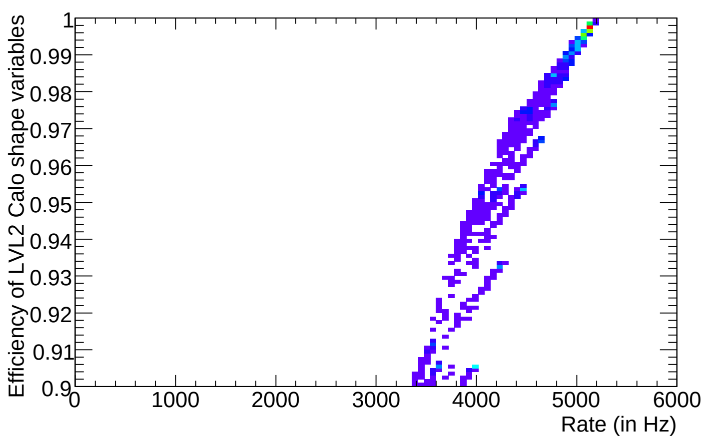

Figure 4.4: Efficiency vs corresponding background rate for all possible combinations of the 3 cut values for an efficiency greater than 90%. This is an example for `tau20i` signature.

[9]Optimal cut values were found to rapidly fluctuate as a function of the efficiency. This was not only due to the very high efficiency required (cuts were set at the very end of the distribution's tail, where the statistics was highly suppressed) but also due to the correlation between the variables (see figure 4.7).

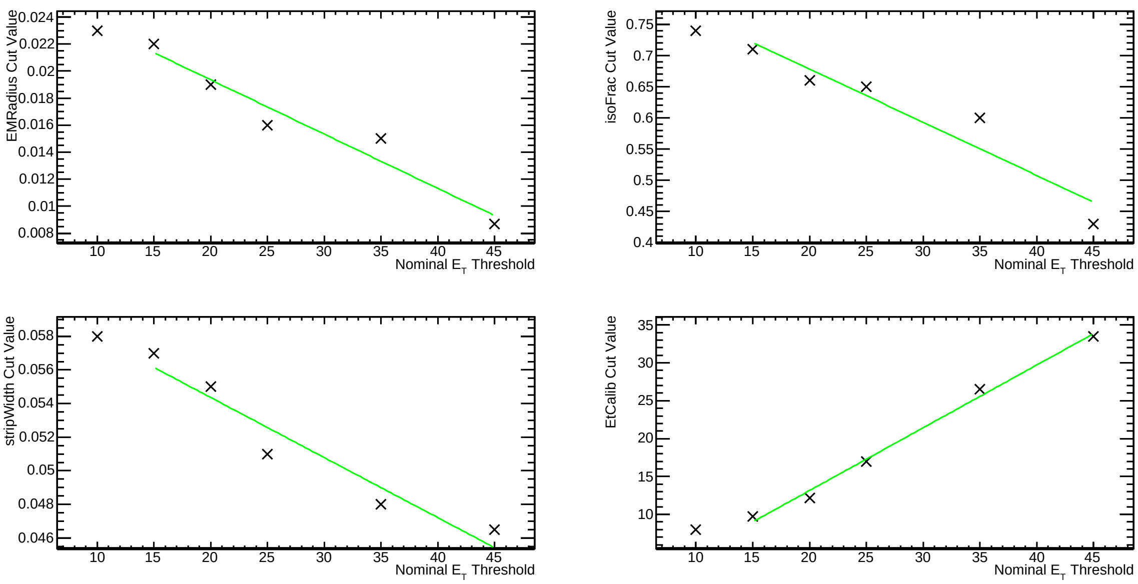

Figure 4.5: L2Calo variables cut value as a function of the nominal p_T threshold of the signature.

4.4 Calorimetric Level 2 Window size studies

At L2Calo, selection variables[10] are calculated in a $\Delta\eta \times \Delta\phi = 0.3 \times 0.3$ window (*full width*) in the second sampling of the EM calorimeter (for the "shower shape" variables) or in the whole EM and hadronic calorimeter (for the "Et" variables).

This region is small compared to the $\Delta R < 0.3$ (equivalent[11] to $\Delta\eta \times \Delta\phi = 0.6 \times 0.6$) region used by the calorimetric EF or the $\Delta R < 0.4$ (equivalent to $\Delta\eta \times \Delta\phi = 0.8 \times 0.8$) cone used by the offline reconstruction algorithms.

The narrowness of the shower from a tau jet is the main characteristic to be exploited at this level to differentiate them from the QCD jets, which for an equivalent energy result in wider showers. If the window used to calculate the shower shape variables is too narrow (narrower than the τ jet) it is more difficult to appreciate the differences between a tau and a QCD jet. Therefore if the performance of the shower shape variables at L2 is worse than at EF is in part due to the different window size used.

A comparison of the L2 Calo variables performance calculated using a $\Delta\eta \times \Delta\phi = 0.3 \times 0.3$ (*small*) or a $\Delta\eta \times \Delta\phi = 0.6 \times 0.6$ (*large*) window is presented in this section.

It is important to mention that a change in the window size would, in principle, have an impact on the execution time of the algorithm. Online timing studies [27] have been performed comparing the execution time as a function of the window size used. Resulting execution times per RoI for L2Calo algorithm are ~6 ms for $\Delta R < 0.2$, ~8 ms for $\Delta R < 0.3$ and ~11 ms for $\Delta R < 0.4$. This results show that the window size is indeed relevant. However, presently the unpacked region is $\Delta R < 0.3$ (even if only cells in a $\Delta R < 0.15$ region are used) and L2Calo algorithm is within the allowed time limitations (about 20 ms). Therefore the decision to use either window can (by now) be taken independently of the time consumption, using as a criteria only the rejection achieved.

4.4.1 Overall distribution comparison

Figure 4.6 shows the different distribution of L2Calo variables for taus from $W \to \tau\nu$ as signal and QCD dijet as background for both window sizes.

As expected, distributions for EMRadius and stripWidth are shifted to higher values for larger window, as more cells are taken into account. In contrast, distributions for isoFrac are shifted to lower values as the energy deposition density decreases with the distance to the center of the cluster. It can be appreciated that the discrimination power of the shape variables tend to increase when a larger window is used.

On the other hand, as the E_T distributions are shifted to higher values (more energy is collected using a larger window) and the shift is bigger for background than for signal, rejection power of the E_T variable will decrease when using a larger window.

In the next section, separation power differences are quantified.

The correlation between the shower shape variables has been studied for both window sizes. In figure 4.7 it can be seen that in general the three variables are quite correlated for $\Delta R < 0.15$ (top-row plots), with a correlation coefficient of about 0.5. EMRadius and stripWidth are naturally correlated, since both measure the angular size of the jet. Yet, as EMRadius is calculated

[10] defined in section 3.2.2.1

[11] In the whole chapter, the two "notations" will be used indifferently. Defining the window size by giving its radius (ΔR) is clearer, as it avoids confusion of interpreting the $\Delta\eta \times \Delta\phi$ as the *full* or *half width* of the window. However it has to be kept in mind that L2Calo uses "squared" windows (and so by ΔR we mean the distance from the center to one of the window edges), while EF and offline algorithms use indeed "round" areas to calculate their variables.

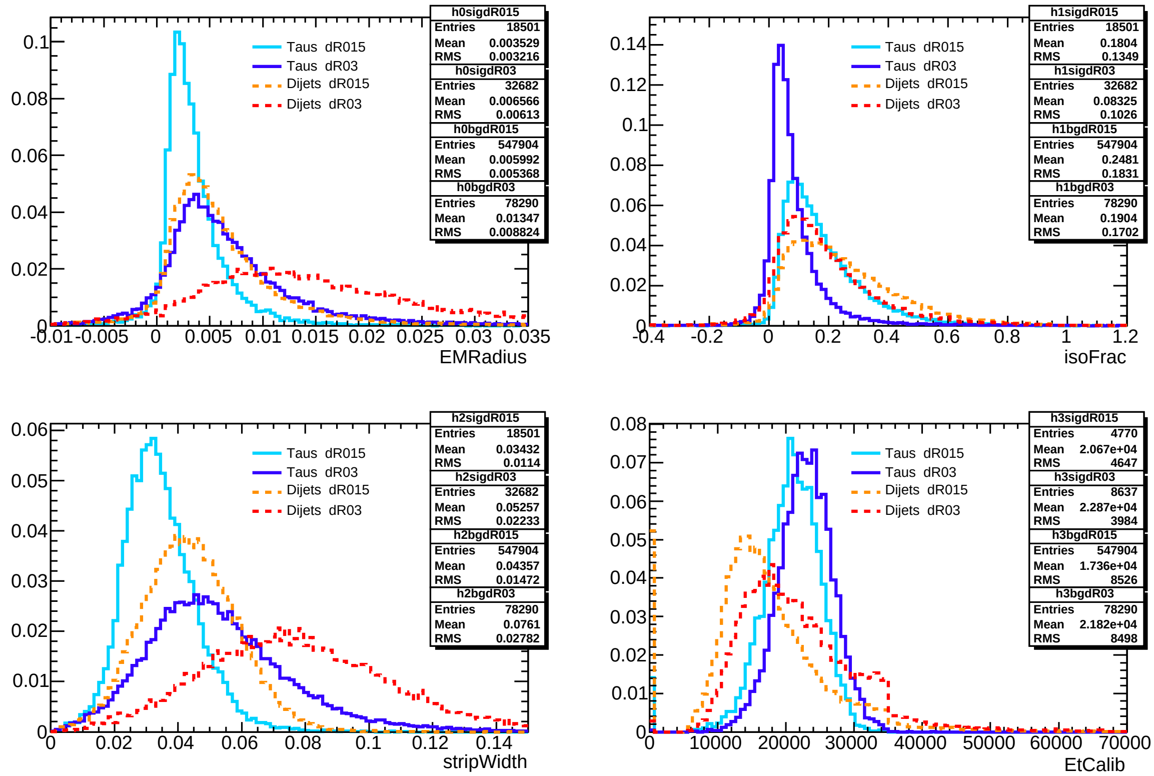

Figure 4.6: L2Calo variables distribution for menu `tau20i`. For each L2Calo variable, distributions of tau signal and dijet background for both window sizes ($\Delta R < 0.15$ and $\Delta R < 0.3$). For signal only tau objects passing L1 selection and matched to an offline identified tau are considered. Moreover for the E_T distribution taus are required to have a visible energy between 20 and 25 GeV. For background only L1 acceptance is required. $W \to \tau\nu$ sample is used as signal, while QCD dijets of 8< p_T < 70 GeV are used as background.

as the squared mean radius of the shower[12], the correlation with stripWidth and isoFrac is not linear but has a square root dependence. It can be appreciated how the distributions change when $\Delta R < 0.3$ is used (bottom-row plots). Correlation between EMRadius and stripWidth increases from 0.58 to 0.78. This is natural since, as already discussed, using a larger window size allows a better estimate of the shower shape and therefore correlation becomes more visible.

4.4.2 Rejection Comparison

To be able to quantify the rejection of each variable using the two window sizes, we compared the background rate obtained after the cut on each variable given a fixed efficiency, common for all variables and window sizes.

Next, taking figure 4.8 as an example, the strategy used is described. First of all, from the signal efficiency curve (figure 4.8, top-right plot) a cut value is set such that the resulting efficiency exceeds a given minimum value (95% in this case). Next, this cuts are applied to the background sample, and corresponding rates are obtained (figure 4.8, bottom-right plot). Finally, rates obtained by using the different window sizes can be compared (horizontal lines). In the example, EMRadius calculated in the larger window gives lower background rate, i.e. the rejection of this variable increases when a larger window is used.

[12] see section 3.2.2.1 for L2Calo variables definition.

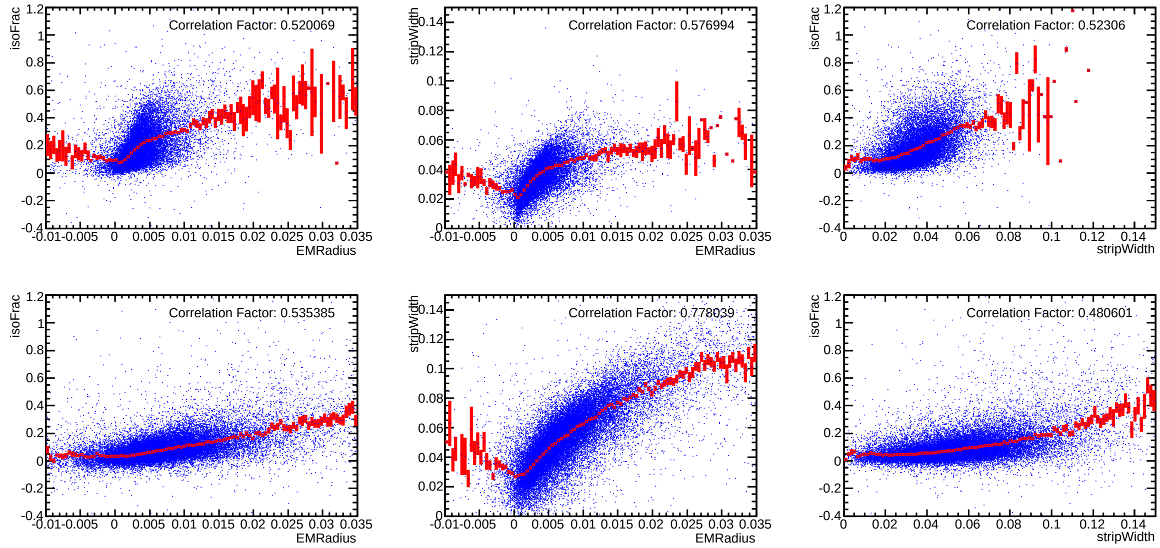

Figure 4.7: Correlation between the L2Calo shower shape variables using $\Delta R < 0.15$ (top plots) and $\Delta R < 0.3$ (bottom plots). For taus passing L1 and offline selection.

The rate values, for all variables and all considered signatures, are plotted versus the nominal p_T threshold in figure 4.9 for a fixed efficiency of 80%. In this plot it can be seen how the shifts in the distributions of figure 4.6 translate in terms of rate differences. The previous conclusions are confirmed: Using a larger window increases the rejection of the shower shape variables, while the rejection due to the E_T cut decreases. This applies to low p_T taus (for menu thresholds up to 45 GeV).

A better comparison can be seen in figure 4.10, where the ratio of the rate value obtained using a a small window divided by the rate obtained using the large window is plotted versus the p_T of the signature's threshold. Comparison is done for 95% signal efficiency (left plot) and 80% efficiency (right plot).

In the first case, the differences observed in the final rates are very small since, as we can see in figure 4.8, in order to reach 95% efficiency we need to set the cut value at the very end of the distribution's tail. Consequently, even if the separation in general increases with the use of a larger window, the tails remain and thus the rejection does not improve. Yet, if a lower efficiency is allowed (80% in this case), the improvement achieved by using a larger window is significant (about a facor of 1.2-1.6) and is systematic for low p_T signatures.

The dependence on the E_T threshold can be explained by the fact that high energy objects generate narrower showers in the calorimeter. For high energy taus, shower is already contained in the small ($\Delta R < 0.15$) window. Therefore using a larger window does not improve the rejection.

4.4.3 Shower Shape Variables Rejection Comparison

The goal of this section is to compare the rejection of each shower shape selection variable individually with respect to the others.

To compare the rejection of the shape variables, figure 4.11 shows the efficiency curves for signal and background and for both windows sizes: small ($\Delta R < 0.15$) on the left, large ($\Delta R < 0.3$) on the right, for `tau20i` signature. In all cases rejection increases when using a large

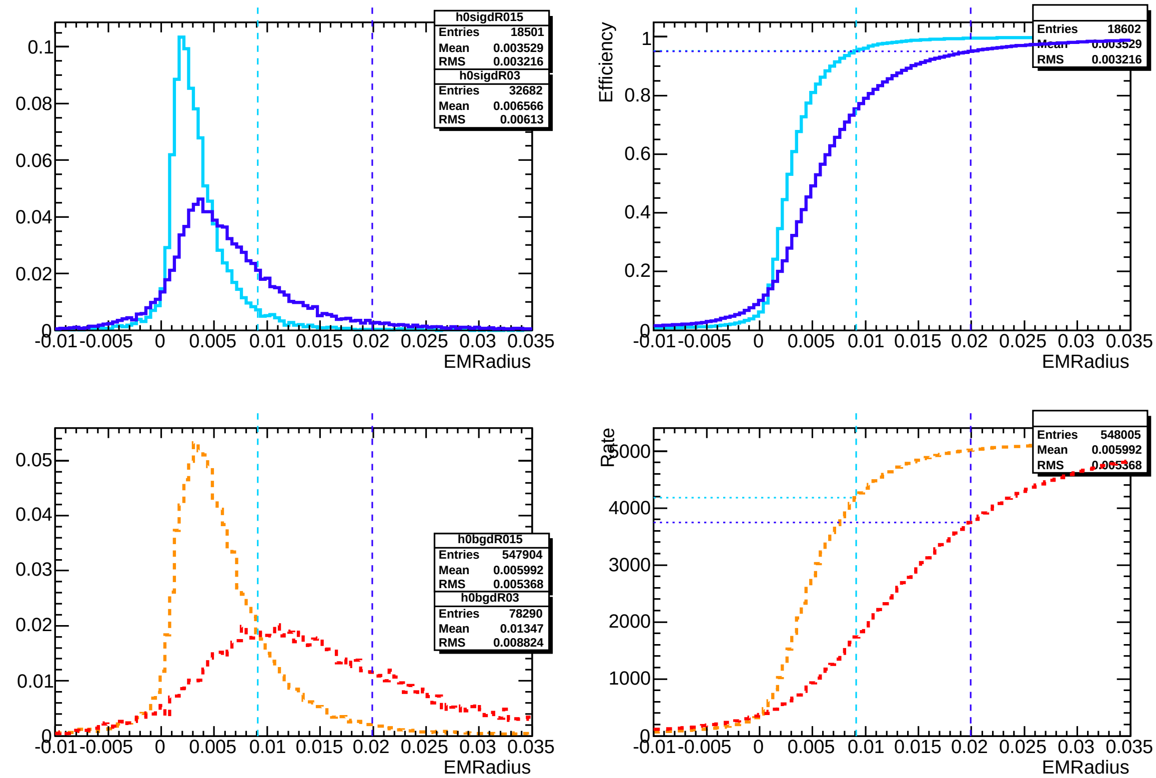

Figure 4.8: EMRadius distribution for menu `tau20i`. Tau signal distribution (top-left plot) for different window sizes. Background distribution (dijets weighted with the corresponding cross section) (bottom-left plot). Efficiency as a function of the cut value (top-right plot). Total rate (weighted dijets) as a function of the cut value (bottom-right plot). Vertical lines indicate cut value corresponding to 95% efficiency for the different window sizes. Horizontal lines are only for visual help and indicate the efficiency (top plot) or rate (bottom plot) for the corresponding cut. Light blue (orange) are curves for small window and in dark blue (red) curves for large window, for tau signal (QCD background). In this particular case, we see that the rate is a bit lower when using a large window.

window. It can be stated as well that, in the small window case, the variable achieving more background rejection is stripWidth, closely followed by EMRadius. While when using a larger window the most powerful variable is EMRadius.

To check that this behavior persists for other menu items, rates for each variable are compared in figure 4.12. Taking as a reference the rate for EMRadius, the ratio of the rates for the other variables is plotted versus the p_T of the signature's nominal threshold.

The same behavior indeed takes place: for small window ($\Delta\eta \times \Delta\phi = 0.3 \times 0.3$) the shape variable with most rejection power is stripWidth (together with EMRadius), while for large window ($\Delta\eta \times \Delta\phi = 0.6 \times 0.6$) it is EMRadius (at least for low p_T). In fact this result is not surprising at all, as EMRadius is also the variable which gives the higher rejection at EF, where the same large window size is used.

It can be appreciated how the rejection of each variable depend differently on the nominal E_T threshold.

The fact that the three variables are correlated and that one of them has a better performance than the other two, is important for the systematic optimization (section 4.3), since the automatic procedure chooses to cut harder on the best variable and the cut values of the other two suffer from fluctuations. Also in next section 4.4.5, this fact will be relevant when the number

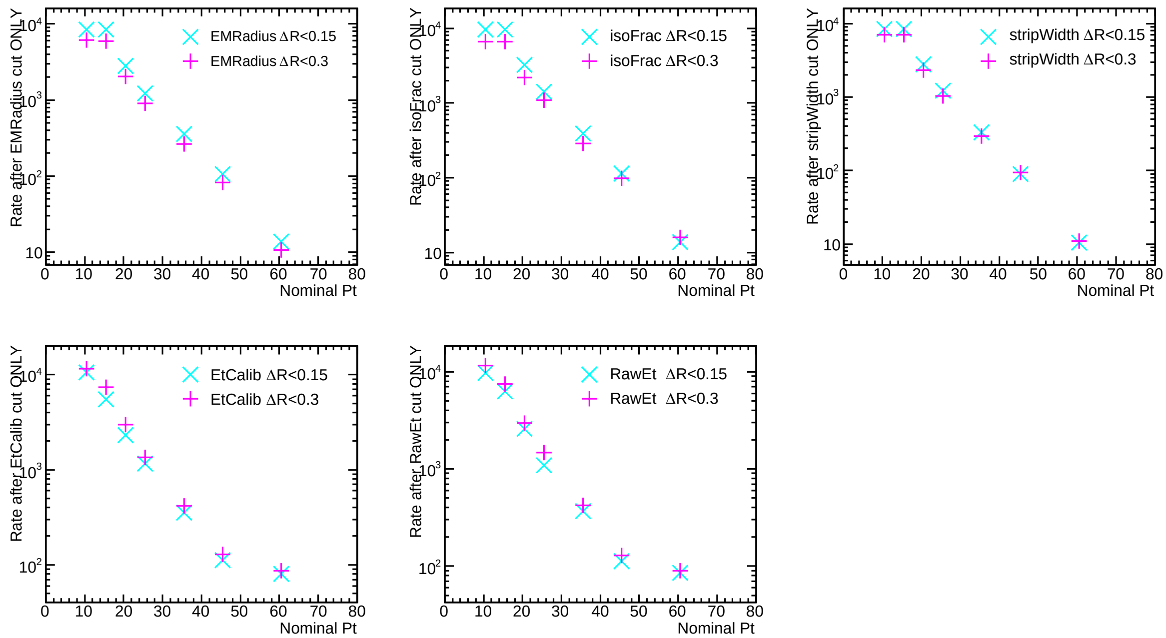

Figure 4.9: Rate as a function of the menu's threshold for an efficiency of 80% (for each variable independently), for the different window sizes. Rates for shape variables are systematically lower when using a large window, specially for EMRadius and isoFrac. However, rejection of Et variables is worse, as expected.

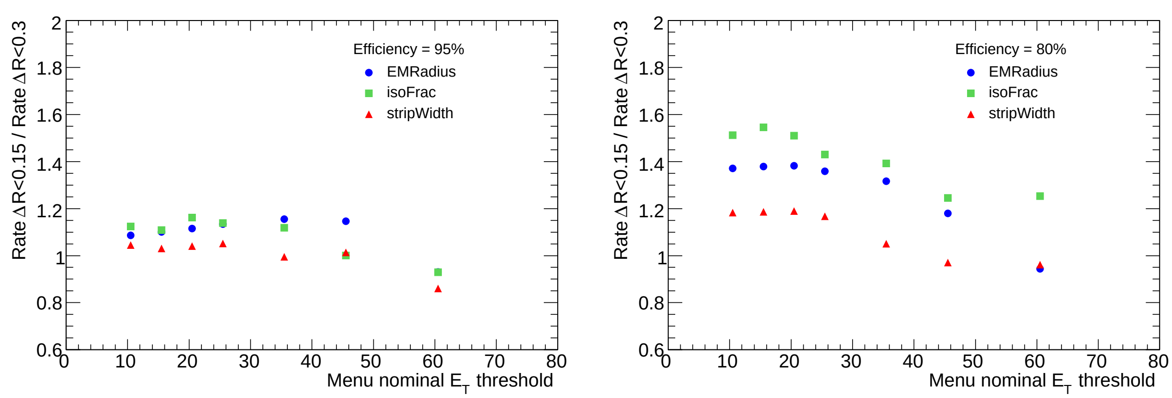

Figure 4.10: Ratio of the rate obtained using small window divided by the rate obtained using large window, as a function of the menu's threshold for an efficiency of 95% (left plot) and 80% (right plot).

of variables used for selection will be discussed.

4.4.4 Systematic optimization results

The systematic optimization of L2Calo variables explained in section 4.3 has been performed for both window sizes. Signal efficiency has been constrained to be $\sim$ 95% for the 3 shape variable cuts toghether, where efficiency is calculated with respect to true taus with visible p_T > threshold matched to an offline identified tau.

The results of this optimization can be seen in tables 4.2 and 4.3, for small and large windows respectively.

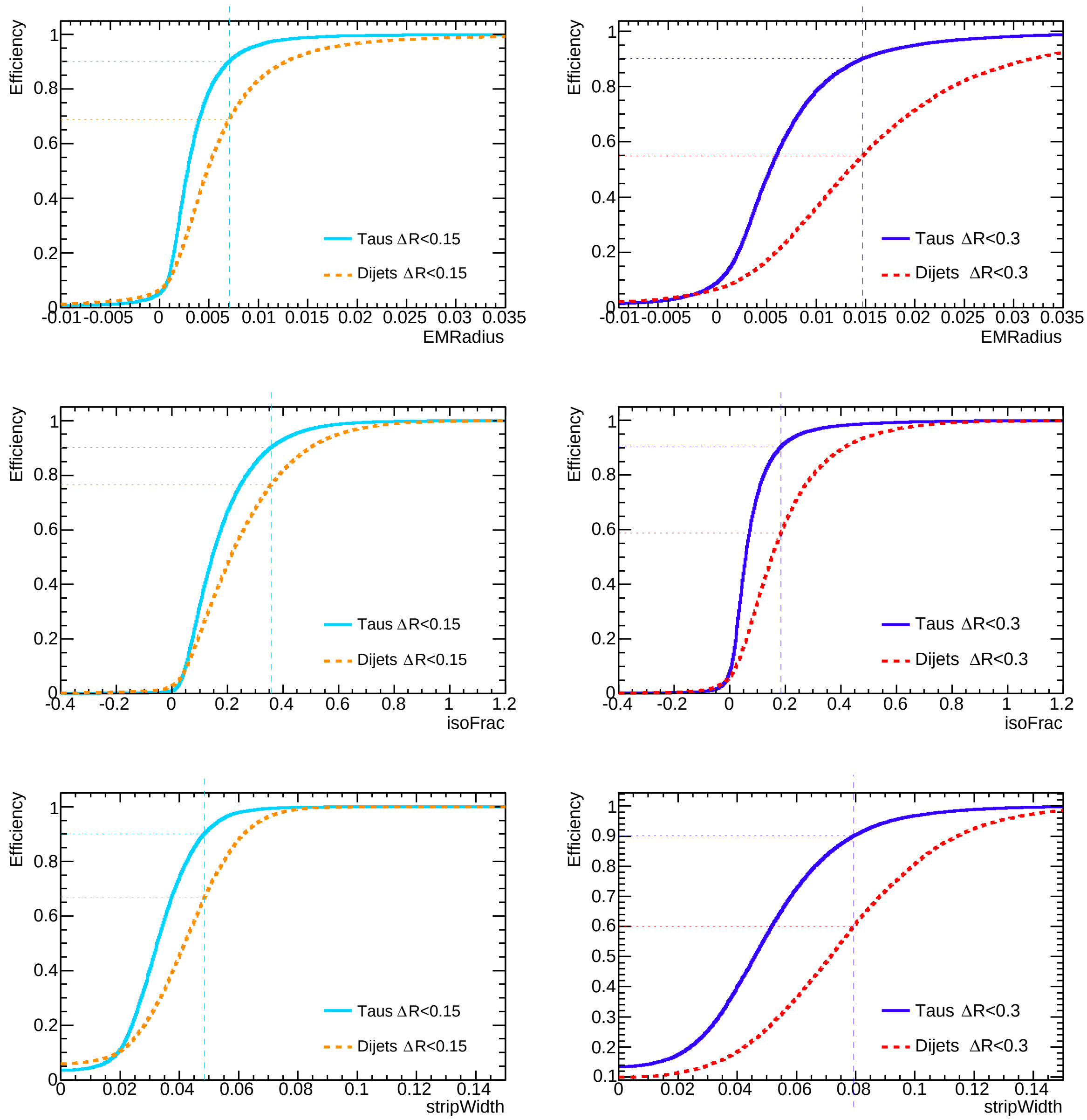

Figure 4.11: Shower Shape variables efficiency for signal and background versus cut value. Different window sizes can be compared, $\Delta\eta \times \Delta\phi = 0.3 \times 0.3$ (left) and $\Delta\eta \times \Delta\phi = 0.6 \times 0.6$ (right). From top to bottom row: EMRadius, IsoFrac, StripWidth. Efficiency for background is calculated by weighting the different dijet sample contribution by their cross-section. Vertical lines indicate cut value corresponding to 90% efficiency. Horizontal lines are for visual help only, they indicate efficiency at the corresponding cut value. This example corresponds to `tau20i` signature.

Equivalent performance in terms of background rejection is achieved in both cases, being the background rate slightly lower in the large window case. This is consistent with the results shown in figure 4.10: if a very high efficiency is required, the improvement that we can get by using a larger window is not significant.

Menu	EMRadius	isoFrac	stripWidth	Effic.	Rate (Hz)
`tau10i`	0.0222	0.74	0.0589	0.958	12107
`tau15i`	0.0222	0.7	0.0589	0.96	12044
`tau20i`	0.0185	0.67	0.0591	0.968	4320.5
`tau25i`	0.0163	0.67	0.0553	0.958	1898.8
`tau35i`	0.0147	0.61	0.0497	0.953	538.95
`tau45i`	0.0082	0.44	0.0436	0.951	170.42
`tau60`	0.0182	0.26	0.0421	0.951	73.077

Table 4.2: Cut values, efficiency and rate for cuts on shower shape variables only, obtained from a systematic cut optimization. Variables calculated in a "small" window $\Delta\eta \times \Delta\phi = 0.3 \times 0.3$. $W \to \tau\nu$ sample has been used for low p_T items, while for high p_T (`tau45i` and `tau60`) $A \to \tau\tau$ sample is used instead.

Menu	EMRadius	isoFrac	stripWidth	Effic.	Rate (Hz)
`tau10i`	0.0277	0.73	0.106	0.951	11397
`tau15i`	0.0295	0.73	0.101	0.949	11094
`tau20i`	0.0248	0.68	0.0979	0.952	3844.5
`tau25i`	0.0222	0.63	0.0936	0.951	1738.3
`tau35i`	0.0188	0.58	0.0855	0.953	529.62
`tau45i`	0.0164	0.56	0.0821	0.95	198.03
`tau60`	0.0113	0.59	0.108	0.954	82.905

Table 4.3: Cut values, efficiency and rate for cuts on shower shape variables only, obtained from a systematic cut optimization. Variables calculated in a "large" window $\Delta\eta \times \Delta\phi = 0.6 \times 0.6$. $W \to \tau\nu$ sample has been used for low p_T items, while for high p_T (`tau45i` and `tau60`) $A \to \tau\tau$ sample is used instead.

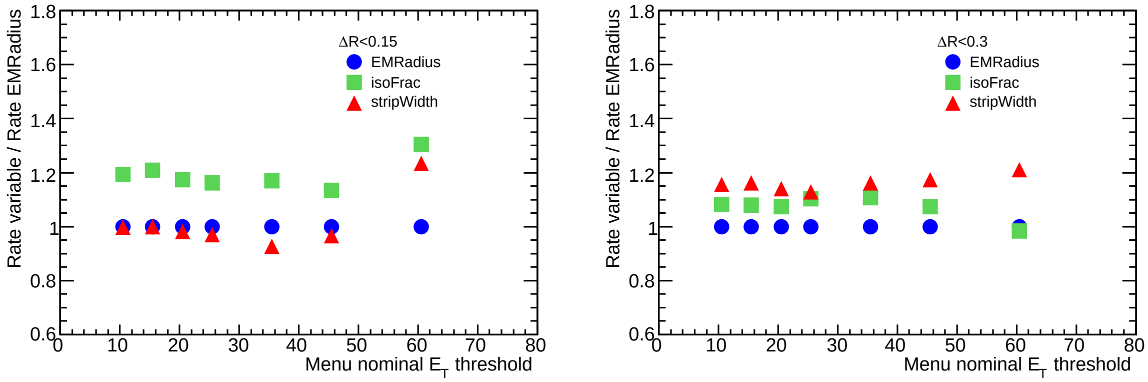

Figure 4.12: Ratio of the rate obtained using the different shape variables taking EMRadius as a reference, as a function of the menu's threshold for an efficiency of 80% for small window (left plot) and large window (right plot). Note that points for EMRadius are all at 1 by definition.

4.4.5 Single cut versus Combined cuts Studies

When a high efficiency is required, cut values are set at the end of the signal distribution's tail. By comparing the cut values in tables 4.2 and 4.3 with the distributions in figure 4.8, it seems that the rejection given by some of the variables is minimal.

It is therefore logical to raise the question if the rejection gained by using the less powerful variables compensates the complication of dealing with combined cuts.

In this section discuss the possibility of using a single cut instead of 3 combined cuts.

Figure 4.13 compares the rejection given by each variable independently with respect to the rejection achieved by the combined cuts on the 3 variables simultaneously optimized. The rate difference is small. The fact that the rejection is slightly higher for single cuts is probably due to the continuity requirement in the systematic optimization[13].

We can conclude that, in terms of background separation, the performance of a single cut selection is comparable to the performance of the combined cuts. Parallel studies in the Tau Trigger Group support this conclusion. Specifically, other L2 studies show that this conclusion applies for all signal efficiencies. Moreover, an equivalent study for calorimetric EF variables leads to similar results, pointing out that using only EMRadius variable leads to the same rejection within a 1% change in signal efficiency.

Conclusions

First conclusion is that it would be optimal to combine large window for shape variables and small window for the energy variable. This possibility has been evaluated, and results obtained are shown in section 4.5.2.

Second conclusion would be that the low rejection that had been observed for the L2 calorimeter variables was a matter of too high efficiency requested.

Thirdly, rejection power of L2 calorimeter variables can be improved by using a wider window. However the improve does not have an impact on the output rate unless a lower efficiency is allowed.

This shows that the signal to background ratio increases for lower efficiencies: rejection im-

[13]Fluctuations in the cut values were observed when performing a scan on efficiency. Cut values were thus forced to be monotonically increasing with efficiency, having to pay the price of allowing a higher rate. The allowed rate increase was higher for high p_T signatures, leading to the p_T dependence on figure 4.13. This discussion and details can be found in section 4.3.

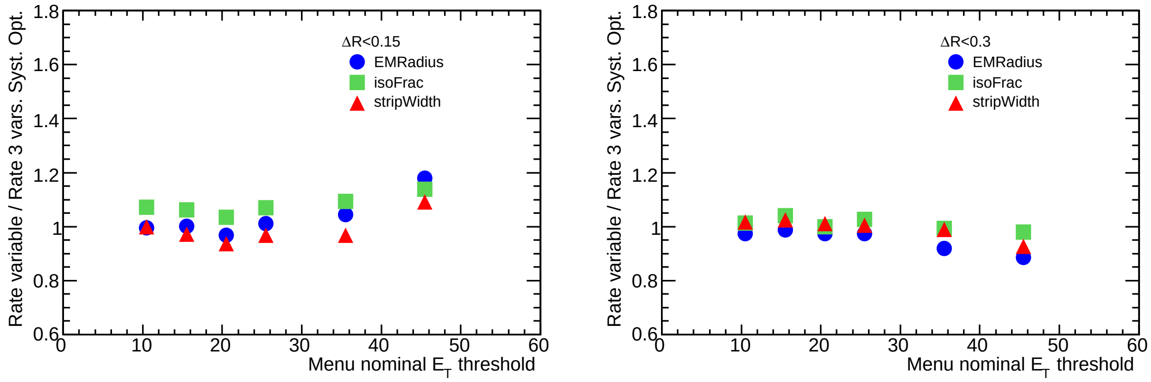

Figure 4.13: Ratio of the rate obtained using the different shape variables independently taking as a reference the rate obtained using all 3 variables with the cuts systematically optimized, as a function of the menu's threshold for an efficiency of 95% for small window (left plot) and large window (right plot).

proves faster than the efficiency loss. Requiring an efficiency of 75% instead of 95%, reduces the rate by a factor of 2. This is a point that should be taken into account when optimizing standalone high p_T menus. If the rate is not affordable two solutions are possible: tighten the cuts and obtain a lower efficiency, or rise the E_T threshold and lose low energy taus. The best solution will depend on the spectra of the signal considered. If the interesting taus are concentrated at low p_T , then it will be better to tighten the cuts, whereas if the spectrum is flat in p_T , the use of a higher p_T cut would be more appropriate.

4.5 Energy measurement at Calorimetric Level 2

The goal of the calibration at the trigger level is not to accurately estimate the energy of the tau candidate but rather to reach the highest background rejection.

Additionally, one cares about linearity (estimated energy / true energy) versus η and p_T . We would like the trigger efficiency to be as constant as possible as a function of η and p_T , in order not to bias the tau samples for offline analysis.

The question if a simple robust calibration scheme fulfills these criteria is investigated in this section. Two issues are considered, the first one is the calibration scheme and the second one is the window size used for energy estimation.

4.5.1 Performance of a simple calibration scheme

Electrons and hadrons have different response in the non-compensated calorimeter. Cell energies are calibrated according to the calorimeter response to electrons. The energy after this first calibration at the EM scale is the so-called *"Raw"* energy. An additional calibration can be applied when dealing with hadrons, that typically deposit less visible energy than electrons in the calorimeters.

At L2, a *Sampling* [29] calibration (introduced in section 3.2.2.2) is used. The current implementation considers only two calibration factors applied to EM and hadronic compartments, since the relative response to electrons and hadrons is different in the two calorimeters. This calibration is applied as follows:

$$E_{calib} = W1 \cdot EM.energy + W2 \cdot had.energy \tag{4.1}$$

Separate weights are derived in 2 energy bins (below and above $E_{cut} = 35\,GeV$) and 44 η bins[14].

Initially all L2Calo variables were calculated in the standard $\Delta\eta \times \Delta\phi = 0.3 \times 0.3$ window (equivalent to $\Delta R < 0.15$). The present calibration weights were extracted for tau energy defined in such region. Therefore in this case this standard window ($\Delta R < 0.15$) is used.

In the present section a comparison between the performance of calibrated (EtCalib) and non calibrated (RawEt) transverse energy variables is presented.

4.5.1.1 Rejection Power

To compare the two energy variables (RawEt and EtCalib) in an objective way, rejection against QCD jets is compared for a fixed signal efficiency. The efficiency is defined for each menu using a tau sample which, apart from the usual optimization requirements (detailed in section 3.3.2), has a true visible p_T in a 5 GeV interval above the menu's threshold (e.g. for `tau20i` menu, the tau visible p_T should stand between 20 and 25 GeV). This interval is of 10 GeV for high p_T menus (`tau45i` and higher). The efficiency is calculated for the energy cut only (all L1 cuts are applied and none of the L2 cuts except E_T calorimetric cut is performed). A cut value for each menu and for each of the two variables is set such that tau signal reaches the desired efficiency.

Resulting rates from QCD dijet events are plotted as a function of the menu's nominal p_T (threshold). Performance of calibrated and non-calibrated energy can be compared in figure 4.14. In the figure it can be noticed that for a fixed 80% efficiency for taus, the two variables have comparable rejection. The same conclusion applies to higher efficiencies. Hence, no significant additional rejection power is gained by calibrating the energy at L2Calo.

[14] The η range for calibration is $|\eta| < 4.4$. However in the present calibration only $|\eta| < 2.5$ is used, taus in $|\eta| > 2.5$ are not interesting for the trigger as there is no tracking information available in such region.

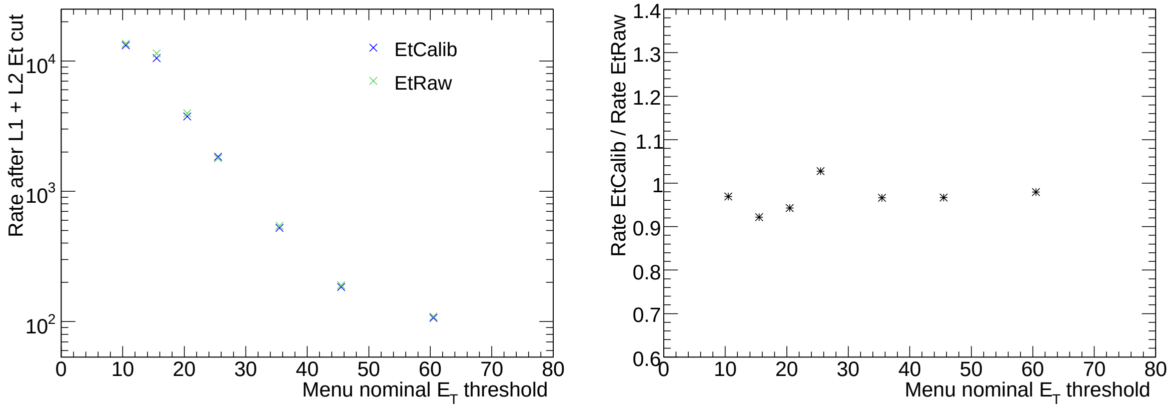

Figure 4.14: Left: Rate as a function of the menu's threshold for an efficiency of 80% , for narrow window ($\Delta\eta \times \Delta\phi = 0.3 \times 0.3$) after L1 selection and L2 E_T cut is applied. Right: Ratio of the left plots: rate obtained using EtCalib divided by that obtained using EtRaw, for each menu. We see that rates are very similar (there is less than 10% difference), and that no general tendency can be appreciated as a function of the threshold.

4.5.1.2 Linearity in E_T and η

Figure 4.15 shows the linearity as a function of true visible p_T and η. In this case all L2 objects matched to a true tau are considered, no offline identification is required, neither a specific L1 selection. Conclusion from these plots is that linearity versus p_T is better when the calibration is used, and also the energy scale in the end-cap region ($1.5 < \eta < 2.5$) and in the barrel ($0 < \eta < 1.3$) are more equal.

Comparing the trigger linearity with that achieved by tauRec (figure 4.16), it is worth to notice that the trigger calibration, which uses a very simple E_T dependence, gives a very uniform p_T response in the low-p_T range. On the other hand, tauRec is able to better recover the energy loss in the crack region (around $\eta \approx 1.5$). Some improvement in this direction is possible in the trigger when re-extracting calibration weights by using new simulated data, as the detector description (amount of material simulated) has changed since the present weights were extracted.

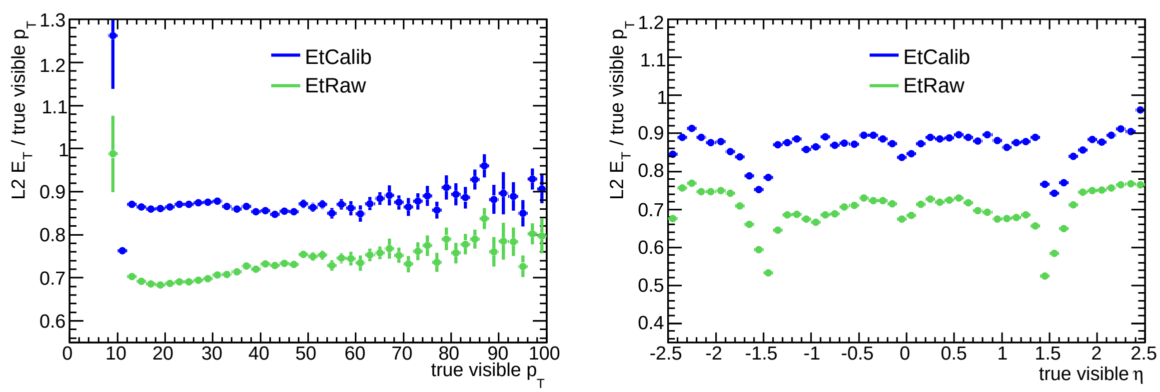

Figure 4.15: Energy scale (L2 measured E_T divided by true tau visible p_T) versus visible E_T (left) and versus visible η (right). L2 objects are only required to match a MC true tau, no offline match is required. $W \rightarrow \tau\nu$ sample is used.

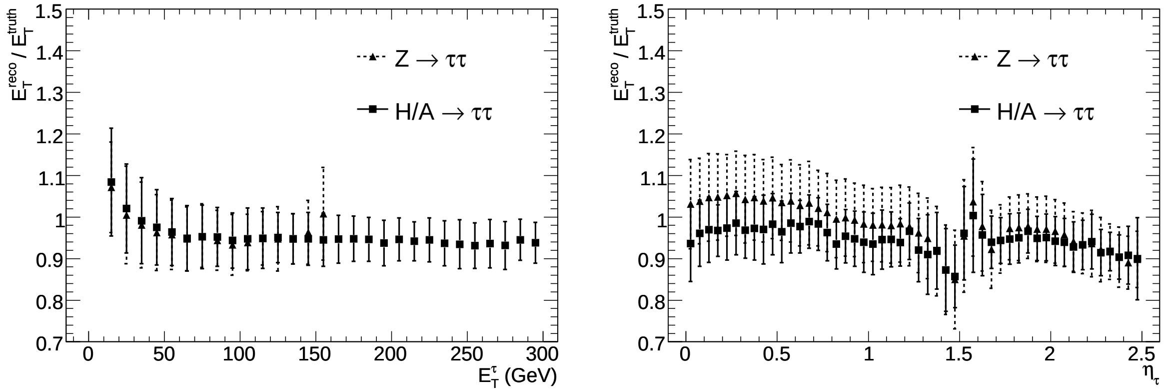

Figure 4.16: Offline tauRec linearity: the ratio between the reconstructed and the true E_T of the hadronic τ decay products is shown as a function of E_T (left) and $|\eta|$ (right). The ordinate value is the mean and sigma of the Gaussian fit performed in the range $0.8 < E_T^{reco}/E_T^{truth} < 1.2$. The triangular points show this ratio for $Z \to \tau\tau$ events, while the square shows this same ratio for $A \to \tau\tau$ events. All considered events pass a loose identification criteria of likelihood LLH > 2.

4.5.1.3 Efficiency Uniformity

Figure 4.17 compares eta dependence of the efficiency for the two E_T variables. Efficiency is calculated with respect to the MC true taus for signal, while for background the reference taken are all objects which pass a very loose L1 selection. The L1 cuts are the standard cuts for `tau20i` menu, whereas the cuts on the two E_T variables are different, and were set to give the same efficiency[15] for taus with true p_T between 20 and 25 GeV. The rejection offered by the two variables is equivalent, the mean efficiency for the background being 0.234 for both EtRaw and EtCalib. However the energy calibration helps to maintain a constant efficiency in η, recovering acceptance in the crack region. The standard deviation from the mean being significantly lower for EtCalib (0.040) than for EtRaw (0.065).

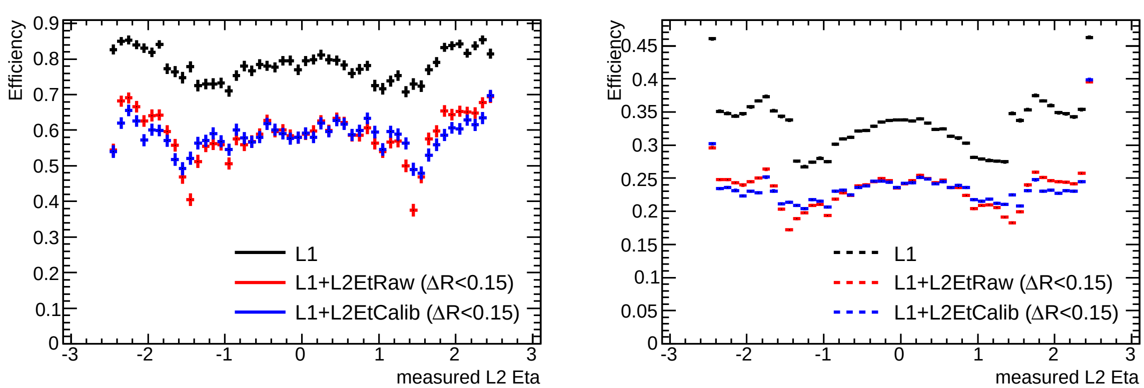

Figure 4.17: Efficiency with respect to true taus, as a function of η for tau signal (left plot) and QCD dijet background weighted by the cross section (right plot). Calibrated (Calib) and non-calibrated (Raw) transverse energy variables calculated in $\Delta R < 0.15$ are compared. The same signal efficiency (90% taking as a reference the offline) for 20-25 GeV taus is required. In the crack region efficiency is in part recovered by the calibration.

[15] 90% with respect to L1 and Offline (standard definition as in 3.3.2)

In summary, the present calibration is not able to improve the discrimination between τ-jets and QCD jets but it improves the linearity and the uniformity of the trigger acceptance versus η. Hence, even if the calibration could be further improved, it is useful and will be applied. More on E_T variables can be found on next section (4.5.2) where a similar comparison is done calculating E_T variables in different RoI window sizes.

4.5.2 Effect of the window size choice

As explained in section 4.4, using a larger window size to calculate the shower shape variables improves their rejection power. However, if the same large ($\Delta R < 0.3$) window is used for the E_T variables, their background rejection power decreases. In order to arrive to a compromise and to take advantage of the maximum rejection possible, different window sizes can be used in each case. Yet, due to technical reasons, if this larger ($\Delta R < 0.3$) window is used by the shape variables, the possible window sizes for E_T variables are only ΔR <0.1, 0.2 and 0.3.

In this section the performance of the E_T variables calculated in two different windows sizes (ΔR <0.1 and ΔR <0.3) is compared. Since calibration weights have not yet been extracted for this window sizes the energy here used is at EM scale (non-calibrated, raw energy).

Figure 4.18 is the equivalent of figure 4.17: it compares the η dependence of the efficiency for the two E_T variables EtRaw ($\Delta R < 0.3$) and EtRawNar ($\Delta R < 0.1$).

For the same efficiency, the rejection of EtRawNar is significantly better. This can be appreciated comparing the mean background efficiency for EtRaw (0.201) and EtRawNar (0.176). This is easily understandable as the QCD jets are on average substantially wider than $\Delta R < 0.1$, and therefore their energy is underestimated in this case. Tau jets are narrower than jets from QCD so more energy is contained in the narrow window. Low energy jets being the main contribution to our background, underestimating QCD jet energy is the best way to reduce the final background rate.

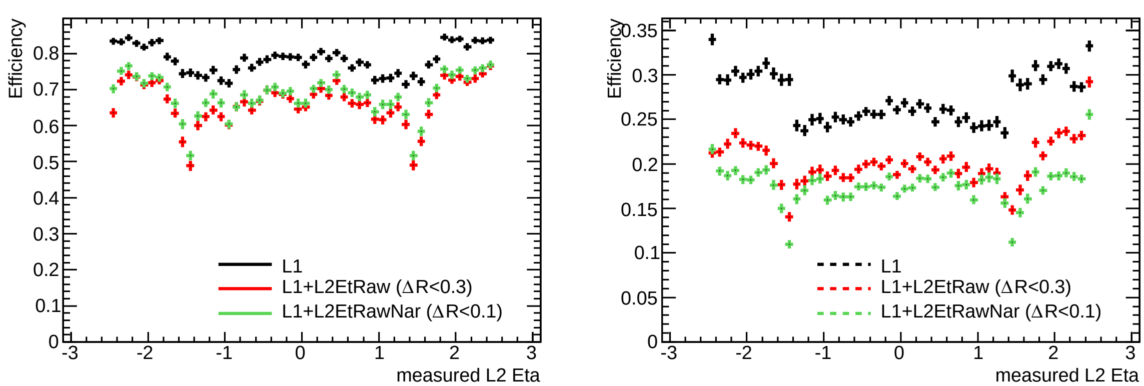

Figure 4.18: Efficiency with respect to true taus, as a function of η for tau signal (left plot) and QCD dijet background weighted by the cross section (right plot). Non calibrated energy in a $\Delta R < 0.3$ window and in a $\Delta R < 0.1$ window are compared. The same signal efficiency for 20-25 GeV taus is required. Background efficiency is significantly lower for energy in a narrower window.

Summary and conclusion

The present simple calibration, even if it has only a first order dependence on the energy, is quite satisfactory in terms of linearity as a function of η and p_T , though it does not help to improve the background rejection.

On the other hand, when the energy is calculated in a small window ($\Delta R < 0.1$) higher background rejection is achieved because the jet energy is underestimated, as QCD jets are wider.

Therefore the optimal combination would be to calibrate the energy in a narrow ($\Delta R < 0.1$) window. This is the option which is foreseen to be implemented. By now, since calibration weights for $\Delta R < 0.1$ window are not yet available, it has been decided to use raw energy instead.

However, in terms of energy measurements at L2, this is not the final nor the only possible approach. The introduction of an *energy-flow* type variable could eventually contribute to the improvement of energy resolution, depending also on the offline reference used.

A new iteration on this topic will be done after the expected convergence of the offline reconstruction algorithms.

5 Conclusions and Outlook

The extremely high energy and luminosity at the LHC needed in order to be sensitive to low cross section processes, will produce a huge amount of interactions and associated volume of data, which can not be all recorded. Therefore, a very selective trigger system is needed to record only the interesting events. The challenge of the trigger system is to make the decision within the available time and using affordable resources.

As it is the heaviest lepton, tau will be an important signature for searches of New Physics such as low mass SM Higgs boson, the MSSM Higgs or Supersymmetry. Taus produced in SM processes like inclusive W, Z boson or top pair production, specially in the early data, will be useful to establish the tau reconstruction and triggering capability in the difficult environment of a hadron collider. Taus can be identified in their hadronic decays, while leptonic decays can not be distinguished easily from primary electrons or muons. There are two offline reconstruction packages exploiting the main features of the tau hadronic decays, narrow jets with a low multiplicity of associated tracks, to separate them from the QCD jets background. One package starts from the calorimeter information, the other from the tracks. The former giving a higher overall QCD jet rejection, while the latter is optimal for low p_T taus and equally efficient for single and multi prong taus.

Tau Trigger is designed to select with high efficiency events in which the tau leptons can be reconstructed and identified offline, and should be efficient for both offline algorithms. Tau/jet separation is not as powerful as electron/jet and hence it is more difficult to trigger on taus than on electrons. At L1 the rejection power is limited by the L1 energy resolution. The thresholds are set to guarantee a high efficiency (90% taking as a reference the offline) for taus of a given true visible energy. The L1 rate is dominated by QCD jets passing the tau L1 selection. A cut on the maximum E_T in the isolation region can be applied at L1. It is useful to reduce the QCD rate in a range of 20-60 GeV, but for higher energies the cut suffers from increasing loss of efficiency. Hence, the highest p_T item at L1 will never use the isolation requirement. At HLT improved resolution and refined shower shape variables are used, in addition to the tracking information. This leads to a further rejection factor of about 5 for L2 and $\sim$2 for EF, maintaining a global tau slice efficiency of the order of $\sim$60% for offline identified taus.

To reduce further the background rate to affordable levels, several options are possible:

- Use higher E_T thresholds (since background is concentrated at low E_T). This has the strong disadvantage that SM physics taus and many of the New Physics signals will appear at low p_T . Even at low 10^{31} luminosity E_T threshold for inclusive tau is already rather high (45-60 GeV) for a good physics acceptance.

- Combine it with other triggers. Events with taus in the final state in general have $\not{E}_T$ associated. $\not{E}_T$ trigger provides good rejection of QCD background, and in combination with taus it can be efficient for W, top and charged higgs decays, among others. Processes in which taus are produced in pairs can be efficiently triggered by tau+lepton (e, μ) selection when one of the taus decays leptonically, and by di-tau triggers when both decay hadronically.

- Use a tighter selection. Some efficiency is lost but E_T threshold can be maintained.

- Introduce a prescale factor. Much more statistics is lost but very low threshold is possible. These triggers are useful for trigger efficiency measurements specially during commissioning.

A lot of optimization has already been done in the Tau Trigger slice. My work has been focused on the optimization of L1 and L2Calo. A systematic optimization method has been designed. The results have helped us to understand many useful features of our selection variables: the first conclusion is that a robust simple trigger can be based in a single variable, since equivalent rejection is achieved. Next is that calibrating the energy is useful, not for background rejection but for linearity in η (some efficiency can be recovered in the crack region) and in p_T , achieving a good uniformity of the efficiency. Finally, we have seen we can improve our background rejection by considering a wider region of the calorimeter, and by estimating the energy in a smaller region. Some further improvements could be possible for example by introducing an *energy-flow* approach at L2, and topological clustering algorithm at EF.

In any case, the optimization will be revised following-up trigger and offline developments and a possible convergence to a unique offline algorithm profiting from the strong aspects of the two approaches that have been developed. Now we are about to start taking the first data, which will allow us to look at important aspects of the trigger selection such as robustness, commissioning strategies and problems associated with the minimum bias.

Selecting and identifying τ leptons in the difficult environment of the LHC will be a challenging task, but it is well worth in view of the potential New Physics discoveries that could be made with τ leptons.

Bibliography

[1] G. Polesello. Introduction to LHC physics. *J. Phys. Conf. Ser.*, 53:107–116, 2006.

[2] ATLAS: Detector and physics performance technical design report. Volume 1,CERN-LHCC-99-14.

[3] A. Airapetian et al. ATLAS calorimeter performance,CERN-LHCC-96-40.

[4] D. Berge et al. The configuration system of the ATLAS Trigger. *IEEE Trans. Nucl. Sci.*, 55:392–398, 2008.

[5] N. Berger et al. The ATLAS High Level Trigger Steering,ATL-DAQ-CONF-2007-026.

[6] ATLAS Collaboration. Identification of hadronic tau decays with ATLAS detector, CSC Note J16.

[7] ATLAS Collaboration. Charged Higgs Boson search in ATLAS, CSC Note HG-10.

[8] ATLAS Collaboration. Search for the SM Higgs via Vector Boson Fusion production process in the di-tau channels, CSC Note HG-3.

[9] ATLAS Collaboration. Discovery potential of A/H $\rightarrow \tau\tau$ in ATLAS, CSC Note HG-7.

[10] Z.Czyczula and T.Vickey. Search for new physics using high-pT tau pairs in ATLAS, ATLAS Physics Communication.

[11] S. Jadach et al. The tau decay library, TAUOLA: version 2.4, Comp. Phys. Commun. **76** (1993) 361.

[12] P. Nevski D. Froidevaux and E. Richter-Was. Energy flow studies for hadronic tau's with DC1 data, ATLAS Physics Communication ATL-COM-PHYS-2005-024.

[13] ATLAS Collaboration. CSC Note CALO-1.

[14] ATLAS Collaboration. J6+J7+J9: Calibration, CSC Note.

[15] M. Heldmann and D. Cavalli. An improved tau-Identification for the ATLAS experiment, ATLAS Physics Note ATL-PHYS-PUB-2006-008.

[16] ATLAS Collaboration. ATLAS Tau Trigger: performance and menus for early running, CSC Note.

[17] D. O. Damazio et al. Data Preparation of the Calorimeter Based Algorithms of the High-Level Trigger for the ATLAS experiment at the LHC. In *COMO2007*, 2007.

[18] ATLAS Collaboration. HLT tracking performance, CSC Note.

[19] ATLAS Collaboration. EG-11 Overall Trigger strategy for Electron and Photon Selection, CSC Note.

[20] ATLAS first-level trigger: Technical design report,CERN-LHCC-98-14.

[21] T. Bold. Trigger menu: http://tbold.web.cern.ch/tbold//view_menu.php?name=full_13.0.30.3.

[22] A. Sidoti et al. Implementation and performance of the ATLAS trigger muon 'vertical slice'. *Nucl. Phys. Proc. Suppl.*, 172:289–291, 2007.

[23] ATLAS Collaboration. Identification of hadronic tau decays with ATLAS detector (long version, not public). http://atlas-sw.cern.ch/cgi-bin/viewcvs-atlas.cgi/groups/JetsEtmissTauC%SC/J16_Tau_CSC/note/TauCSC.ps?revision=1.36&view=markup.

[24] The CDF Collaboration A. Safanov et al. Nucl. phys. proc. supl. **144** (2005) 323.

[25] The CDF Collaboration D. Acosta et al. Phys. rev. d **75** (2007) 092004.

[26] The CDF Collaboration D. Abulencia et al. Phys. lett. b **639** (2005) 112002.

[27] ATLAS Collaboration. ATLAS Tau Trigger: performance and menus for early running (long version, not public). http://atlas-sw.cern.ch/cgi-bin/viewcvs-atlas.cgi/groups/TauTrigger/Tau%TriggerCSC/tautriggerCSC.tex?revision=1.43&view=markup.

[28] P. Casado on behalf of the Tau Trigger Group. Tau trigger: LvL1 and LvL2 calorimeter. http://indico.cern.ch/getFile.py/access?contribId=80&sessionId=3&resId=%1&materialId=slides&confId=16155.

[29] A. Gupta et al. Jet Energy Correction Using Longitudinal Weighting, ATLAS Internal Note Phys-2006-062, 2007.

Acknowledgments

First of all, I would like to thank the Tau Trigger Group for their patience and support. Also all people in ATLAS who have helped me and have been comprehensive with my inexperience. Special thanks to Olya and Imma, for showing their interest in this work which has been definitively encouraging.

Of course, I am grateful to Martine for all the knowledge received and specially for the time taken on my *tesina* during these tough weeks.

This work would not have been possible without Carlos, first of all for the knowledge inherited from him but most important for his personal support in the difficult times, wise advice, and infinite patience. Thanks.

I also wish to thank Volker for all interesting exchanges and technical help provided.

I am certainly grateful to my parents, who encouraged me from the very beginning. I must acknowledge their patience, advice, and unconditional support.

I want to sincerely thank my *"family"*: Pau, Gaëlle, Laura, Albert and also Xavi. Their everyday support is very much appreciated.

Finally, I am thankful to all my friends for sharing lunches, dinners, teas, parties and lots of good moments together.

This work has received financial support from *Ministerio de Educación y Ciencia* (FPU, AP2006-01735).